Copyright

by

Jai-Pil Choi

2003

The Dissertation Committee for Jai-Pil Choi Certifies that this is the approved version of the following dissertation:

ELECTROGENERATED CHEMILUMINESCENCE WITH AMINE AND BENZOYL PEROXIDE COREACTANTS: REACTIVITY AND REACTION MECHANISM STUDIES

Committee:

Allen J. Bard, Supervisor

Eric V. Anslyn

Keith J. Stevenson

David A. Vanden Bout

Arumugam Manthiram

ELECTROGENERATED CHEMILUMINESCENCE WITH AMINE AND BENZOYL PEROXIDE COREACTANTS: REACTIVITY AND REACTION MECHANISM STUDIES

by

Jai-Pil Choi, B.S., M.S.

Dissertation

Presented to the Faculty of the Graduate School of

The University of Texas at Austin

in Partial Fulfillment

of the Requirements

for the Degree of

Doctor of Philosophy

The University of Texas at Austin

December, 2003

Dedication

To my family who have endlessly supported and encouraged me: my precious daughter, Seung Hye Choi, my loving wife, Hee Sun Yang, my esteemed parents and parents-in-law, Myung Hwan Choi, Se Ja Moon, Jae Cheon Yang, and Kil Soon Cho.

Acknowledgements

The author would like to acknowledge Professor Allen J. Bard in gratitude for his guidance and support of author's research. The author would like to thank Dr. Wujian Miao for his helpful discussion on the ECL mechanism of amine coreactants, Dr. Don O'Connor for fluorescence lifetime measurements, Dr. Ken-Tsung Wong for providing ter(9,9-diarylfulorene)s. The author would also like to thank Drs. Fu-Ren F. Fan, Katherine Holt, Bob LeSure, and Donald Pile for their revision of this dissertation.

ELECTROGENERATED CHEMILUMINESCENCE WITH AMINE AND BENZOYL PEROXIDE COREACTANTS: REACTIVITY AND REACTION MECHANISM STUDIES

Publication No._____

Jai-Pil Choi, Ph.D.

The University of Texas at Austin, 2003

Supervisor: Allen J. Bard

The electrogenerated chemiluminescence (ECL) of tris(2,2′-bipyridine)ruthenium(II), $Ru(bpy)_3^{2+}$, was investigated using amine coreactants. When amine coreactants were oxidized, they produced both sufficiently strong reducing ($R_2NC^{\bullet}HR'$) and oxidizing ($R_2N^{\bullet+}CH_2R'$) agents and these agents were relatively stable to diffuse and react with $Ru(bpy)_3^{2+}$ or electrochemically generated $Ru(bpy)_3^{3+}$ to generate $Ru(bpy)_3^{2+}*$. Most amine coreactants produced two ECL waves in a plot of ECL vs electrode potentials: the first occurred before the oxidation of $Ru(bpy)_3^{2+}$ and the second occurred immediately after the oxidation of $Ru(bpy)_3^{2+}$, implying two different ECL mechanisms participate in the first and second ECL, except for *N*, *N*, *N*′, *N*′-tetra-*n*-propylmethane diamine

and *N*, *N*, *N*′, *N*′-tetra-*n*-propylethylene diamine. ECL produced by monoamine coreactants gave stronger emissions than diamines, and acyclic amines produced stronger ECL than heteroalicyclic amines. The ECL intensity increased as the number of carbon atoms increased in the same group of amines except for those with the piperazine group. Tri-*n*-propylamine produced the most intense first and second ECL.

Benzoyl peroxide (BPO) was studied as a new coreactant for neutral red (NR), ter(9,9-diarylfluorene)s (TDAFs) and $Ru(bpy)_3^{2+}$. When BPO was reduced, it produced the strong oxidizing agent, $C_6H_5CO_2^{\bullet}$ via an ECE process. Then electrochemically reduced $NR^{\bullet-}$, $TDAF^{\bullet-}$, or $Ru(bpy)_3^{+}$ reacted with $C_6H_5CO_2^{\bullet}$ to produce ECL. At a high concentration of BPO (e.g. > 10 mM compared to 0.5 mM NR), ECL quenching by BPO was significant, as confirmed by fluorescence quenching experiments. NR could be used as both a pH indicator and ECL emitter in acetonitrile. A yellow-to-red color change was observed when a NR solution was titrated with acids. The protonated form of NR (NRH^+) did not produce ECL due to two-electron reduction of NRH^+ and lack of sufficient energy for the ECL reaction. However, NR generated ECL emission of 610 nm. TDAFs emitted at ~ 400 nm (blue ECL). In annihilation ECL, significant emission of TDAF excimers, mainly formed by coulombic interactions when radical cations were annihilated by radical anions, interfered with their blue emission ($\phi_{ECL} \leq 0.05$ %) Excimers

were not observed in fluorescence. No significant excimer emission was found when BPO coreactant was used.

Table of Contents

List of Tables xiii

List of Figures xiv

List of Schemes xxiii

Chapter 1 Fundamentals of Electrogenerated Chemiluminescence (ECL) 1

1.1 Introduction 1

1.2 Ion Annihilation 2

1.3 Coreactants 5

1.4 Formation of Excimers or Exciplexes 6

1.5 Preannihilation ECL 9

1.6 Concluding Remark 10

References 11

Chapter 2 Electrogenerated Chemiluminescence of Tris(2,2′-bipyridine)ruthenium(II), $Ru(bpy)_3^{2+}$/Tri-*n*-propylamine (TPrA) System – A New Route Involving $TPrA^{\bullet+}$ Cation Radicals 14

2.1 Introduction 14

2.2 Experimental Section 18

Chemicals 18

Immobilization of $Ru(bpy)_2[bpy(COOH)_2]^{2+}$ on an ITO Electrode 18

Electrochemical and ECL measurements 19

ESR Experiments 20

2.3 Results and Discussion 22

Electrochemical and ECL behavior of the $Ru(bpy)_3^{2+}$/TPrA system 22

SECM – ECL Experiments 30

Fast scan CV and digital simulations 38

ESR of $TPrA^{\bullet+}$ in aqueous solution 42
2.4 Conclusions 46
References 48

Chapter 3 Structure and Reactivity Aspects of Various Amine Coreactants and Coreactive Buffers on the Electrogenerated Chemiluminescence of Tris(2,2′-bipyridine)ruthenium(II) Complex, $Ru(bpy)_3^{2+}$, in Aqueous Media 50
3.1 Introduction 50
3.2 Experimental Section 54
Chemicals and Solutions 54
Syntheses of TPDAM, TPDAE, TPDAP, PP, DEPz, and DPPz 59
N,N,N',N'-Tetra-n-propylmethanediamine (TPDAM) 59
N,N,N',N'-Tetra-n-propylethylenediamine (TPDAE) 60
N,N,N',N'-Tetra-n-propylpropane-1,3-diamine (TPDAP) 60
1-Propylpiperidine (PP) 60
1,4-Diethylpiperazine (DEPz) 61
1,4-Dipropylpiperazine (DPPz) 61
Instruments and Procedures 61
3.3 Results and Discussion 62
Electrochemistry of $Ru(bpy)_3^{2+}$ and 14 Different Amine Coreactants 62
ECL of $Ru(bpy)_3^{2+}$ by amine coreactants 66
The first ECL 72
The second ECL 74
ECL of $Ru(bpy)_3^{2+}$ in Coreactive Buffers 83
3.4 Conclusions 87
References 89

Chapter 4 Acid-Base Properties, Electrochemistry, and Electrogenerated Chemiluminescence of Neutral Red in Acetonitrile 92
4.1 Introduction 92

4.2 Experimental Section 95
Materials 95
Spectroscopy 96
Electrochemistry 96
Electrogenerated Chemiluminescence (ECL) 97
4.3 Results and Discussion 98
Acid-Base Properties of NR in MeCN 98
Electrochemistry of NR and NRH^+ 101
Electrogenerated Chemiluminescence (ECL) of NR 114
Concentration effects on the ECL of NR 121
ECL of $Ru(bpy)_3^{2+}$ with BPO and ECL Efficiency 127
4.4 Conclusions 131
Supporting Information 132
References 135

Chapter 5 Electrogenerated Chemiluminescence of Ter(9,9-diarylfluorene)s: Excited Singlet State Emission vs. Excimer Emission 138
5.1 Introduction 138
5.2 Experimental Section 141
Chemicals 141
Apparatus and Instrumentation 143
Calculations 144
5.3 Results and Discussion 144
Absorbance, Fluorescence, and Phosphorescence 144
Electrochemistry 148
Electrogenerated Chemiluminescence (ECL) – Ion annihilation 154
Electrogenerated Chemiluminescence (ECL) – Coreactant 160
Modeling the Excimer 165
Triplet ECL Emission 166

ECL Efficiency 168
5.4 Conclusions 169
Supporting Information 170
References 174
Chapter 6 Concluding Remarks 177
References 181
Appendix A List of Symbols 182
Roman Symbols 182
Greek Symbols 184
Glossary 186
References 190
Vita 202

List of Tables

Table 3.1: Summary of Electrochemical Data for the Oxidation of Amines 68

Table 3.2: List of pK_a Values of Coreactants, Optimum pH for the Second ECL and Its ECL intensities 82

Table 3.3: pK_a, Anodic Peak Potential (E_p), the First and Second ECL wave Intensities, and the Relative second ECL wave Intensity (I_{CB}/I_{TPrA}) of Coreactant Buffers 86

Table 4.1: Summary of $E_{1/2}$, n, and D for the Reductions of NR and NRH^+ 112

Table 5.1: Summary of Spectroscopic Data 149

Table 5.2: Summary of Electrochemical Data 153

Table 5.3.: Physical Data of Ion annihilation Reaction and Coreactant Reaction for ECL 155

List of Figures

Figure 2.1: Setup for SECM – ECL 21

Figure 2.2: (a) ECL and (b) cyclic voltammogram of 1.0 nM $Ru(bpy)_3^{2+}$ in the presence of 0.10 M TPrA with 0.1 M Tris/0.10 M $LiClO_4$ buffer (pH = 8) at a 3 mm diameter glassy carbon electrode at scan rate 50 mV/s. (c) As (a) but with 1.0 μM $Ru(bpy)_3^{2+}$. The ECL intensity scale is given for (c) and should be multiplied by 100 for (a). 24

Figure 2.3: Linear sweep voltammograms (LSV) and their corresponding ECL signals for 1 μM $Ru(bpy)_3^{2+}$ and 50 mM TPrA in pH 8.5 PBS at a 3 mm diameter glassy carbon electrode at different scan rates. Inset, plot of the first and the second ECL signals versus $v^{1/2}$. 25

Figure 2.4: (a) The first ECL peak intensity as a function of TPrA concentration with 1 μM $Ru(bpy)_3^{2+}$ (0.20 M PBS, pH 7.5). A 3 mm diameter glassy carbon electrode was used at a scan rate of 100 mV/s. 27

(b) The first ECL peak intensity as a function of $Ru(bpy)_3^{2+}$ concentration with 100 mM TPrA (0.20 M PBS, pH 8.5). A 3 mm diameter glassy carbon electrode was used at a scan rate of 100 mV/s. 28

(c) The first and the second ECL responses in 100 mM TPrA (0.20 M PBS, pH 8.5) with different $Ru(bpy)_3^{2+}$ concentrations: 1 mM (solid line), 0.50 mM (dashed line), 0.10 mM (dotted line) and 0.05 mM (dash-dotted line). A 3 mm diameter glassy carbon electrode was used at a scan rate of 100 mV/s. 29

Figure 2.5: An approach curve obtained for the oxidation of 10.0 mM TPrA (0.10 M Tris/0.10 M $LiClO_4$ buffer, pH = 8) at a 1.5 mm diameter hemispherical Au electrode held at 0.85 V vs. Ag/AgCl. An ITO/OSiRu^{II} electrode at open circuit served as the substrate 31

Figure 2.6: Cyclic voltammogram and ECL signal obtained in 10.0 mM TPrA (0.10 M Tris/0.10 M $LiClO_4$ buffer, pH = 8) at a 1.5 mm diameter hemispherical Au electrode when the tip/substrate separation distance, *d,* was 1.92 μm. A scan rate of 50 mV/s was used, and the substrate was an ITO/OSiRu^{II} electrode at open circuit 33

Figure 2.7: ECL peak intensity as a function of tip distance 34

Figure 2.8: (a) A simulated CV of TPrA oxidation in pH 8 solution at a scan rate of 900 V/s. Parameters used in the simulation were (see Scheme 2.4 for further information): $E°_{TPrA^{\bullet+}/TPrA}$ = 0.88 V vs. Ag/AgCl, k_s (for eqs. 4.2 & 4.4) = 0.01 cm/s, $E°_{P1/TPrA^{\bullet}}$ = – 1.7 V vs. Ag/AgCl, for eq. 4.3 $k_f = 3500\ s^{-1}$ & $k_b = 7\times10^6\ s^{-1}$, $c_{(TPrA+TPrAH^+)}$ = 10 mM. All species were assumed to have a diffusion coefficient of 5×10^{-6} cm^2/s except for H^+ (D_{H^+} = 5×10^{-5} cm^2/s) 40

(b) to (e) the concentration profiles for $TPrA^{\bullet+}$ (solid line) and $TPrA^{\bullet}$ (dotted line) at a specific points, A, B, C, and D, shown in (a). Parameters used in the simulation were (see Scheme 2.4 for further information): $E°_{TPrA^{\bullet+}/TPrA}$ = 0.88 V vs. Ag/AgCl, k_s (for eqs. 4.2 & 4.4) = 0.01 cm/s, $E°_{P1/TPrA^{\bullet}}$ = -1.7 V vs. Ag/AgCl, for eq. 4.3 $k_f = 3500\ s^{-1}$ & $k_b = 7\times10^6\ s^{-1}$, $c_{(TPrA+TPrAH^+)}$ = 10 mM. All species were assumed to have a

diffusion coefficient of 5 x 10^{-6} cm^2/s except for H^+ (D_{H^+} = 5 x 10^{-5} cm^2/s) 41
Figure 2.9: A simulated concentration profile for $TPrA^{+\bullet}$ formed at a 1.5 mm diameter hemispherical tip. This curve corresponds to potential A on the cyclic voltammogram (inset) for 10.0 mM TPrA (0.10 M Tris/0.10 M $LiClO_4$, pH 8) with a scan rate of 50 mV/s. Other parameters required for the simulation are as in Figure 2.8 43
Figure 2.10: Experimentally measured (dotted line) and simulated (solid line) ESR spectra of $TPrA^{+\bullet}$ generated by the oxidation of TPrA by $Ru(bpy)_3^{3+}$ in an aqueous pH 7 solution at 20 ˚C 45

Figure 3.1: Molecular structures of amine coreactants. Acronyms are defined in the text 55
Figure 3.2: Molecular structures of coreactant buffers (CB). Acronyms are defined in the text 56
Figure 3.3: Cyclic voltammograms (CV) of 1 mM $Ru(bpy)_3^{2+}$ in (a) pH 2.5, (b) pH 6.5, (c) pH 9.5, (d) pH 10.5, (e) pH 11.5, and (f) pH 12.5 of 0.2 M PBS at 0.1 V/s using a glassy carbon electrode (area = 0.07 cm^2). The dotted lines are background CVs 63
Figure 3.4: (a) Cyclic voltammograms of 10 mM TEtA in pH 12.5 PBS measured at various scan rates (ν). (b) Dependence of peak potentials for TEtA oxidation on log ν. A GCE (area = 0.07 cm^2) was used as a working electrode 67
Figure 3.5: Simultaneous CV and ECL of 1 μM $Ru(bpy)_3^{2+}$ with 10 mM *N,N,N′,N′*-tetraethyl-1,3-propanediamine (TEDAP) in pH 7.5 PBS. Scan rate. = 0.1 V/s. A GCE (area = 0.07 cm^2) was used 70

Figure 3.6: Simultaneous CV and ECL of 1 μM $Ru(bpy)_3^{2+}$ with 10 mM *N,N,N′,N′*-tetra-*n*-propylethylenediamine (TPDAE) in pH 7.5 PBS. Scan rate. = 0.1 V/s. A GCE (area = 0.07 cm^2) was used 71

Figure 3.7: Comparison of the first ECL wave intensities of 1 μM $Ru(bpy)_3^{2+}$ generated with various amine coreactants (10 mM) in pH 7.5 PBS. Scan rate = 0.1 V/s. A GCE (area = 0.07 cm^2) was used 73

Figure 3.8: Dependence of the second ECL produced in a solution of 1 μM $Ru(bpy)_3^{2+}$ and 10 mM acyclic monoamine group coreactant (TEtA or TPrA) on the pH of PBS. Each data point is the average value of three measurements and contains less than 10 % deviation. A GCE (area = 0.07 cm^2) was used. 75

Figure 3.9: Dependence of the second ECL produced in a solution of 1 μM $Ru(bpy)_3^{2+}$ and 10 mM acyclic *N*,*N*,*N*′,*N*′-tetraethyldiamine group coreactant (TEDAM, TEDAE, or TEDAP) on the pH of PBS. Each data point is the average value of three measurements and contains less than 10 % deviation. A GCE (area = 0.07 cm^2) was used 76

Figure 3.10: Dependence of the second ECL produced in a solution of 1 μM $Ru(bpy)_3^{2+}$ and 10 mM acyclic *N*,*N*,*N*′,*N*′-tetra-*n*-propyldiamine group coreactant (TPDAM, TPDAE, or TPDAP) on the pH of PBS. Each data point is the average value of three measurements and contains less than 10 % deviation. A GCE (area = 0.07 cm^2) was used 77

Figure 3.11: Dependence of the second ECL produced in a solution of 1 μM $Ru(bpy)_3^{2+}$ and 10 mM heteroalicyclic monoamine group coreactant (MP, EP, or PP) on the pH of PBS. Each data point is the average value of three measurements and contains less than 10 % deviation. A GCE (area = 0.07 cm^2) was used 78

Figure 3.12: Dependence of the second ECL produced in a solution of 1 μM $Ru(bpy)_3^{2+}$ and 10 mM heteroalicyclic diamine group coreactant (DMPz, DEPz, or DPPz) on the pH of PBS. Each data point is the average value of three measurements and contains less than 10 % deviation. A GCE (area = 0.07 cm^2) was used. 79

Figure 3.13: Dependence of the anodic current for the oxidation of 10 mM TPDAP on pH of PBS. Scan Rate = 0.1 V/s. A GCE (area = 0.07 cm^2) was used..... 81

Figure 3.14: Simultaneous CV and ECL 1 μM $Ru(bpy)_3^{2+}$ in pH 7.5 of DIPSO buffer (0.2 M) solution containing 0.1 M NaCl as a supporting electrolyte. Scan rate = 0.1 V/s. A GCE (area = 0.07 cm^2) was used..... 84

Figure 4.1: Electronic absorption spectra of 10 μM NR titrated with (a) 0 μM (b) 2 μM (c) 3 μM (d) 4 μM (e) 5 μM (f) 6 μM (g) 7 μM (h) 10 μM of anhydrous $HClO_4$ in MeCN. Inset is a plot of log $\{[ClO_4^-] - [NRH^+]\}$ vs. log $\{[NRH^+]/[NR]\}$ 99

Figure 4.2: Cyclic voltammograms of 1 mM neutral red (NR) in 0.1 M TBAP/MeCN. Scan rate = 0.1 V/s. A Pt electrode was used (area = 0.03 cm^2) 102

Figure 4.3: Dependence of peak potentials (E_p) and peak currents (i_{pc} and i_{pa}) for the NR reduction on the scan rate (ν). i_{pc} represents the reduction peak current of NR and i_{pa} denotes the corresponding oxidation current of reduced NR. 1mM NR in 0.1 M TBAP/MeCN and a Pt electrode (area = 7.9×10^{-3} cm^2) were used 103

Figure 4.4: Cyclic voltammograms of 1 mM neutral red (NR) with (a) 0.00 mM, (b) 0.26 mM, (c) 0.52 mM, (d) 0.78 mM, (e) 1.04 mM, (f) 1.30 mM, (g) 1.56 mM, and (h) 1.82 mM trifluoroacetic acid (TFA) in 0.1 M TBAP/MeCN. Scan Rate = 0.1 V/s. The same Pt electrode was used for each measurement (area = 0.03 cm^2) 105

Figure 4.5: Dependence of reduction peak currents (i_p) NR and NRH^+ on the concentration of TFA in 0.1 M TBAP/MeCN. 1 mM NR was titrated with 0.13 M TFA/0.1 M TBAP /MeCN stock solution. Scan rate = 0.1 V/s. A same Pt electrode was used for each measurement (area = 0.03 cm^2) 106

Figure 4.6: Cyclic voltammograms of 1 mM NR and NRH^+ produced by adding 2 mM TFA in 0.1 M TBAP/MeCN. A Pt-UME of 25μm (a = 12.5 μm) was used. Scan rate = 10 mV/s 109

Figure 4.7: Plots of the normalized current ratio, $i_d(t)/i_{ss}$, against the inverse square root of time for the reductions of (a) 1 mM NR and (b) 1 mM NRH^+ in 0.1 M TBAP/MeCN. The sampling rate is 100 μsec per point. 12.5 μm radius Pt-UME employed 110

Figure 4.8: Simultaneous (a) ECL and (b) CV of 1 mM NR and 5 mM BPO in 0.1 M TBAP/MeCN at 0.1 V/s. A Pt electrode was used (area = 0.03 cm^2) 115

Figure 4.9: ECL (solid line) spectrum of 1 mM NR and fluorescence spectra of 5 μM NR (dotted line) and 5 μM NRH^+ (dashed line). ECL was generated with 10 mM BPO by pulsing the electrode potential between 0 V and – 1.6 V vs. Ag QRE (0.1 sec pulse-width and 5 min integration). λ_{ex} for NR and NRH^+ were 440 nm and 530 nm, respectively..... 118

Figure 4.10: ECL spectra of 1 mM NR with 10 mM BPO in MeCN (dotted line) and CH_2Cl_2 (solid line). ECL was generated by pulsing the potential between 0 V and – 1.6 V vs. Ag QRE with 5 min integration time. The same Pt electrode was used for each measurement (area =0.03 cm^2)..... 120

Figure 4.11: Effect of NR concentrations on its ECL produced with a fixed 5 mM BPO. ECL was measured with a PMT and by sweeping an electrode potential at 0.1 V/s. The same Pt electrode was used for each measurement (area =0.03 cm^2)..... 122

Figure 4.12: Effect of TFA concentrations on the ECL of 1 mM NR produced with 5 mM BPO. ECL was measured with a PMT and by sweeping an electrode potential at 0.1 V/s. The same Pt electrode was used for each measurement (area =0.03 cm^2) 123

Figure 4.13: Effect of BPO concentrations on the ECL of 0.5 mM NR. ECL was measured with a PMT and by sweeping the electrode potential at 0.1 V/s. Inset represents the low concentration region (0 mM to 2.5 mM BPO). The same Pt electrode was used for each measurement (area =0.03 cm^2)..... 125

Figure 4.14: Stern-Volmer plot of the NR fluorescence quenching by BPO in the absence of molecular oxygen. C_{NR} = 1 μM. λ_{ex} = 440 nm..... 128

Figure 4.15: Simultaneous (a) cyclic voltammogram and (b) ECL wave of 1 mM $Ru(bpy)_3^{2+}$ and 5 mM BPO in 0.1 M TBAP/MeCN at 0.1 V/s. Inset of (b) represents the ECL spectra measured under the same condition..... 129
Supporting Information Figure 4.1..... 132
Supporting Information Figure 4.2..... 133
Supporting Information Figure 4.3..... 134

Figure 5.1: Molecular structures of TDAF-1, TDAF-2 and BPO 142
Figure 5.2: Absorption and fluorescence (λ_{ex} = 350 nm) spectra of (a) TDAF-1 and (b) TDAF-2 in MeCN:Bz (1:1,v:v) at room temperature under atmospheric conditions. Absorbance: 10 μM of TDAF; fluorescence: 1 μM of TDAF. (c) Phosphorescence (λ_{ex} = 355 nm) spectra of 10.1 μM TDAF-1 (I) and 9.8 μM TDAF-2 (II) obtained at 77 K in deoxygenated methylcyclohexane. The spectra were taken at a delay time of 5 ms 145
Figure 5.3: Cyclic voltammograms of (a) 0.5 mM TDAF-1 and (b) 0.5 mM TDAF-2 in MeCN:Bz (1:1,v:v)/0.1 M TBAP at 0.1 V/s. Inset: differential pulse voltammogram (DPV) with increment potential, 4 mV, amplitude, 0.05 V, pulse width, 0.05 s 151
Figure 5.4: ECL spectra of (a) 0.5 mM TDAF-1 and (b) 0.5 mM TDAF-2 in MeCN:Bz (1:1,v:v)/0.1 M TBAP. 0.1 s pulses by alternating between + 1.58 V and – 1.95 V vs. Ag QRE for (a) and + 1.54 V and – 1.97 V vs. Ag QRE for (b). All spectra were obtained with an integration time of 5 min 156

Figure 5.5: Schematic diagram of ECL and excimer formation mechanism 159
Figure 5.6: ECL (solid line) spectra of (a) 0.5 mM TDAF-1 and (b) 0.5 mM TDAF-2 with 5 mM BPO in MeCN:Bz (1:1,v:v)/ 0.1 M TBAP. 0.1 s pulses alternating 0 V and – 1.96 V vs. Ag QRE for (a) and + 0 V and – 1.98 V vs. Ag QRE for (b). All ECL spectra were obtained with an integration time of 5 min. Fluorescence spectra (dotted line) were obtained with (a)1 μM TDAF-1 and (b) 1μM TDAF-2 without BPO. λ_{ex} = 350 nm for both (a) and (b) 162
Figure 5.7: Model of a dimer of TDAF-1 from radical ions 167
Supporting Information Figure 5.1 170
Supporting Information Figure 5.2 172
Supporting Information Figure 5.3 173

Figure 6.1: Structures of (a) PIPES, (b) PIPPS, and (c) PIPBS 179

List of Schemes

Scheme 1.1 2

Scheme 1.2 6

Scheme 1.3 8

Scheme 1.4 9

Scheme 2.1 15

Scheme 2.2 15

Scheme 2.3 16

Scheme 2.4 35

Scheme 2.5 37

Scheme 2.6 37

Scheme 3.1 52

Scheme 3.2 53

Scheme 3.3 53

Scheme 3.4 65

Scheme 4.1 113

Scheme 4.2 116

Scheme 4.3 130

Scheme 5.1 139

Scheme 5.2 140

Scheme 5.3 141

Scheme 5.4 161

Scheme 5.5 164

Chapter 1: Fundamentals of Electrogenerated Chemiluminescence (ECL)

1.1 Introduction

Electrogenerated chemiluminescence (ECL) is a phenomenon where light emission arises from a high energy electron transfer reaction between electrogenerated species, which is usually accompanied with the regeneration of the emitting species. Although luminescence during electrolysis was already observed[1,2] in the 1920's, the first detailed ECL[3] study was reported by Hercules in 1964. Since 1964, ECL has been extensively investigated to elucidate the mechanism and the origin of ECL, and many reviews[4–9] are available in the literature.

ECL is a kind of chemiluminescence (CL), in that light emission is produced by an energetic electron transfer reaction. However, the difference between CL and ECL is how the light emission is controlled. In CL, luminescence is governed by merely mixing or flowing an emitter with necessary reagents in a reaction vessel. In contrast, in ECL, light emission is controlled by turning on/off the electrode potential. As an analytical technique, ECL has some advantages over CL: (1) ECL has more spatial freedom than CL, in that the emission spot can be controlled and manipulated by moving an electrode or varying the size/number

of electrodes because the ECL reaction occurs only in the diffusion layer of an electrode, (2) ECL can be more selective than CL, in that the generation of excited states can be selectively controlled by varying the electrode potentials, (3) ECL is usually a non-destructive technique because ECL emitters are regenerated after the ECL emission. In this chapter, the fundamental principles of ECL will be reviewed before the main topics are discussed.

1.2 Ion Annihilation

ECL can be generated by ion annihilation when the ECL emitters (R) are electrochemically oxidized and reduced to sufficiently stable radical cations ($R^{\bullet+}$) and anions ($R^{\bullet-}$), respectively. The produced radical ions are annihilated by the oppositely charged radical ions to generate the excited state species (R*), as shown in Scheme 1.1.

Scheme 1.1

$$R - e \longrightarrow R^{\bullet+} \quad (1.1)$$

$$R + e \longrightarrow R^{\bullet-} \quad (1.2)$$

$$R^{\bullet+} + R^{\bullet-} \longrightarrow R + R^{*} \quad (1.3)$$

$$R^{*} \longrightarrow R + h\nu \quad (1.4)$$

Depending on the energy available in the ion annihilation, eq. (1.3), the produced R* could be either the lowest excited singlet state species (^{1}R*) or the triplet state species (^{3}R*). The energy available in eq. (1.3) can be calculated from the electrode potentials for eq. (1.1) and eq. (1.2) as defined in eq. (1.5)[4].

$$-\Delta H_{ann} = E_p\,(R/R^{\bullet+}) - E_p\,(R/R^{\bullet-}) - 0.1\ eV \qquad (1.5)$$

where $-\Delta H_{ann}$ is the enthalpy for the ion annihilation of eq. (1.3), E_p is the peak potential for the electrochemical oxidation or reduction of R, and 0.1 eV is an estimate of the temperature-entropy approximation term ($T\Delta S$) at 25 °C. If the energy ($-\Delta H_{ann}$) estimated from eq. (1.5) is larger than the energy (E_s) required to produce the lowest excited singlet state (^{1}R*) from the ground state of R, it is possible to directly generate ^{1}R* from eq. (1.3), and this system is called *an energy-sufficient system* or *the S-route.* A typical example of an energy-sufficient system is the $DPA^{\bullet+}/DPA^{\bullet-}$ (DPA = 9,10-diphenylanthracene) system.[10,11]

S-route

$$R^{\bullet+} + R^{\bullet-} \longrightarrow R + {}^1R^* \qquad (1.3a)$$

In contrast, if $-\Delta H_{ann}$ is smaller than E_s but larger than the triplet state energy (E_t), the triplet state (^{3}R*) is initially formed, and then ^{1}R* can be formed by triplet-triplet annihilation (TTA) as shown in eq. (1.6). This is called *an energy-deficient system* or *the T-route*. Typical examples of energy deficient systems are the $TMPD^{\bullet+}/DPA^{\bullet-}$ and the $TMPD^{\bullet+}/AN^{\bullet-}$ systems (TMPD = *N*,*N*,*N*′,*N*′-tetramethyl-*p*-phenylenediamine and AN = anthracene).[10,12] The efficiency of the direct emission from ^{3}R* is usually low in a solution phase because of the long radiative lifetime of ^{3}R* and its quenching by radical ions or other species, such as molecular oxygen (O_2).

T-route

$$R^{\bullet+} + R^{\bullet-} \longrightarrow R + {}^3R^* \qquad (1.3b)$$

$$^3R^* + {}^3R^* \longrightarrow R + {}^1R^* \qquad (1.6)$$

If $-\Delta H_{ann}$ is nearly marginal to E_s, the T-route can contribute to the formation of ^{1}R* in addition to the S-route, and it is called *the ST-route*. Although the T-route is inefficient in the presence of considerable S-route,[11,13–15] it is still possible for the ST-route to exist. A typical example is the rubrene anion-cation annihilation in benzonitrile.[16–18]

1.3 Coreactants

A coreactant is a compound that can produce a reactive intermediate (a strong reducing or oxidizing agent) by a reaction following the electrochemical or chemical electron transfer reaction. Employing a coreactant is useful especially when either $R^{\bullet+}$ or $R^{\bullet-}$ is not stable enough for ECL reaction, or when the ECL solvent has a narrow potential window so that $R^{\bullet+}$ or $R^{\bullet-}$ cannot be formed. In an aqueous solvent, the use of a coreactant is very important because water has a narrow potential window, many organic compounds have a low solubility, and many radical ions of organic emitters are unstable in an aqueous solvent.

The first coreactant used for ECL was oxalate ion ($C_2O_4^{2-}$).[19,20] When $C_2O_4^{2-}$ is oxidized, it produces the sufficiently strong reducing agent, $CO_2^{\bullet-}$ ($E°$ = – 1.9 V vs. NHE[21]), and CO_2. For example, $Ru(bpy)_3^{2+}$ dissolved in an aqueous solution can produce ECL in the presence of $C_2O_4^{2-}$ via Scheme 1.2. In addition, various amines[22–25] and peroxydisulfate ($S_2O_8^{2-}$)[26–28] have been used as coreactants.

The following conditions are suggested for an efficient coreactant candidate: (1) the coreactant should be reasonably soluble in a solvent because the ECL intensity is generally proportional to its concentration, (2) the reactive intermediate species generated electrochemically and/or chemically should be stable enough to undergo the ECL reaction with an emitting species, (3) the rate of reaction between the intermediate and the radical ion of an ECL emitter must

be rapid, (4) the coreactant and its intermediate should have inert or weak quenching effect on ECL, and (5) the coreactant itself should not produce any light emission.

Scheme 1.2

$$Ru(bpy)_3^{2+} - e \longrightarrow Ru(bpy)_3^{3+} \quad (1.7)$$

$$Ru(bpy)_3^{3+} + C_2O_4^{2-} \longrightarrow Ru(bpy)_3^{2+} + C_2O_4^{\bullet-} \quad (1.8)$$

$$C_2O_4^{\bullet-} \longrightarrow CO_2^{\bullet-} + CO_2 \quad (1.9)$$

$$Ru(bpy)_3^{3+} + CO_2^{\bullet-} \longrightarrow Ru(bpy)_3^{2+*} + CO_2 \quad (1.10)$$

$$Ru(bpy)_3^{2+*} \longrightarrow Ru(bpy)_3^{2+} + h\nu \quad (1.11)$$

or

$$Ru(bpy)_3^{2+} + CO_2^{\bullet-} \longrightarrow Ru(bpy)_3^{+} + CO_2 \quad (1.12)$$

$$Ru(bpy)_3^{3+} + Ru(bpy)_3^{+} \longrightarrow Ru(bpy)_3^{2+*} + Ru(bpy)_3^{2+} \quad (1.13)$$

1.4 Formation of Excimers or Exciplexes

The term, excimer, introduced by Stevens and Hutton[29] represents an electronically excited dimeric species, which is immediately dissociated after its emission. The usual characteristics of excimer emission are the broad structureless emission band appearing at the longer wavelength side of the monomeric fluorescence and its increasing emission intensity with increasing concentration. In addition, the absorption spectra of the sample show the only monomeric characters. In fluorescence, the excimer [(RR)*] is usually formed by

the association of an excited state (R*) species with the corresponding ground state species (R) [eq. (1.14)]. Depending on the spin multiplicity of R*, the excimers may be singlet or triplet. In ECL, on the other hand, the excimers can be formed not only by the direct generation during the ion annihilation [eq. (1.15)], but also by the association of R* with R [eq. (1.14)]. However, depending on the molecular structure of R and the lifetime of R*, eq. (1.14) may be negligible in ECL.

$$R^* + R \longrightarrow (RR)^* \qquad (1.14)$$

$$R^{\bullet -} + R^{\bullet +} \longrightarrow (RR)^* \qquad (1.15)$$

Chandross, *et. al.* [30] first reported the excimer emissions in ECL with anthracene, 9,10-dimethylanthracene, phenanthrene, perylene, and 3,4-benzpyrene and they suggested that the excimer might be mainly formed by eq. (1.15), because the fluorescence spectra of anthracene, 9,10-dimethylanthracene, and phenanthrene did not show any excimer emission.

The excimer can also be formed via the triplet-triplet annihilation (TTA). Maloy and Bard[31] demonstrated that the TTA of triplet state pyrene (^{3}Py*) contributed to the formation of excimer when the radical anion of pyrene (Py) was annihilated by the radical cation of TMPD (T-route) at the rotating ring-disk electrode (RRDE) as shown in Scheme 1.3.

Scheme 1.3

$$Py^{\bullet-} + TMPD^{\bullet+} \longrightarrow {}^3Py^* + TMPD \quad (1.16)$$

$${}^3Py^* + {}^3Py^* \longrightarrow {}^1Py^* + Py \quad (1.17)$$

$${}^3Py^* + {}^3Py^* \longrightarrow (Py_2)^* \quad (1.18)$$

Similar to the formation of excimers, the exciplex (excited complex or hetero-excimer) can be formed by the annihilation of radical ions [eq. (1.19)], the association of $^1A^*$ with D (or *vice versa*) [eq. (1.20)], and the TTA of $^3A^*$ and $^3D^*$ [eq. (1.21)]. In ECL, exciplex emission arises mainly through eq. (1.19)[32], although the mode of exciplex formation depends primarily on the energy available in ion annihilation. The singlet quenching path, eq. (1.20), is inefficient in ECL unless the excited singlet state ($^1A^*$) is directly produced by the S-route in the proximity of the ground state (D).

$$A^{\bullet-} + D^{\bullet+} \longrightarrow {}^1(A^-D^+)^* \quad (1.19)$$

$${}^1A^* + D \text{ or } A + {}^1D^* \longrightarrow {}^1(A^-D^+)^* \quad (1.20)$$

$${}^3A^* + {}^3D^* \longrightarrow {}^1(A^-D^+)^* \quad (1.21)$$

where A represents an electron acceptor molecule and D denotes an electron donor molecule. The emission from formed exciplexes may be rationalized by the

following scheme 1.4.

Scheme 1.4

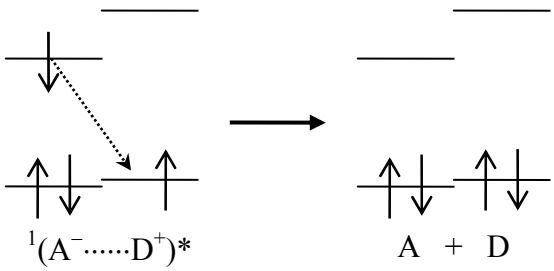

A typical example of an exciplex observed in ECL is the $PTP^{\bullet-}/TPTA^{\bullet+}$ (PTP = *p*-terphenyl and TPTA = tri-*p*-tolylamine) system in acetonitrile.[33]

1.5 Preannihilation ECL

It was reported that weak ECL was produced when only $R^{\bullet+}$ or $R^{\bullet-}$ was generated in a solvent without any coreactants,[34–37] and the ECL spectrum was identical to the fluorescence spectrum in all cases. Such luminescence is called the preannihilation ECL and it is usually thought that the light emission may be generated by a reacting species produced from solvents, electrolytes, or impurities. For example, when rubrene was electrochemically reduced at – 1.6 V in DMF and then the electrode potential was scanned back to – 0.2 V where rubrene was not oxidized yet, light emission was observed.[35]

1.6 Concluding Remark

Recently, ECL is of great interest for analytical applications as a result of its high sensitivity and selectivity. ECL produced by a coreactant has been employed in a variety of areas: fiber optic ECL sensor,[38–40] detection method for HPLC,[41–43] ECL biosensing,[44–46] immunoassay and DNA-probe assay analyses,[47–49] etc. Therefore, it is important to understand ECL reaction mechanisms and reactivities of coreactants. In this dissertation, the reaction mechanisms and reactivities of amine (Chapters 2 and 3) and benzoyl peroxide (Chapters 4 and 5) coreactants are described for the ECL of $Ru(bpy)_3^{2+}$, neutral red, and ter(9,9-diarylfluorene)s.

References

(1) Dufford, R. T.; Nightingale, D.; Gaddum, L. W. *J. Am. Chem. Soc.* **1927**, *49*, 1858.

(2) Harvey, N. *J. Phys. Chem.* **1929**, *33*, 1456.

(3) Hercules, D. M. *Science* **1964**, *145*, 808.

(4) Faulkner, L. R.; Bard, A. J. In *Electroanalytical Chemistry*; Bard, A. J., Ed., Marcel Dekker: New York, 1977; Vol. 10, p1.

(5) Faulkner, L. R. *Methods Enzymol.* **1978**, *57*, 494.

(6) Glass, R. S.; Faulkner, L. R. In *Chemical and Biological Generation of Excited States*; Adam, W.; Cilento, G., Eds., Academic Press, New York, 1982, Chapter 6.

(7) Knight, A. W.; Greenway, G. M. *Analyst* **1994**, *119*, 879.

(8) Lee, W. Y. *Mikrochim. Acta* **1997**, *127*, 19.

(9) Bard, A. J.; Debad, J. D.; Leland, J. K.; Sigal, G. B.; Wilbur, J. L.; Wohlstadter, J. N. In *Encyclopedia of Analytical Chemistry: Applications, Theory, and Instrumentation*, Meyer, R. A. Ed.; John Wiley & Sons: New York, 2000, p. 9842.

(10) Faulkner, L. R.; Tachikawa, H.; Bard, A. J. *J. Am. Chem. Soc.* **1972**, *94*, 691.

(11) Bezman, R.; Faulkner, L. R. *J. Am. Chem. Soc.* **1972**, *94*, 6317.

(12) Faulkner, L. R.; Bard, A. J. *J. Am. Chem. Soc.* **1969**, *91*, 209.

(13) Bezman, R.; Faulkner, L. R. *J. Am. Chem. Soc.* **1973**, *95*, 3083

(14) Bezman, R.; Faulkner, L. R. *J. Am. Chem. Soc.* **1972**, *94*, 6324.

(15) Bezman, R.; Faulkner, L. R. *J. Am. Chem. Soc.* **1972**, *94*, 6331.

(16) Tachikawa, H.; Bard, A. J. *Chem. Phys. Letters* **1974**, *26*, 246.

(17) Periasamy, N.; Santhanam, K. S. V. *Proc. Ind. Acad. Sci.* **1974**, *80A*, 821.

(18) Pighin, A.; Conway, B. E. *J. Electrochem. Soc.* **1975**, *122*, 619.

(19) Chang, M. –M.; Saji, T.; Bard, A. J. *J. Am. Chem. Soc.* **1977**, *99*, 5399.

(20) Rubinstein, I.; Bard, A. J. *J. Am. Chem. Soc.* **1981**, *103*, 512.

(21) Butler, J.; Hengline, A. *Radiat. Phys. Chem.* **1980**, *15*, 603.

(22) Noffsinger, J. B.; Danielson, N. D. *Anal. Chem.* **1987**, *59*, 865.

(23) Leland, J. K.; Powell, M. J. *J. Electrochem. Soc.* **1990**, *137*, 3127.

(24) Zu, Y.; Bard, A. J. *Anal. Chem.* **2000**, *72*, 3223.

(25) Kanoufi, F.; Zu, Y.; Bard, A. J. *J. Phys. Chem. B* **2001**, *105*, 210.

(26) White, H. S.; Bard, A. J. *J. Am. Chem. Soc.* **1982**, *104*, 6891.

(27) Becker, W. G.; Seung, H. S.; Bard, A. J. *J. Electroanal. Chem.* **1984**, *167*, 127.

(28) Fabrizio, E. F.; Prieto, I.; Bard, A. J. *J. Am. Chem. Soc.* **2000**, *122*, 4996.

(29) Stevens, B.; Hutton, E. *Nature*, **1960**, *186*, 1045.

(30) Chandross, E. A.; Longworth, J. W.; Visco, R.E. *J. Am. Chem. Soc.* **1965**, *87*, 3259.

(31) Maloy, J. T.; Bard, A. J. *J. Am. Chem. Soc.* **1971**, *93*, 5968.

(32) Bard, A. J.; Park, S. M. In *The Exciplex*; Gordon, M.; Ware, W. R., Eds.; Academic Press: New York, 1975, p. 305.

(33) Keszthelyi, C. P.; Bard, A. J. *Chem. Phys. Letters* **1974**, *24*, 300.

(34) Hercules, D. M.; Lansbury, R. C.; Roe, D. K. *J. Am. Chem. Soc.* **1966**, *88*, 4578.

(35) Maricle, D. L.; Maurer, A. *J. Am. Chem. Soc.* **1967**, *89*, 188.

(36) Zweig, A.; Hoffman, A. K.; Maricle, D. L.; Maurer, A. H. *Chem. Commun.* **1967**, 106.

(37) Zweig, A.; Maricle, D. L.; Brinen, J. S.; Maurer, A. H. *J. Am. Chem. Soc.* **1967**, *89*, 473.

(38) Egashira, N.; Kumasako, H.; Ohga, K. *Anal. Sci.* **1990**, *6*, 903.

(39) Kuhn, L. S.; Weber, A.; Weber, S. G. *Anal. Chem.* **1990**, *62*, 1613.

(40) Preston, J.; Nieman, T. A. *Anal. Chem.* **1996**, *68*, 966.

(41) Noffsinger, J. B.; Danielson, N. D. *J. Chromatogr.* **1987**, *387*, 520.

(42) Uchikura, K.; Kirisawa, M. *Anal.Sci.* **1991**, *7*, 971.

(43) Skotty, D. R.; Lee, W. Y.; Nieman, T. A. *Anal. Chem.* **1996**, *68*, 1530.

(44) Martin, A. F.; Nieman, T. A. *Anal. Chim. Acta* **1993**, *281*, 475.

(45) Yokoyama, K.; Sasaki, S.; Ikebukuro, K.; Takeuchi, T.; Karube, I.; Tokitsu, Y.; Masuda, Y. *Talanta* **1994**, *31*, 1035.

(46) Jameison, F.; Sanchez, R. I.; Dong, L.; Leland J. K.; Yost, D.; Martin, M. T. *Anal. Chem.* **1996**, *68*, 1298.

(47) Blackburn, G. F.; Shah, H. P.; Kenten, J. H.; Leland, J.; Kamin, R. A.; Link, J.; Peterman, J.; Powell, M. J.; Shah, A.; Talley, D. B.; Tyagi, S. K.; Wilkins, E.; Wu, T. G.; Massey, R. J. *Clin. Chem.* **1991**, *37*, 1534.

(48) Kenten, J. H.; Casadei, J.; Link, J.; Lupold, S.; Willey, J.; Powell, M. J.; Rees, A.; Massey, R. J. *Clin. Chem.* **1991**, *37*, 1626.

(49) DiCesare, J.; Grossman, B.; Katz, E.; Picozza, E.; Ragusa, R.; Woundenberg, T. *Biotechniques* **1993**, *15*, 152.

Chapter 2: Electrogenerated Chemiluminescence of Tris(2,2′-bipyridine)ruthenium(II), $Ru(bpy)_3^{2+}$/Tri-*n*-propylamine (TPrA) System – A New Route Involving $TPrA^{\bullet+}$ Cation Radicals

2.1 Introduction

Noffsinger and Danielson[1] first reported the chemiluminescence of tris(2,2′-bipyridine)ruthenium(III), $Ru(bpy)_3^{3+}$ (bpy = 2,2′-bipyridine), with aliphatic amines. Following this study, Leland and Powell[2] reported the electrogenerated chemiluminescence (ECL) of the $Ru(bpy)_3^{2+}$ with tri-*n*-propylamine (TPrA) as a coreactant. Since then, a wide range of ECL analytical applications involving $Ru(bpy)_3^{2+}$ or its derivatives as labels have been reported.[3] The $Ru(bpy)_3^{2+}$ (or its derivatives) with TPrA exhibit the highest ECL efficiency and this system forms the basis of commercial systems for immunoassay and DNA analysis.[2–4] The ECL intensity for this system is proportional to the concentration of both $Ru(bpy)_3^{2+}$ and TPrA species,[2,4-6] and also depends on the solution pH and the electrode material.[1,2,5] The ECL mechanism of this reaction has been investigated by many workers, [1,2,4,5,7] and follows the now familiar coreactant mechanism[8] where the oxidation of TPrA generates a strongly reducing species. This oxidation can be via a catalytic route where electrogenerated

$Ru(bpy)_3^{3+}$ reacts with TPrA as well as by the direct reaction of TPrA at the electrode described by both Scheme 2.1 and Scheme 2.2:

Scheme 2.1

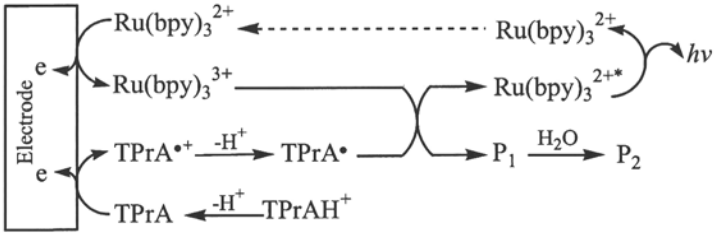

Scheme 2.2

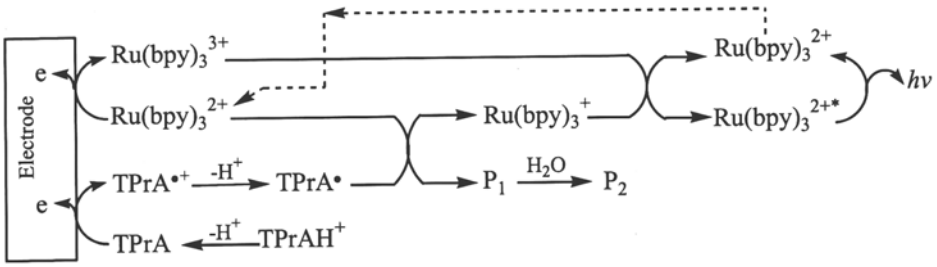

where $TPrA^{\bullet+}$ = $(CH_3CH_2CH_2)_3N^{\bullet+}$, $TPrAH^+$ = Pr_3NH^+, $TPrA^{\bullet}$ = $Pr_2NC^{\bullet}HCH_2CH_3$, $P_1 = Pr_2N^+C{=}HCH_2CH_3$, and $P_2 = Pr_2NH + CH_3CH_2CHO$. The "catalytic" route involving homogeneous oxidation of TPrA with $Ru(bpy)_3^{3+}$ is shown in Scheme 2.3. The contribution of this process to the overall ECL intensity, depends upon the $Ru(bpy)_3^{2+}$ concentration, and is small when relatively

low concentrations of $Ru(bpy)_3^{2+}$ are used.[5]

Scheme 2.3

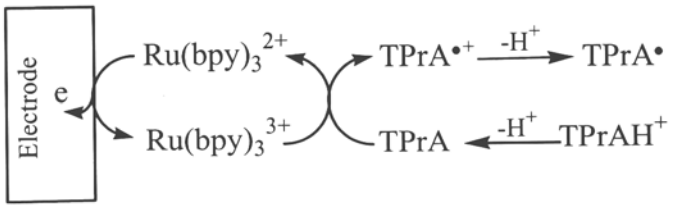

The mechanisms proposed above, however, do not account for a number of observations made for this ECL system. The strong dependence of ECL efficiency on electrode material[5] and surfactants[9] strongly supports the importance of the direct oxidation of TPrA. However, two ECL waves occur at a glassy carbon and a gold electrode, with the first ECL wave in a potential range less positive than that for the oxidation of $Ru(bpy)_3^{2+}$ (while the second wave occurs at potentials for $Ru(bpy)_3^{2+}$ oxidation). Both waves were associated with the emission of $Ru(bpy)_3^{2+}$* to $Ru(bpy)_3^{2+}$. The necessary oxidant to produce ECL at this first wave is not apparent. Moreover, in the commercial Origen analyzer (IGEN International, Inc., Gaithersburg, MD), the $Ru(bpy)_3^{2+}$-tagged species in immunoassay are immobilized on 2.8 μm diameter magnetic beads that are brought to an electrode by a magnetic field. Direct oxidation of $Ru(bpy)_3^{2+}$ on the beads would only occur for those within electron tunneling distance from the electrode, ~ 1 to 2 nm, so most of the labels on the bead would not contribute to

the ECL response. However, the high sensitivity of the technique indicates that most of the labels on the beads participate in the reaction, so that some other reactions involving the TPrA coreactant must generate precursors that can form $Ru(bpy)_3^{2+}$*. Clearly, the present ECL mechanisms proposed above (Schemes 2.1 – 2.3) cannot explain these results. Moreover, there has been no convincing explanation of the relative efficiencies of related coreactants, e.g., Et_3N vs. TPrA, based on the mechanism that only involves the free radical reductant as an intermediate (e.g., correlating the reducing power of the radical with observed ECL emission efficiency).

An understanding of the mechanism of the $Ru(bpy)_3^{2+}$/TPrA system is important in designing and selecting new coreactants and in improving the sensitivity and reproducibility of the ECL system. In this chapter, a new route involving $TPrA^{\bullet+}$ cation radical reduction for the generation of the excited state $Ru(bpy)_3^{2+}$* is presented. This mechanism is supported by a scanning electrochemical microscopy (SECM) – ECL experiment, cyclic voltammetry (CV) and CV digital simulations, and the direct detection by electron spin resonance (ESR) showing that the $TPrA^{\bullet+}$ cation radical is relatively stable under conditions similar to those used in the ECL experiments, i.e., in aqueous solutions at neutral pH.

2.2 Experimental Section

Chemicals. Tris(2,2'-bipyridyl)ruthenium(II) dichloride hexahydrate ($Ru(bpy)_3Cl_2 \cdot 6H_2O$), tri-*n*-propylamine (TPrA, 99+ %), and Fremy's salt [$(KSO_3)_2NO$] from Aldrich (Milwaukee, WI), (3-aminopropyl)-trimethoxysilane [$(CH_3O)_3Si(CH_2)_3NH_2$, ≥ 97 %] and lithium perchlorate ($LiClO_4$, > 99 %) from Fluka (Milwaukee, WI), potassium permanganate ($KMnO_4$), sodium phosphate dibasic heptahydrate ($Na_2HPO_4 \cdot 7H_2O$, 98.0 %), and phosphoric acid (H_3PO_4, 85 %) from Fisher (Fairlawn, NJ), potassium phosphate monobasic (KH_2PO_4, 99.6 %) from J. T. Baker (Phillipsburg, NJ), tris(hydroxymethyl)aminomethane (Tris, ultrapure) from Life Technologies (Rockville, MD), 1-ethyl-3-(3-dimethylaminopropyl) carbodiimide hydrochloride (EDAC, SigmaUltra) and 1-methylimidazole from Sigma (Louis, MO), hydrochloric acid (HCl, GR) from EM (Gibbstown, NJ), toluene (A.R.) from Mallinckrodt (Hazelwood, MO), and EtOH (200-proof) from Aaper Alcohol (Shelbyville, KY) were used without further purification. Bis(2,2′-bipyridine)-4,4′-dicarboxy-2,2′-bipyridineruthenium(II) hexafluorophosphates, $Ru(bpy)_2[bpy(COOH)_2](PF_6)_2$, was prepared by following a procedure in the literature.[10] Unless otherwise stated, all solutions were freshly prepared with deionized water (Milli Q, Millipore).

Immobilization of $Ru(bpy)_2[bpy(COOH)_2]^{2+}$ on an ITO Electrode. A clean and dried indium tin oxide (ITO) electrode (resistance, 30-60 ohm/square; Delta Technologies, Stillwater, MN) with dimensions of ~ 1×1 cm^2 was immersed

in a 5 % of $(CH_3O)_3Si(CH_2)_3NH_2$ toluene solution and kept in a desiccator for 24 hrs. During this process, $(CH_3O)_3Si(CH_2)_3NH_2$ becomes immobilized by formation of ITO/O-$Si(CH_2)_3NH_2$ bonds.[11] The electrode was then washed with EtOH and transferred into a 0.10 M 1-methylimidazole/HCl buffer solution (pH = 7) containing ~ 10 mM $Ru(bpy)_2[bpy(COOH)_2]^{2+}$ and 10 mM EDAC. After a 45 min incubation at 70 °C, the ITO electrode was washed thoroughly with EtOH and then water. By this treatment, a monolayer of $Ru(bpy)_2[bpy(COOH)_2]^{2+}$ was covalently attached to the aminosilane formed previously on the ITO, to produce ITO/O-$Si(CH_2)_3$NH-[CO(bpy)(COOH)](bpy)$_2$Ru(II) (designated as ITO/OSiRu^{II}). The ITO/OSiRu^{II} electrode was subsequently immersed in a 0.10 M Tris/HCl buffer (pH = 8) and maintained in the dark until further use.

Electrochemical and ECL measurements. Fast scan CV was performed with the model 660 electrochemical workstation (CH Instruments, Austin, TX). A conventional three-electrode cell was used, with a Pt wire as the counter electrode and an Ag/AgCl/KCl(sat.) as the reference electrode. The working electrodes used for the examination of TPrA redox behavior at fast scan rates were of different materials [Pt, Au, carbon fiber, and glassy carbon (GC)] and different dimensions (3 mm, 100 μm, 25 μm, 5 μm diameter Pt; 2 mm diameter Au; 3 mm diameter GC and 10 μm diameter carbon fiber). The ECL along with the CV signals were measured simultaneously with a home-built potentiostat combined with a photomultiplier tube (PMT, Hamamatsu R4220p, Japan) installed under the

electrochemical cell. A voltage of – 750 V was supplied to the PMT with a high-voltage power supply series 225 (Bertan High Voltage Corp., Hicksville, NY). A 3 mm diameter GC working electrode, and the counter and reference electrodes the same as those used for fast scan CV were used.

The SECM-ECL experiments were taken with a CHI 900 SECM system (CH Instruments, Austin, TX) combined with the ECL instrument described. Figure 2.1 shows a schematic diagram of the setup. The working electrode (tip), was a 1.5 mm diameter hemispherical Au, and the ITO/OSiRu^{II} ("modified ITO") served as the substrate. The direct oxidation of covalently attached $Ru(bpy)_2[bpy(COOH)_2]^{2+}$ species at the ITO electrode was avoided by holding the electrode at an open circuit. A Pt wire and an Ag/AgCl/KCl (sat.) electrode were also used as the counter and reference electrodes, respectively.

The simulation of the cyclic voltammogram of TPrA oxidation in aqueous solution was carried out by using the simulation package DigiSim® V 3.03 (Bioanalytical System Inc., West Lafayette, IN).

ESR Experiments. The cation radical of TPrA, $TPrA^{\bullet+}$, was generated by flowing 0.10 M TPrA (pH 7, adjusted by HNO_3) and ~ 0.030 M $Ru(bpy)_3^{3+}$ solutions through a quartz flat cell[12] via a two-jet mixing chamber (Wilmad, Prod. No. WG-801-Q, Buena, NJ). The $Ru(bpy)_3^{3+}$ solution was freshly prepared by bubbling Cl_2 gas generated via the reaction of solid $KMnO_4$ and concentrated HCl directly into a 0.030 M $Ru(bpy)_3Cl_2$ solution. A clear color change from reddish

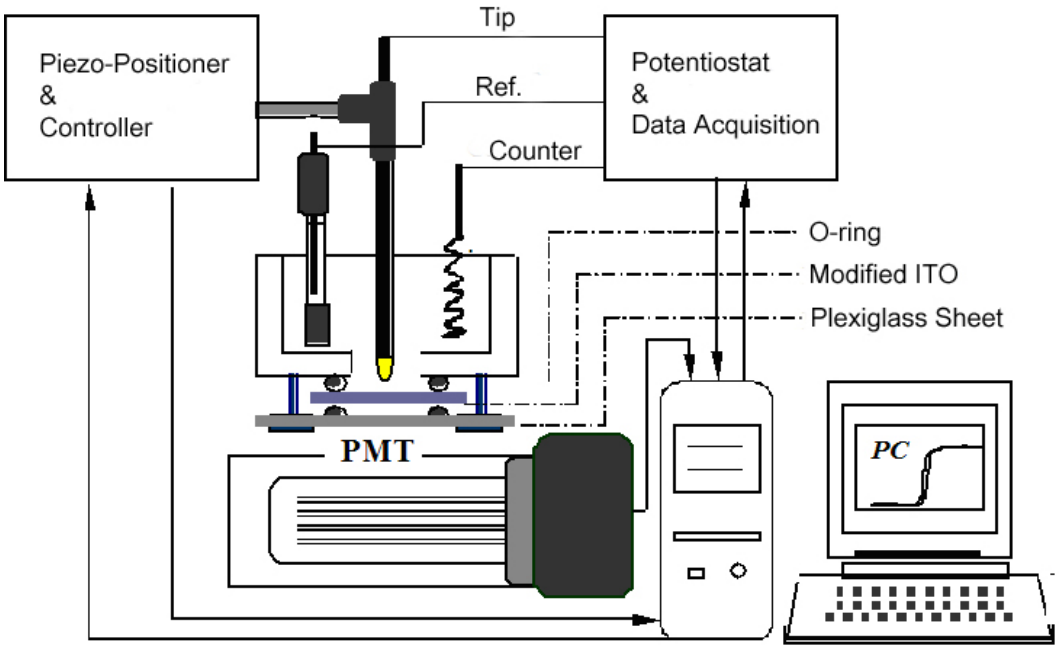

Figure 2.1. Setup for SECM – ECL.

orange to dark greenish blue was observed upon the complete oxidation of $Ru(bpy)_3^{2+}$ to $Ru(bpy)_3^{3+}$.

X-band ESR spectra were recorded on an ER-300 ESR spectrometer (IBM Instruments Inc.) with a modulation frequency of 100 kHz and microwave power at 12.6 mW. The swept field and the *g* value were calibrated externally using a 5.0 mM aqueous Fremy's salt solution.[13,14] The quartz flat cell was installed in a TE_{102} rectangular cavity. Overall, solution flow rates of 2 to 5 mL/s were employed and the relative flow rates for the TPrA and $Ru(bpy)_3^{3+}$ solutions were adjusted so that an orange color appeared at the outlet of the flow cell.

The spectra were simulated using PEST Winsim Software[15] (National Institute of Environmental Health Sciences, National Institute of Health, Research Triangle Park, NC).

All experiments were conducted at a temperature of 20 ± 2 ˚C, unless otherwise stated.

2.3 Results and Discussion

Electrochemical and ECL behavior of the $Ru(bpy)_3^{2+}$/TPrA system. An earlier report[5] showed that at low concentrations of $Ru(bpy)_3^{2+}$ (~ μM) and 10 to 100 mM TPrA in aqueous 0.15 M phosphate buffer, pH 7.5, the ECL emission vs. potential curves displayed two broad waves. Similar behavior was also observed when a much lower concentration of $Ru(bpy)_3^{2+}$, 1.0 nM,

[Figure 2.2 (a)] and a different buffer solution, 0.10 M Tris/0.10 M $LiClO_4$, pH = 8, were used [Figure 2.2]. The initial ECL signal started at potentials where the direct oxidation of TPrA at the GC electrode occurs [Figure. 2.2 (a) and (b)], and reached a first maximum at a potential of about 0.90 V vs. Ag/AgCl, about 50 mV less positive than the peak potential for TPrA oxidation, and well before $Ru(bpy)_3^{2+}$ oxidation. The second ECL signal has a peak potential value of 1.14 V vs. Ag/AgCl, in the potential region of the direct oxidation of $Ru(bpy)_3^{2+}$ at a GC electrode.[5] For comparison, Figure 2.2 also includes the ECL signal profile obtained with the $Ru(bpy)_3^{2+}$ concentration of 1.0 μM [Figure. 2.2 (c)]. The corresponding TPrA oxidation CV is not included, since it is essentially the same as that in Figure 2.2 (b). The relative ECL intensity from the first wave is significant, particularly in the 1.0 nM $Ru(bpy)_3^{2+}$ solution, and thus the bulk of the ECL signal obtained in this system with low concentrations of analytes, as in immunoassays and DNA probes with $Ru(bpy)_3^{2+}$ as an ECL label, probably originates from the first ECL wave. Note that even with a high concentration of $Ru(bpy)_3^{2+}$ (~ mM), the ECL signal first appeared in a potential range less positive than that for the oxidation of $Ru(bpy)_3^{2+}$. However, the initial ECL signal is relatively small compared to the large ECL signal generated via Schemes 2.1 and 2.2.

Figure 2.3 shows linear sweep voltammograms (LSV) and the corresponding ECL signals obtained from 1 μM $Ru(bpy)_3^{2+}$ and 50 mM TPrA in

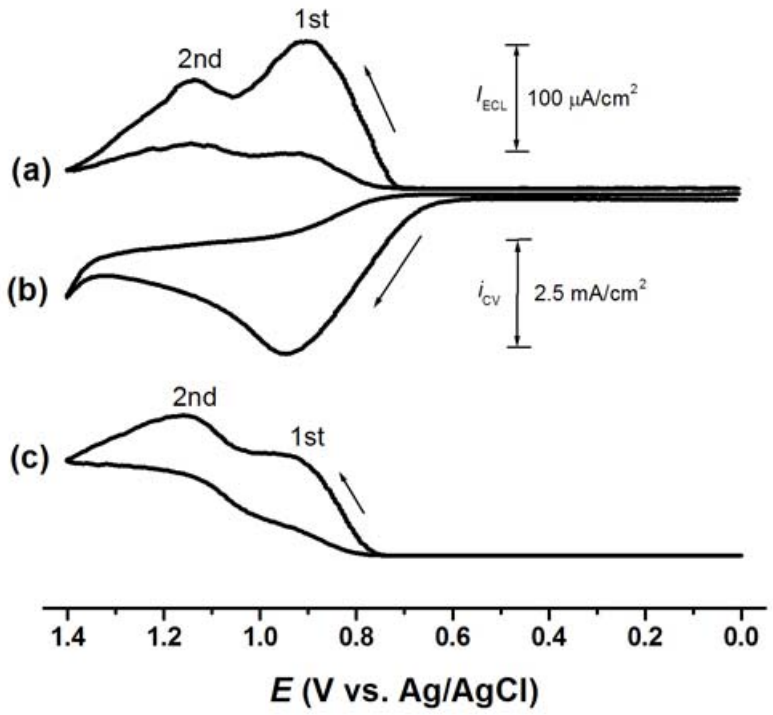

Figure 2.2. (a) ECL and (b) cyclic voltammogram of 1.0 nM $Ru(bpy)_3^{2+}$ in the presence of 0.10 M TPrA with 0.1 M Tris/0.10 M $LiClO_4$ buffer (pH = 8) at a 3 mm diameter glassy carbon electrode at scan rate 50 mV/s. (c) As (a) but with 1.0 μM $Ru(bpy)_3^{2+}$. The ECL intensity scale is given for (c) and should be multiplied by 100 for (a).

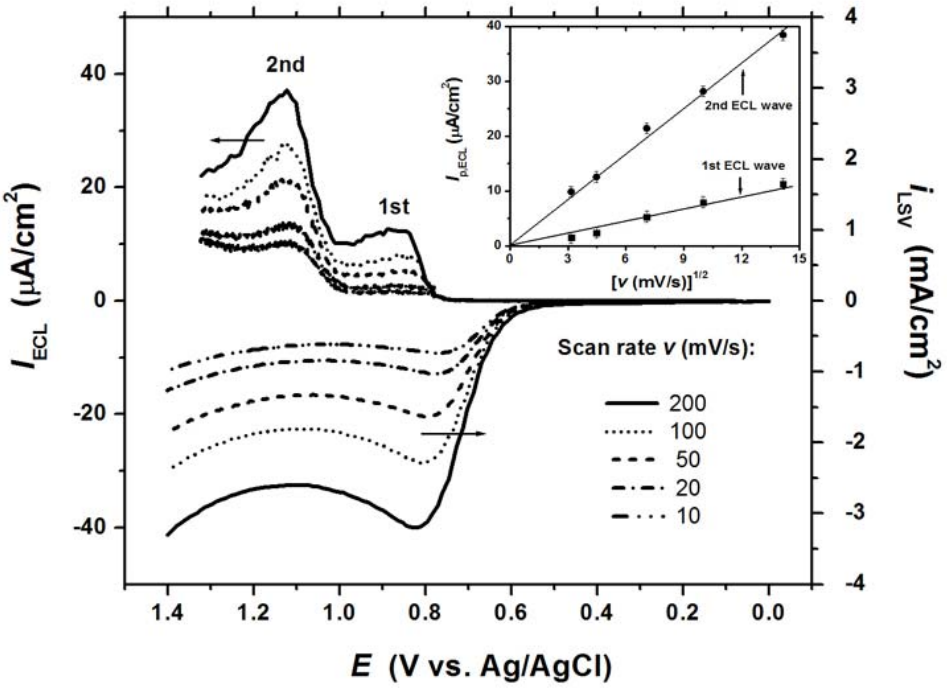

Figure 2.3. Linear sweep voltammograms (LSV) and their corresponding ECL signals for 1 μM $Ru(bpy)_3^{2+}$ and 50 mM TPrA in pH 8.5 PBS at a 3 mm diameter glassy carbon electrode at different scan rates. Inset, plot of the first and the second ECL signals versus $v^{1/2}$.

0.20 M phosphate buffer solution (PBS, pH 8.5) at a GC electrode at different potential scan rates (v). A linear relationship between the ECL peak intensity ($I_{p,ECL}$) for both the first and the second ECL waves and $v^{1/2}$ was observed [Figure 2.3, inset], consistent with the linear relationship between the peak current for the oxidation of TPrA and $v^{1/2}$. These results suggest that the first ECL signal is directly related to the oxidation of TPrA.

The effect of both TPrA and $Ru(bpy)_3^{2+}$ concentrations on the first ECL peak intensity ($I_{p1,ECL}$) was also investigated. As shown in Figure 2.4 (a), in 1 μM $Ru(bpy)_3^{2+}$ (0.20 M PBS, pH 7.5), the $I_{p1,ECL}$ is linearly proportional to the concentration of TPrA. No ECL signal was detected in the absence of either TPrA or $Ru(bpy)_3^{2+}$, so the first ECL signal must be associated with a reaction between the species generated from TPrA and $Ru(bpy)_3^{2+}$. Figure 2.4 (b) shows the $I_{p1,ECL}$ changes as a function of $Ru(bpy)_3^{2+}$ concentration when TPrA concentration kept at a constant value of 100 mM (0.20 M PBS, pH 8.5). In the range of 10 pM to 50 μM of $Ru(bpy)_3^{2+}$, $I_{p1,ECL}$ steadily rises with an increase of $Ru(bpy)_3^{2+}$ concentration. Beyond 50 μM, $I_{p1,ECL}$ reaches a plateau. In contrast, the ECL intensity of the second wave was always proportional to the concentration of $Ru(bpy)_3^{2+}$, for concentrations up to at least 1 mM. Figure 2.4 (c) shows both the first and the second ECL responses when the $Ru(bpy)_3^{2+}$ concentration was in the "plateau" range of 50 μM to 1.0 mM. These results clearly indicate that the mechanism for the first ECL signal is different from the second one.

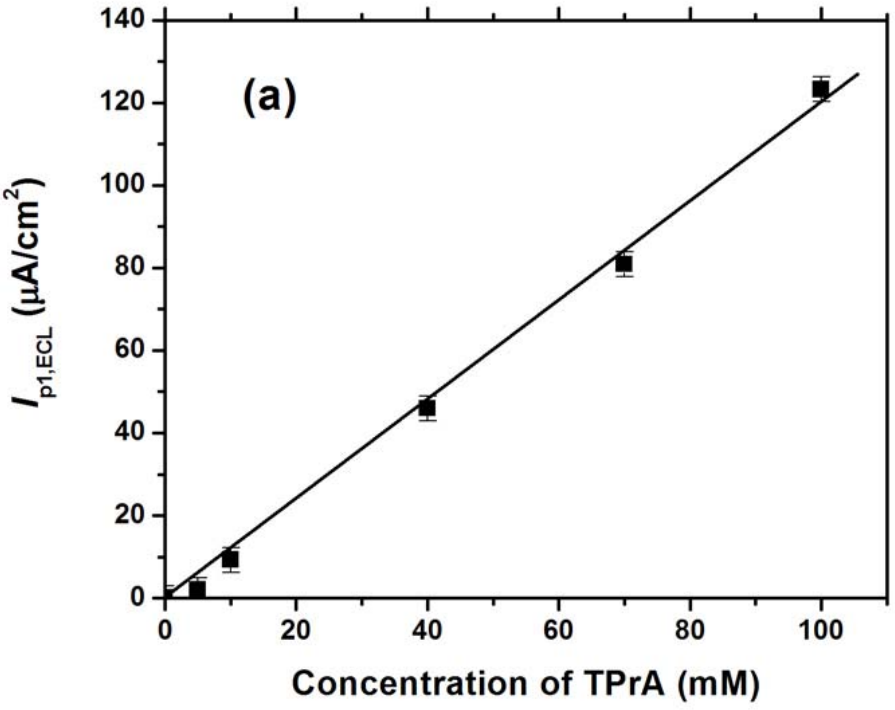

Figure 2.4. (a) The first ECL peak intensity as a function of TPrA concentration with 1 μM $Ru(bpy)_3^{2+}$ (0.20 M PBS, pH 7.5). A 3 mm diameter glassy carbon electrode was used at a scan rate of 100 mV/s.

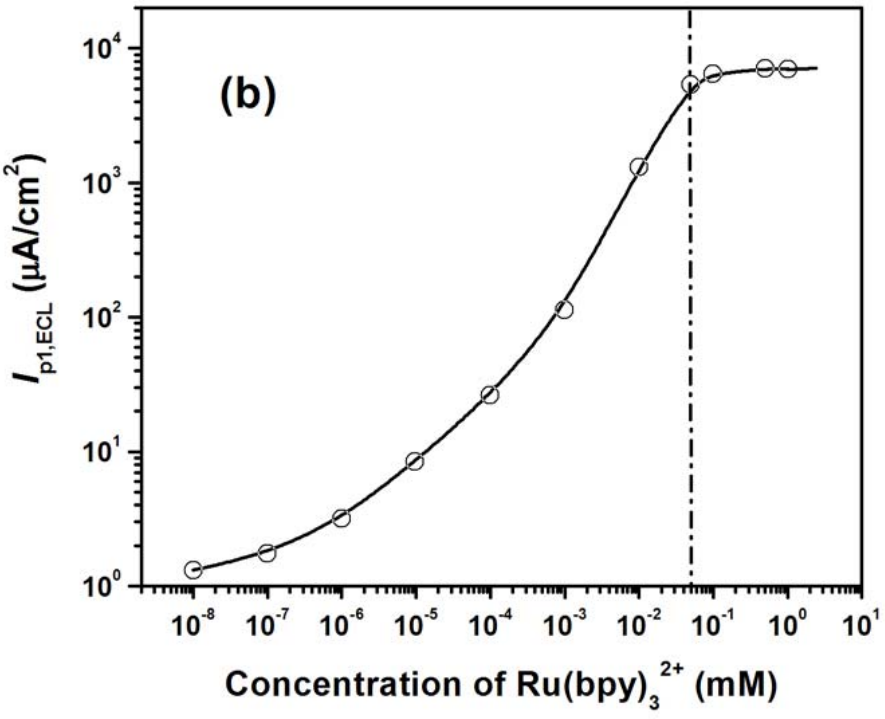

Figure 2.4. (b) The first ECL peak intensity as a function of $Ru(bpy)_3^{2+}$ concentration with 100 mM TPrA (0.20 M PBS, pH 8.5). A 3 mm diameter glassy carbon electrode was used at a scan rate of 100 mV/s.

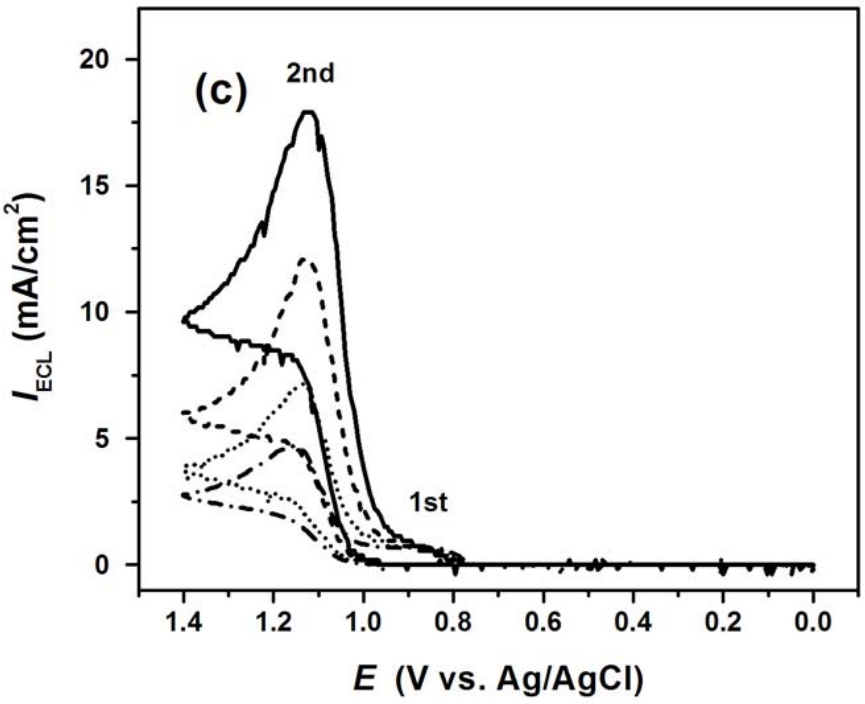

Figure 2.4. (c) The first and the second ECL responses in 100 mM TPrA (0.20 M PBS, pH 8.5) with different $Ru(bpy)_3^{2+}$ concentrations: 1 mM (solid line), 0.50 mM (dashed line), 0.10 mM (dotted line) and 0.05 mM (dash-dotted line). A 3 mm diameter glassy carbon electrode was used at a scan rate of 100 mV/s.

As demonstrated later, the intensity of the first ECL signal is determined by the quantity of TPrA derived radicals (cation and free) generated from the oxidation of TPrA at the electrode. In a relative excess of $Ru(bpy)_3^{2+}$ solution, the $I_{1st,ECL}$ is governed by the concentration of TPrA [Figure 2.4 (a)]. On the other hand, when the reaction produces excess TPrA radicals relative to the concentration of $Ru(bpy)_3^{2+}$, the $I_{1st,ECL}$ will be controlled by the concentration of $Ru(bpy)_3^{2+}$. When the $Ru(bpy)_3^{2+}$ concentration is equivalent to or greater than the concentration of radicals formed from TPrA oxidation, the $I_{1st,ECL}$ will be independent of the concentration of $Ru(bpy)_3^{2+}$. Figure 2.4 (c) exhibits these two features simultaneously.

SECM – ECL Experiments. To prove that oxidation of TPrA generates an ECL signal without direct oxidation of $Ru(bpy)_3^{2+}$, experiments with the instrumental setup shown in Figure 2.1 were carried out. In this experiment, $\{Ru(bpy)_2[bpy(COOH)_2]\}^{2+}$ was covalently immobilized on an ITO electrode. During the course of the SECM – ECL experiment, this modified ITO electrode was at an open circuit potential and served as the substrate. The reaction medium used was 10.0 mM TPrA solution in 0.10 M Tris/0.10 M $LiClO_4$ buffer (pH = 8). Note that the tip in this experiment was considerably larger than those usually employed in SECM[16] to generate a sufficient flux of TPrA radicals to obtain an observable emission signal. However, this electrode still showed a decreasing SECM current response on approach to a substrate that blocked diffusion of

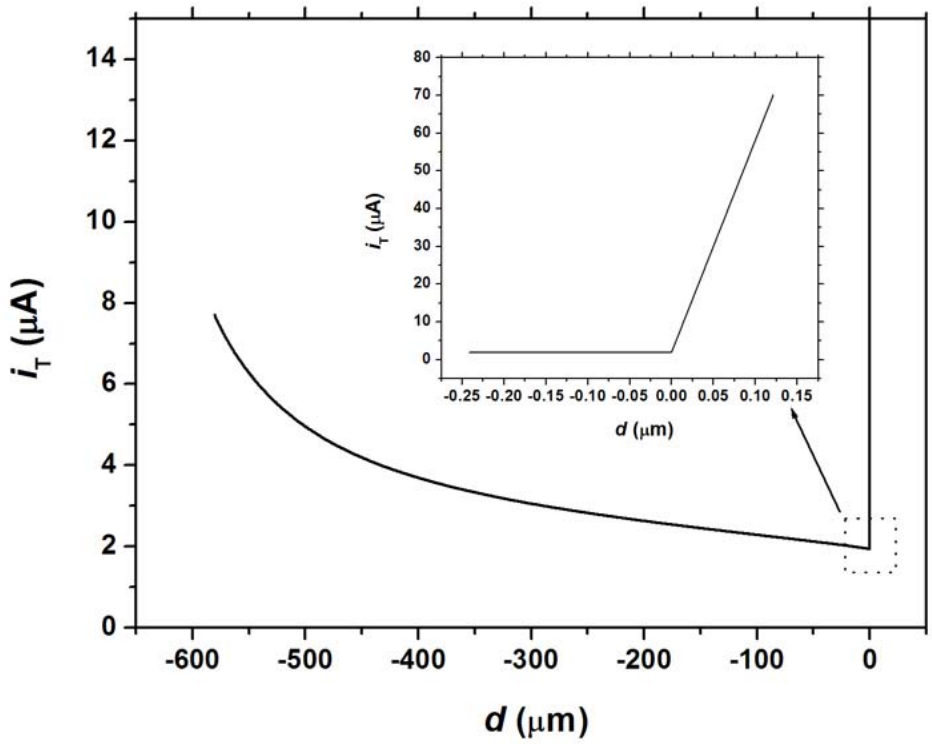

Figure 2.5. An approach curve obtained for the oxidation of 10.0 mM TPrA (0.10 M Tris/0.10 M $LiClO_4$ buffer, pH = 8) at a 1.5 mm diameter hemispherical Au electrode held at 0.85 V vs. Ag/AgCl. An ITO/OSiRu^{II} electrode at open circuit served as the substrate.

reactant to the tip [Figure 2.5]. The distance between the tip and the substrate (*d*) was estimated from this approach curve. By holding the tip potential at 0.85 V vs. Ag/AgCl, where TPrA oxidation occurs, a gradual decrease in tip current was initially observed as the tip slowly approached the substrate (~ 0.05 μm/s at the last stage). The zero distance was indicated by a sudden increase in the tip current when contact is made between the tip and ITO. The tip was withdrawn from the substrate a given distance and cycled between 0 and 1.0 V vs. Ag/AgCl at v = 50 mV/s, and the current and any ECL signal generated in the electrochemical cell were monitored. A typical experimental result for d = 1.92 μm is given in Figure 2.6. Upon oxidation of TPrA at ~ 0.80 V vs. Ag/AgCl, an ECL signal appears and tracks the tip current during potential cycling. A pair of pre-waves located at ~ 0.5 V vs. Ag/AgCl on the CV was frequently observed during the oxidation of TPrA, and may be attributed to the gold surface oxide formation and reduction.[5] The ECL signal could be detected only within a very small d (< ~ 5 to 6 μm); the maximum intensity as a function of the tip distance is shown in Figure 2.7. At short distance, the ECL intensity decreased almost exponentially with the tip distance, indicating that the amount of dissolved $Ru(bpy)_2[(bpy(COOH)_2)]^{2+}$ species from the substrate in the solution phase (if any) is negligible under the experimental conditions. This experiment clearly demonstrates that by simply oxidizing TPrA intermediates are formed that can

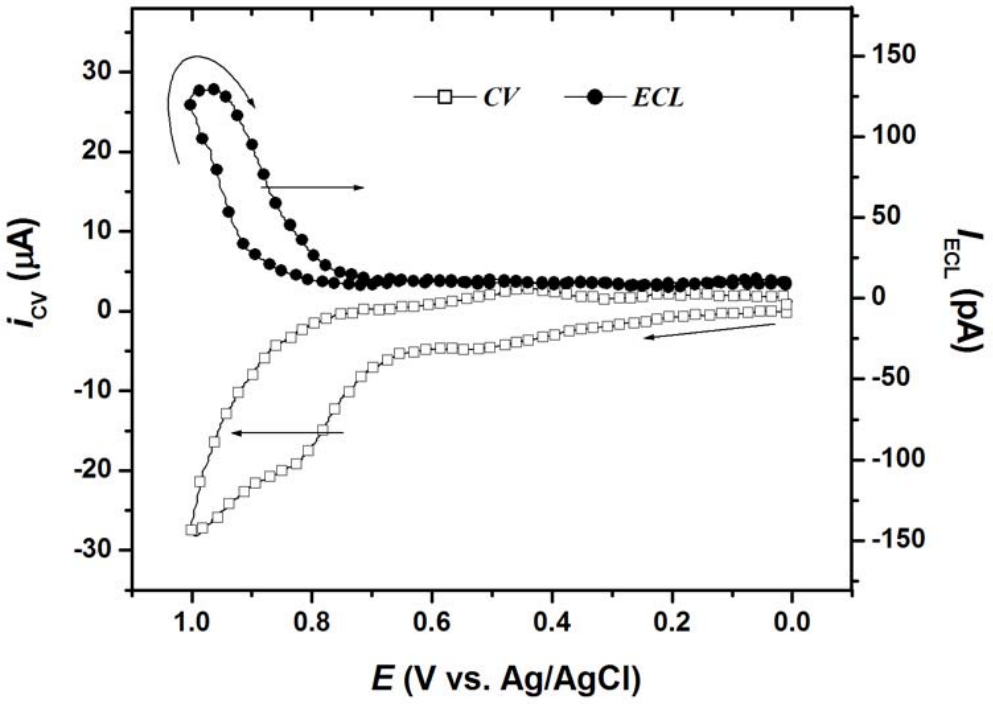

Figure 2.6. Cyclic voltammogram and ECL signal obtained in 10.0 mM TPrA (0.10 M Tris/0.10 M $LiClO_4$ buffer, pH = 8) at a 1.5 mm diameter hemispherical Au electrode when the tip/substrate separation distance, *d,* was 1.92 μm. A scan rate of 50 mV/s was used, and the substrate was an ITO/OSiRu^{II} electrode at open circuit.

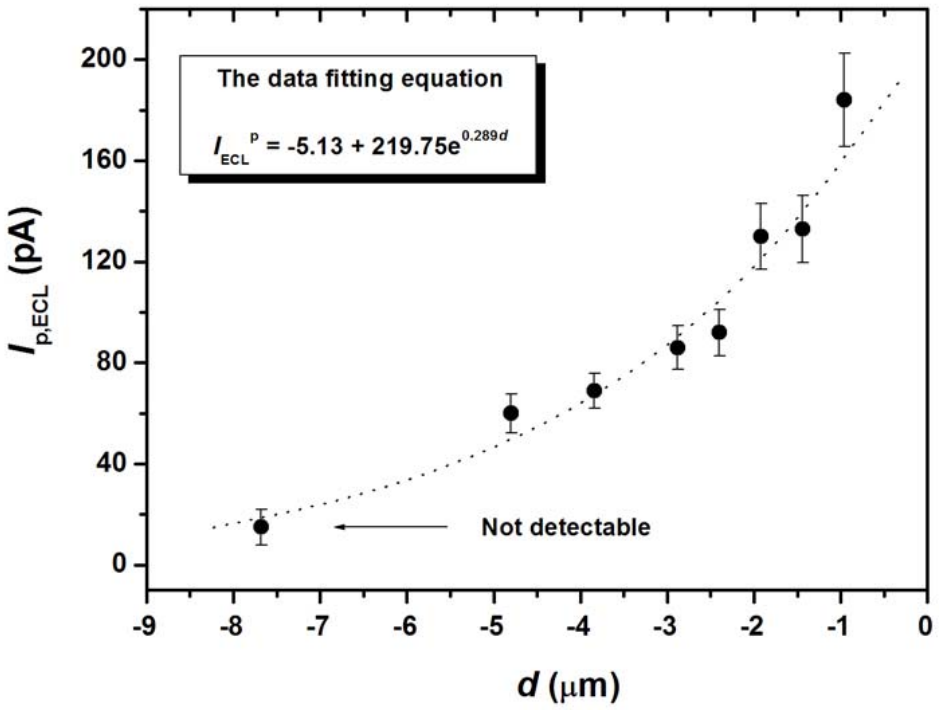

Figure 2.7. ECL peak intensity as a function of tip distance.

cause excitation of $Ru(bpy)_3^{2+}$ and is a direct confirmation of the ability to form excited states at all positions of a 2.8 μm bead on an electrode surface.

The electrochemical oxidation of TPrA under various conditions has been extensively studied and the following mechanism for reactions occurring in aqueous solution is generally accepted (Scheme 2.4):[4,17–21]

Scheme 2.4

$$TPrAH^+ \overset{pK_a = 10.4}{\rightleftharpoons} TPrA + H^+ \qquad (2.1)$$

$$TPrA \xrightarrow{k_s} TPrA^{\bullet +} + e \qquad (2.2)$$

$$TPrA^{\bullet +} \underset{k_b}{\overset{k_f}{\rightleftharpoons}} TPrA^{\bullet} + H^+ \qquad (2.3)$$

$$TPrA^{\bullet} \xrightarrow{k_s} P1 + e \qquad (2.4)$$

$$P1 + H_2O = P2 \qquad (2.5)$$

and $$TPrA^{\bullet +} + TPrA^{\bullet} = TPrA + P1 \qquad (2.6)$$

where $TPrA^{\bullet +}$, $TPrA^{\bullet}$, P1 and P2 species have the same significance as in Scheme 2.2.

Deprotonated TPrA molecules first undergo one-electron oxidation to form TPrA cation radicals ($TPrA^{\bullet +}$), which rapidly deprotonate to form TPrA free radicals ($TPrA^{\bullet}$). These oxidize further by losing one electron to produce the iminium ion (P1), which subsequently hydrolyzes to products, P2.

On the basis of previous study,[5] we believe that the ECL signal generated under the present conditions is the emission of immobilized $Ru(bpy)_2[(bpy(COOH)_2)]^{2+}$*, simplified as $Ru(bpy)_3^{2+}$* in the following discussions, since $Ru(bpy)_2[(bpy(COOH)_2)]^{2+}$ and $Ru(bpy)_3^{2+}$ species exhibit very similar electrochemical behavior.[22] According to Scheme 2.4, the direct oxidation of TPrA at the tip of SECM - ECL experiments leads to the formation of reducing radicals ($TPrA^{\bullet}$, $E° = \sim -1.7$ V vs. Ag/AgCl[23]) that can diffuse away from the tip and reach the substrate and react with immobilized $Ru(bpy)_3^{2+}$ to generate $Ru(bpy)_3^{+}$. To produce $Ru(bpy)_3^{2+}$*, some oxidant is required to remove an electron from $Ru(bpy)_3^{+}$. The most likely oxidant candidate in this system is the cation radical $TPrA^{\bullet+}$, $E° = \sim 0.83$ to 0.95 V vs. Ag/AgCl. However the deprotonation process of $TPrA^{\bullet+}$ to $TPrA^{\bullet}$ has usually been taken to be an extremely rapid process, resulting in an insufficient flux of $TPrA^{\bullet+}$ from the tip to produce measurable ECL. We considered the possible production of $Ru(bpy)_3^{3+}$ from reaction of $Ru(bpy)_3^{2+}$ with $TPrA^{\bullet+}$, but the redox potential of the $TPrA^{\bullet+}$/ TPrA couple is not sufficient for this reaction (see Scheme 2.5,[24] where the potentials have been converted to Ag/AgCl by taking $E°_{Ag/AgCl} = 0.20$ V vs. NHE[25]).

Scheme 2.5

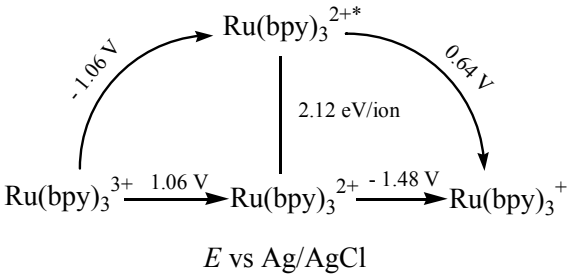

Scheme 2.6 summarizes a new route for the generation of ECL within the potential range before direct oxidation of $Ru(bpy)_3^{2+}$ at the electrode, involving formation of excited state on reaction of $TPrA^{\bullet+}$ with $Ru(bpy)_3^{+}$ (formed by reaction of $Ru(bpy)_3^{2+}$ with $TPrA^{\bullet}$).

Scheme 2.6

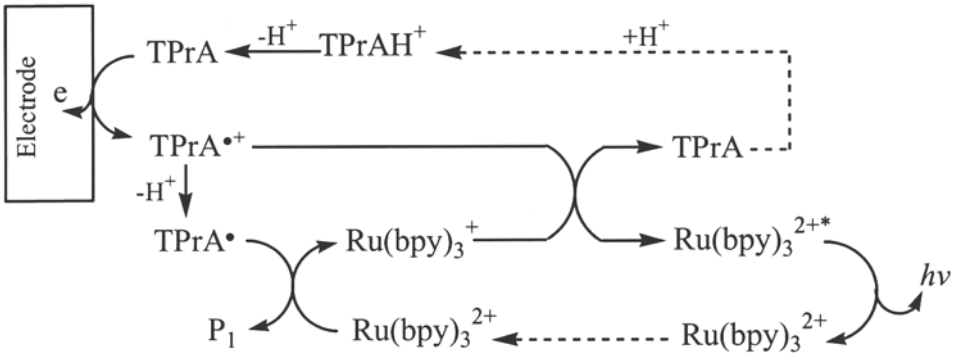

If the maximum distance at which light is observed, ~ 6 μm, represents the distance that $TPrA^{\bullet+}$ can diffuse before deprotonation, given a typical diffusion

coefficient of 4×10^{-6} cm^2/s, the lifetime, τ, of the cation radical would be ~ 0.1 ms.

Fast scan CV and digital simulations. With τ ~ 0.1 ms, one would estimate that $TPrA^{\bullet+}$ could be detected by CV, if v > ~260 V/s (~ $RT/F\tau$).[25] Fast scan CV experiments were thus carried out to detect $TPrA^{\bullet+}$ species after TPrA oxidation at the electrode by scan reversal. A wide range of TPrA aqueous solutions (~ 0.010 to 0.10 M) with different supporting electrolytes and different pHs (from 0.2 M H_2SO_4 to pH ~ 10), different materials of the working electrode (GC, carbon fiber, Au, Pt) with different dimensions (from 5 μm to 3 mm diameters), and different scan rates between 20 mV/s to 1000 V/s were used. However no wave associated with the reduction of $TPrA^{\bullet+}$ on the reverse scan of the CVs was ever found. Scan rates faster than 1000 V/s and CV with background subtraction were also tried without success, since in these cases, significant charging currents and probably limitations from the rate of the heterogeneous electron transfer from TPrA interfered.

The failure to detect the cation radical can be ascribed to the fact that the oxidation of TPrA is an ECE process[25] and that at potentials where $TPrA^{\bullet+}$ is reduced, the radical $TPrA^{\bullet}$ is oxidized, so that a cathodic current is at least partially compensated by an anodic one. To investigate this effect, CV digital simulations following Scheme 2.4 were carried out assuming different values for

the heterogeneous electron transfer rate constants [k_s in eqs. 2.1 and 2.4], and the k_f and k_b values of eq. 2.3. Other parameters were either adopted from the literature or assigned to reasonable values. Figure 2.8 (a) shows a simulated CV of TPrA oxidation in pH 8 solution at a scan rate of 900 V/s, with the parameters shown in the figure caption. The cross over on the reverse scan, where the anodic current is larger on the reverse scan than it is on the forward scan current (at ~ 0.96 V vs. Ag/AgCl), can be attributed to the greater contribution of $TPrA^{\bullet}$ to the measured current. The concentration profiles (c vs. x) for both $TPrA^{\bullet+}$ and $TPrA^{\bullet}$ at specific potential values are shown in Figures 2.8 (b) to (e). Upon the oxidation of TPrA, a significant amount of $TPrA^{\bullet+}$ cation radical is formed at the electrode surface [Figure 2.8 (b)], which further dissociated to $TPA^{\bullet}$. Since the free radical is a very strong reducing agent and can be oxidized immediately at the electrode, its surface concentration equaling zero is expected. During the potential scan period of A to B [Figures. 2.8 (b) and (c)], due to the continuous conversion of $TPrA^{\bullet+}$ to $TPrA^{\bullet}$, as well as diffusion to the bulk solution, the surface concentration of $TPrA^{\bullet+}$ starts to decrease, while the overall amount of $TPrA^{\bullet}$ in the electrode surface region increases. After potential B, substantial reduction of $TPrA^{\bullet+}$ to TPrA is expected, which results in a cathodic current and the surface concentration of $TPrA^{\bullet+}$ species decreases dramatically [Figure 2.8 (d)]. Note that even in this potential region, the overall current at the electrode is always anodic,

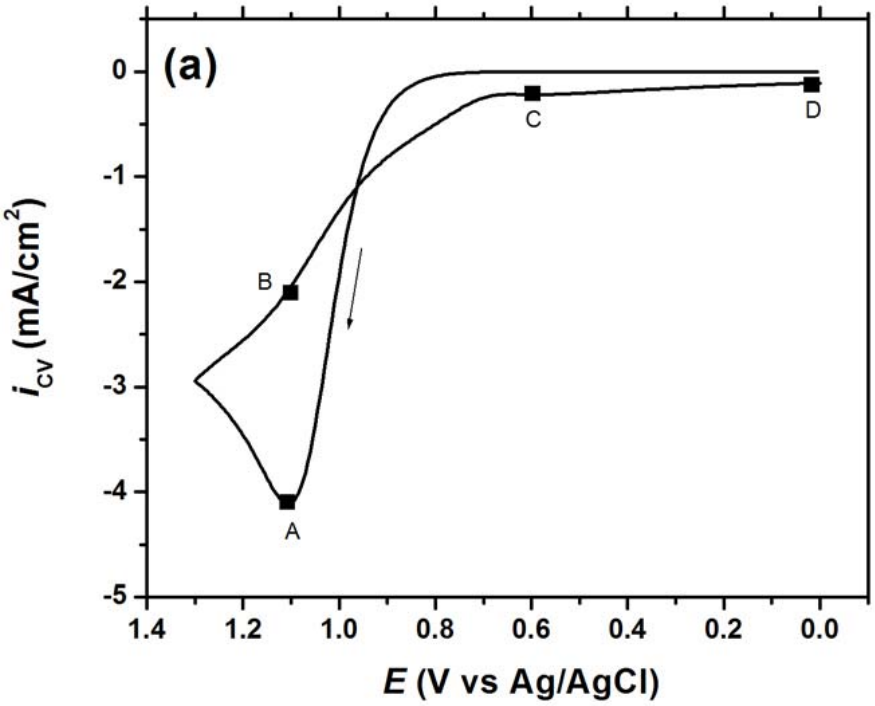

Figure 2.8. (a) A simulated CV of TPrA oxidation in pH 8 solution at a scan rate of 900 V/s. Parameters used in the simulation were (see Scheme 2.4 for further information): $E°_{TPrA^{\bullet+}/TPrA}$ = 0.88 V vs. Ag/AgCl, k_s (for eqs. 4.2 & 4.4) = 0.01 cm/s, $E°_{P1/TPrA^{\bullet}}$ = – 1.7 V vs. Ag/AgCl, for eq. 4.3 k_f = 3500 s^{-1} & $k_b = 7\times10^6$ s^{-1}, $c_{(TPrA+TPrAH^+)}$ = 10 mM. All species were assumed to have a diffusion coefficient of 5×10^{-6} cm^2/s except for H^+ ($D_{H^+} = 5 \times 10^{-5}$ cm^2/s).

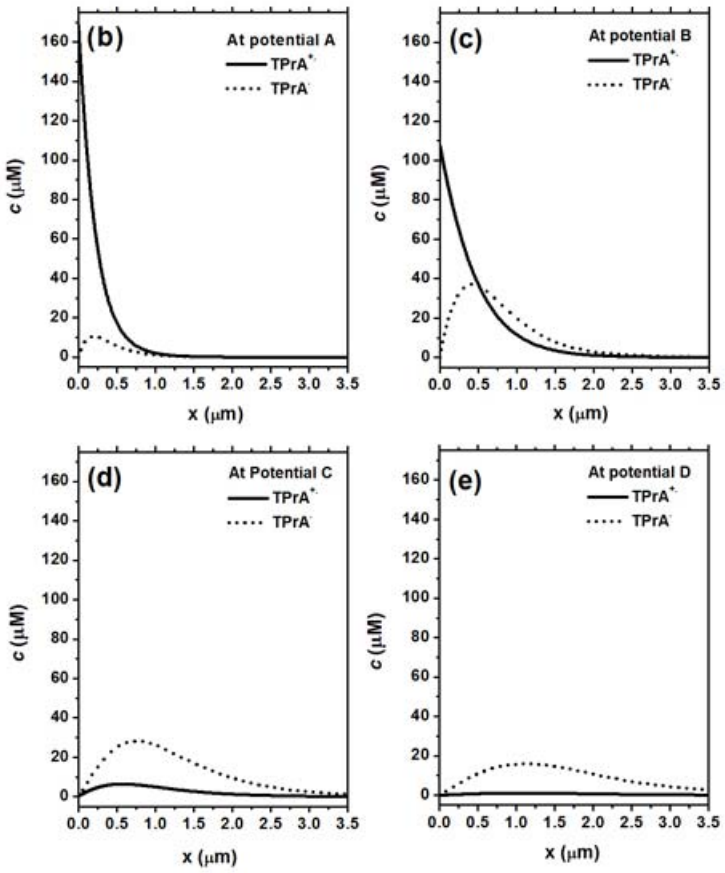

Figure 2.8. (b) to (e) the concentration profiles for $TPrA^{\bullet+}$ (solid line) and $TPrA^{\bullet}$ (dotted line) at a specific points, A, B, C, and D, shown in (a). Parameters used in the simulation were (see Scheme 2.4 for further information): $E°_{TPrA^{\bullet+}/TPrA} = 0.88$ V vs. Ag/AgCl, k_s (for eqs. 4.2 & 4.4) = 0.01 cm/s, $E°_{P1/TPrA^{\bullet}} = -1.7$ V vs. Ag/AgCl, for eq. 4.3 $k_f = 3500\ s^{-1}$ & $k_b = 7\times10^6\ s^{-1}$, $c_{(TPrA+TPrAH^+)} = 10$ mM. All species were assumed to have a diffusion coefficient of 5×10^{-6} cm^2/s except for H^+ ($D_{H^+} = 5 \times 10^{-5}$ cm^2/s).

because the current contribution from the oxidation of $TPrA^{\bullet}$ is larger. Therefore, the absence of a reduction wave following the oxidation of TPrA with fast scan CV does not indicate that $TPrA^{\bullet+}$ is so unstable that it cannot participate in the ECL reaction.

These digital simulations were carried out using the lifetime of $TPrA^{\bullet+}$ obtained from the previous SECM – ECL experiment in 10 mM TPrA (pH 8). Figure 2.9 shows the simulated concentration distribution for $TPrA^{\bullet+}$ formed at the tip as a function of distance from the tip. This curve was recorded at the potential A on the CV [inset of Figure 2.9], at which a maximum surface concentration and a maximum diffusion distance of $TPrA^{\bullet+}$ was observed. By comparing the data shown in Figure 2.9 with those in Figure 2.7, about 3.6 % of the initial $TPrA^{\bullet+}$ (or 71 nM, at x = 6 μm, Figure 2.9) are needed to diffuse to the substrate and react with immobilized $Ru(bpy)_3^{2+}$ to generate an ECL signal.

With the assumption that the $TPrA^{\bullet+}$ deprotonation reaction (eq. 2.3) is a first-order process, the half-life ($\tau_{1/2}$) of $TPrA^{\bullet+}$ is $\tau_{1/2} = 0.693/k_f$, where k_f is the forward rate constant of eq. 2.3, ~ 3500 s^{-1} based on the digital simulation.

ESR of $TPrA^{\bullet+}$ in aqueous solution. With the above estimated life time, it should be possible to detect $TPrA^{\bullet+}$ by ESR. Tertiary amine radical cations are generally believed to be short-lived intermediates in amine oxidation because of rapid deprotonation at the α-carbon to produce α-aminoalkyl free radicals.[17]

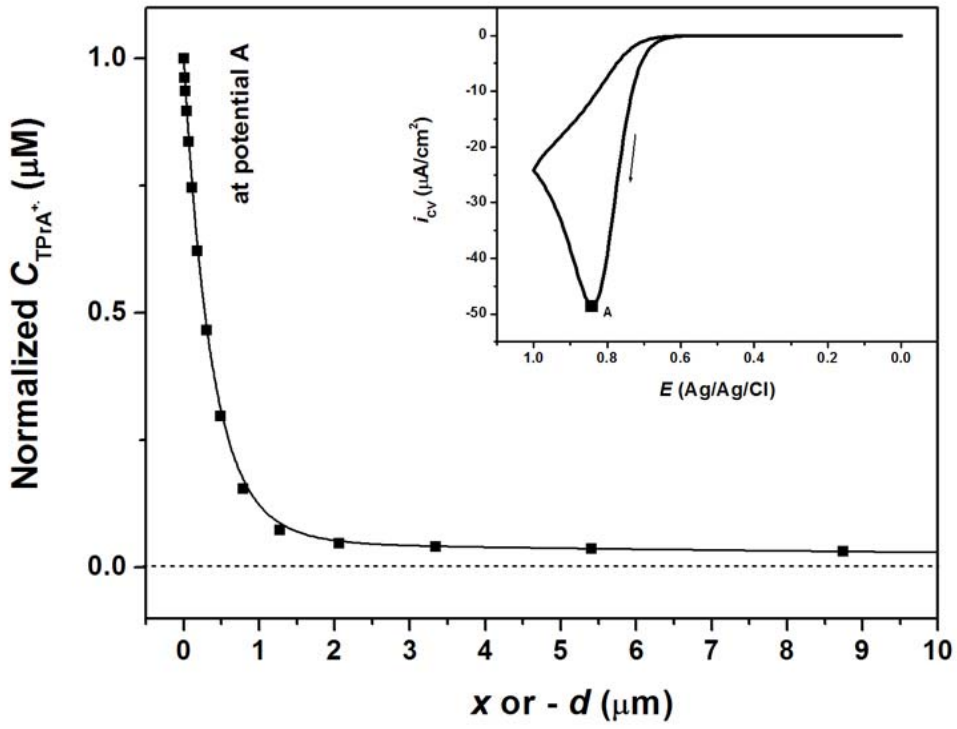

Figure 2.9. A simulated concentration profile for $TPrA^{+\bullet}$ formed at a 1.5 mm diameter hemispherical tip. This curve corresponds to potential A on the cyclic voltammogram (inset) for 10.0 mM TPrA (0.10 M Tris/0.10 M $LiClO_4$, pH 8) with a scan rate of 50 mV/s. Other parameters required for the simulation are as in Figure 2.8.

Under some experimental conditions, such as strongly acidic solution and formation by ionizing radiation, the ESR of several small aliphatic amines cation radicals has been reported.[17,26,27]

To detect the $TPrA^{\bullet+}$ cation radicals, an ESR quartz flat flow cell was used. Such cells have proven effective in producing a steady-state concentration of many reactive intermediates within the microwave cavity of the ESR instrument. Freshly prepared ~ 0.03 M $Ru(bpy)_3^{3+}$ and 0.10 M TPrA (pH 7) aqueous solutions were flowed into the mixing chamber at a rate of 2 to 5 mL/s and the ESR spectrum of the product in the quartz cell obtained. The major advantages of using $Ru(bpy)_3^{3+}$ as the oxidant are that the reaction between $Ru(bpy)_3^{3+}$ and TPrA is rapid at neutral pH[4] and it is a one-electron transfer process. Many other oxidants, such as Ce^{4+}, $KMnO_4$, $KBrO_3$ and Cl_2, were found to be unsuitable for TPrA oxidation, because either they required the use of strongly acidic solutions, where TPrA oxidation was slow, the oxidant itself or its reduction products gave strong ESR background, or the redox reaction was not fast enough. Figure 2.10 shows the experimentally measured (dotted line) as well as the simulated (solid line) ESR spectra of $TPrA^{\bullet+}$ generated in the flow cell at 20 °C. The spectrum consists of a relatively intense and sharp septet with a splitting of ~ 20 G due to the six equivalent α-hydrogens. On the basis of the simulation, hyperfine coupling constants of 19.87 G and 20.05 G for ^{14}N (1N, I = 1) and α-^{1}H (6H, I = 1/2) were evaluated. The experimental ESR spectrum had a

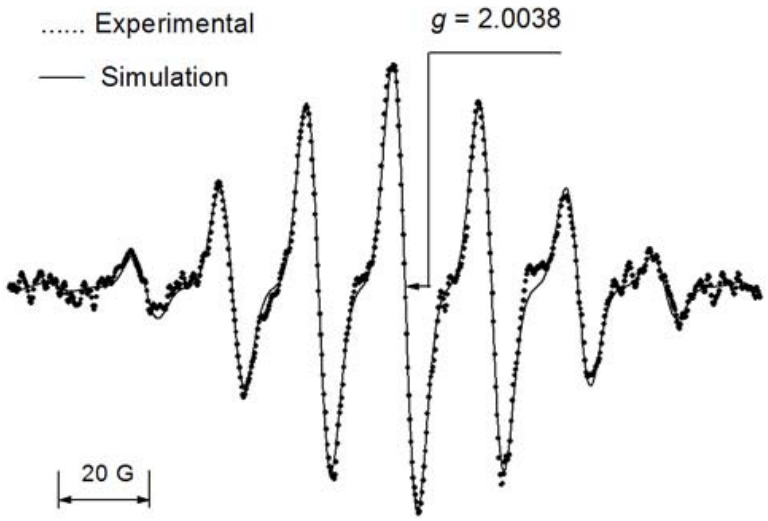

Figure 2.10. Experimentally measured (dotted line) and simulated (solid line) ESR spectra of $TPrA^{+\bullet}$ generated by the oxidation of TPrA by $Ru(bpy)_3^{3+}$ in an aqueous pH 7 solution at 20 ˚C.

g-value of 2.0038. Recently, Liu *et. al.*[27] have reported the structure and dynamics of $TPrA^{\bullet+}$ cation radicals generated in solid $AlPO_4$-5 by ionizing radiation. Our solution-phase ESR spectrum is consistent with their solid-state ESR spectrum at 300 K.

During the ESR experiments, $Ru(bpy)_3^{3+}$ and $Ru(bpy)_3^{+}$ species can also produce signals. However, they have no effect on the ESR spectrum of $TPrA^{\bullet+}$, since the *g*-values of these two species are very different than that of $TPrA^{\bullet+}$.[28-31] No ESR signal associated with $TPrA^{\bullet}$ was observed, probably because they were oxidized by excess oxidant in the solution. Note that the expected ESR spectrum of the carbon-centered $TPrA^{\bullet}$ would be very different than the one observed.

2.4 Conclusions

The ECL emission as a function of potential for the $Ru(bpy)_3^{2+}$/TPrA system consists of two waves. The first occurs with the direct oxidation of TPrA at the electrode, and the second where $Ru(bpy)_3^{2+}$ is oxidized. In dilute $Ru(bpy)_3^{2+}$ solutions (< ~ μM) containing mM TPrA, the intensity of the first ECL wave is significant and can be larger than that for the second ECL wave. A new route for the generation of $Ru(bpy)_3^{2+}$* at potentials of the first wave is proposed, where $TPrA^{\bullet+}$ formed during TPrA oxidation is a sufficiently stable intermediate that can oxidize $Ru(bpy)_3^{+}$ (formed from the reduction of $Ru(bpy)_3^{2+}$ by $TPrA^{\bullet}$ free radical) to give $Ru(bpy)_3^{2+}$*. Based on SECM – ECL experiments and digital

simulation, a half-life of ~ 0.2 ms was estimated for $TPrA^{\bullet+}$ in aqueous solution. An ESR spectrum of $TPrA^{\bullet+}$ in aqueous solution was obtained via flow mixing experiments. Fast scan CV experiments and simulations revealed that the absence of reduction wave for $TPrA^{\bullet+}$ on the reverse scan can be attributed to the cancellation of the component of current from the reduction of $TPrA^{\bullet+}$ by the anodic current contribution from the oxidation of $TPrA^{\bullet}$. These results also explain why selection of highly efficient coreactants is difficult for determination of low concentrations of Ru-label. The coreactant must form both oxidant (e.g. $TPrA^{\bullet+}$) and reductant (e.g. $TPrA^{\bullet}$) with appropriate redox potentials and lifetimes. Thus, the deprotonation rate of $TPrA^{\bullet+}$ must be just right to build up the needed concentrations of both species.

References

(1) Noffsinger, J. B.; Danielson, N. D. *Anal. Chem.* **1987**, *59*, 865.

(2) Leland, J. K.; Powell, M. J. *J. Electrochem. Soc.* **1990**, *137*, 3127.

(3) Bard, A. J.; Debad, J. D; Leland, J. K.; Sigal, G. B.; Wilbur, J. L.; Wohlstadter, J. N., "Chemiluminescence, Electrogenerated," in *Encyclopedia of Analytical Chemistry: Applications, Theory and Instrumentation*, R. A. Meyers, Ed., John Wiley & Sons: New York, 2000, Vol. 11, p. 9842 and references therein.

(4) Kanoufi, F.; Zu, Y.; Bard, A. J. *J. Phys. Chem. B* **2001**, *105*, 210.

(5) Zu, Y.; Bard, A. J. *Anal. Chem.* **2000**, *72*, 3223.

(6) Gross, E. M.; Pastore, P.; Wightman, R. M. *J. Phys. Chem. B* **2001**, *105*, 8732.

(7) He, L.; Cox, K. A.; Danielson, N. D. *Anal. Lett.* **1990**, *23*, 195.

(8) Rubinstein, I.; Bard, A. J. *J. Am. Chem. Soc.* **1981**, *103*, 512.

(9) Zu, Y.; Bard, A. J. *Anal. Chem.* **2001**, *73*, 3960.

(10) Sprintschnik, G.; Sprintschnik, H. W.; Kirsch, P. P.; Whitten, D. G. *J. Am. Chem. Soc.* **1977**, *99*, 4947.

(11) Murray, R. W. In *Electroanalytical Chemistry*; Bard, A. J., Ed.; Marcel Dekker, Inc.: New York, 1984; Vol. 13, p 191.

(12) Charkoudian, J. C. *J. Magn. Reson.* **1984**, *57*, 287.

(13) Windle, J. J.; Wiersema, A. K. *J. Chem. Phys.* **1963**, *39*, 1139.

(14) Pake, G. E.; Townsend, J.; Weissman, S. I. *Phys. Rev.* **1952**, *85*, 682.

(15) Duling, D. R. *J. Magn. Reson., Ser. B* **1994**, *104*, 105.

(16) Bard, A. J.; Mirkin, M. V., Eds., *Scanning Electrochemical Microscopy*, Marcel Dekker, New York, 2001.

(17) Chow, Y. L.; Danen, W. C.; Nelsen, S. F.; Rosenblatt, D. H. *Chem. Rev.* **1978**, *78*, 243.

(18) Mann, C. K. *Anal. Chem.* **1964**, *36*, 2424.

\
(19) Masui, M.; Sayo, H.; Tsuda, Y. *J. Chem. Soc., B* **1968**, 973.

(20) Portis, L. C.; Bhat, V. V.; Mann, C. K. *J. Org. Chem.* **1970**, *35*, 2175.

(21) Ross, S. D. *Tetrahedron Lett.* **1973**, 1237.

(22) Elliott, C. M.; Hershenhart, E. J. *J. Am. Chem. Soc.* **1982**, *104*, 7519.

(23) Lai, R., Bard, A. J., *unpublished experiments.*

(24) Roundhill, D. M. In *Photochemistry and Photophysics of Metal Complexes*; Fackler, J. J. P., Ed.; Plenum Press: New York, 1994, p 165.

(25) Bard, A. J.; Faulkner, L. R. *Electrochemical Methods*; 2nd ed.; John Wiley & Sons. Inc.: New York, 2000.

(26) Eastland, G. W.; Rao, D. N. R.; Symons, M. C. R. *J. Chem. Soc., Perkin Trans. 2* **1984**, 1551.

(27) Liu, W.; Yamanaka, S.; Shiotani, M.; Michalik, J.; Lund, A. *Phys. Chem. Chem. Phys.* **2001**, *3*, 1611.

(28) Ledney, M.; Dutta, P. K. *J. Am. Chem. Soc.* **1995**, *117*, 7687.

(29) Quayle, W. H.; Lunsford, J. H. *Inorg. Chem.* **1982**, *21*, 97.

(30) Matsuura, K.; Kevan, L. *J. Phys. Chem.* **1996**, *100*, 10652.

(31) Matsuura, K.; Kevan, L. *Radiat. Phys. Chem.* **2001**, *62*, 399.

Chapter 3: Structure and Reactivity Aspects of Various Amine Coreactants and Coreactant Buffers on the Electrogenerated Chemiluminescence of Tris(2,2′-bipyridine)ruthenium(II) Complex, $Ru(bpy)_3^{2+}$, in Aqueous Media

3.1 Introduction

Generally, electrogenerated chemiluminescence (ECL)[1–3] can be achieved either by ion annihilation or by use of coreactants. In the ion annihilation mode, the excited state (R*) of an emitter (R) is produced by an energetic electron transfer reaction between electrochemically generated $R^{\bullet+}$ and $R^{\bullet-}$.

$$R^{\bullet+} + R^{\bullet-} \longrightarrow R^* + R \qquad (3.1)$$

However, this mode requires that both $R^{\bullet+}$ and $R^{\bullet-}$ are accessible and fairly stable with a sufficiently long lifetime in the diffusion layer of the electrode to obtain the ECL reaction.

If these conditions cannot be obtained, coreactants can be employed. A coreactant is an electrochemically active reagent that can produce a reactive species, which can reduce $R^{\bullet+}$ or oxidize $R^{\bullet-}$ to generate R*. Therefore, ECL can

be achieved by sweeping or pulsing the electrode potential in only one direction, either cathodic or anodic. Using a coreactant for ECL has some advantages over the ion annihilation mode; (a) it is not necessary to generate both $R^{\bullet+}$ and $R^{\bullet-}$ at the electrode, (b) it is useful when an emitter has an unstable $R^{\bullet+}$ or $R^{\bullet-}$ form, and (c) it is useful for solvents having a narrow potential window, such as water, so that either $R^{\bullet+}$ or $R^{\bullet-}$ cannot be formed.

Amines are good candidates as coreactants in aqueous media, and tri-*n*-propylamine (TPrA) among them has been studied intensively[4–8]. In chapter 1 and previous studies,[9,10] tris(2,2′-bipyridine)ruthenium(II), $Ru(bpy)_3^{2+}$ (bpy = 2,2′-bipyridine), was shown to generate two ECL waves in a plot of the ECL intensity vs. potential when TPrA was used as a coreactant. The first ECL wave began at the same potential where TPrA was oxidized, but before $Ru(bpy)_3^{2+}$ was oxidized. This ECL continued until $Ru(bpy)_3^{2+}$ was oxidized. According to the proposed mechanism of the first ECL wave, TPrA produces a radical cation ($Pr_3N^{\bullet+}$) [eq. (3.2)] and a free radical ($Pr_2NC^{\bullet}HEt$) [eq. (3.3)] both having a sufficiently long lifetime,[10] when TPrA is oxidized at an electrode. The produced $Pr_2NC^{\bullet}HEt$ reduces $Ru(bpy)_3^{2+}$ to $Ru(bpy)_3^{+}$, which will be oxidized to the excited state of $Ru(bpy)_3^{2+}$ by $Pr_3N^{\bullet+}$ later. The mechanism of this first ECL wave is shown in Scheme 3.1.

Scheme 3.1

$$Pr_3N - e \longrightarrow Pr_3N^{\bullet+} \quad (3.2)$$

$$Pr_3N^{\bullet+} \longrightarrow Pr_2NC^{\bullet}HEt + H^+ \quad (3.3)$$

$$Pr_2NC^{\bullet}HEt + Ru(bpy)_3^{2+} \longrightarrow Pr_2N^+{=}CHEt + Ru(bpy)_3^{+} \quad (3.4)$$

$$Ru(bpy)_3^{+} + Pr_3N^{\bullet+} \longrightarrow Ru(bpy)_3^{2+}* + Pr_3N \quad (3.5)$$

$$Ru(bpy)_3^{2+}* \longrightarrow Ru(bpy)_3^{2+} + h\nu \quad (3.6)$$

where Pr is $CH_3CH_2CH_2-$ and Et is CH_3CH_2-.

The second ECL wave arises at potentials where both $Ru(bpy)_3^{2+}$ and TPrA are oxidized. Two routes[6,7], direct oxidation (Scheme 3.2) and catalytic (Scheme 3.3) routes, contribute to the second ECL wave. The excited state of $Ru(bpy)_3^{2+}$ is formed by an electron transfer reaction between $Ru(bpy)_3^{3+}$ and $Pr_2NC^{\bullet}HEt$ in both routes [eq. (3.8)]. In the direct oxidation route (Scheme 3.2), the generation of $Pr_2NC^{\bullet}HEt$ is initiated by a heterogeneous electrode reaction, while this radical ion ($Pr_2NC^{\bullet}HEt$) is produced by a homogeneous oxidation by electrochemically generated $Ru(bpy)_3^{3+}$ in the catalytic route (Scheme 3.3). The relative contribution of these different routes to the second ECL wave depends on the experimental conditions, such as electrode potential and relative concentration of $Ru(bpy)_3^{2+}$ and TPrA.[7]

Scheme 3.2 ***(Direct Oxidation Route)***

$$Pr_3N - e \longrightarrow Pr_3N^{\bullet+} \quad (3.2)$$

$$Pr_3N^{\bullet+} \longrightarrow Pr_2NC^{\bullet}HEt + H^+ \quad (3.3)$$

$$Ru(bpy)_3^{2+} - e \longrightarrow Ru(bpy)_3^{3+} \quad (3.7)$$

$$Pr_2NC^{\bullet}HEt + Ru(bpy)_3^{3+} \longrightarrow Pr_2N^+{=}CHEt + Ru(bpy)_3^{2+}* \quad (3.8)$$

Scheme 3.3 ***(Catalytic Route)***

$$Ru(bpy)_3^{2+} - e \longrightarrow Ru(bpy)_3^{3+} \quad (3.7)$$

$$Ru(bpy)_3^{3+} + Pr_3N \longrightarrow Ru(bpy)_3^{2+} + Pr_3N^{\bullet+} \quad (3.9)$$

$$PrN^{\bullet+} \longrightarrow Pr_2NC^{\bullet}HEt + H^+ \quad (3.3)$$

$$Pr_2NC^{\bullet}HEt + Ru(bpy)_3^{3+} \longrightarrow Pr_2N^+{=}CHEt + Ru(bpy)_3^{2+}* \quad (3.8)$$

In both routes, the generation of $Ru(bpy)_3^+$ by $PrNC^{\bullet}HEt$ [eq. (3.4)] is also possible, so an annihilation reaction between $Ru(bpy)_3^+$ and $Ru(bpy)_3^{3+}$ may also occur.

ECL by amine coreactants is strongly dependent on the stability and reactivity of amine radicals produced on oxidation, which depends on the molecular structures of amines. Therefore, it is important to correlate the stability and reactivity of amines to their molecular structures. Noffsinger, *et. al.*[11] reported that the chemiluminescence (CL) intensity of $Ru(bpy)_3^{3+}$ in aqueous media

increased in order of primary < secondary < tertiary amine, and Nieman[12], *et. al.* demonstrated that the ECL intensity of $Ru(bpy)_3^{2+}$ increased in order of mono-*n*-propylamine < di-*n*-propylamine < tri-*n*-propylamine. However, there has been no report concerning on the relative stability and reactivity of cationic and free radicals of amine coreactants for the first and second ECL waves.

In this chapter, the structure and reactivity aspects of 14 different amine coreactants toward the ECL of $Ru(bpy)_3^{2+}$ in phosphate buffer solutions (PBS) at different pH are discussed. The use of coreactant buffers, which function as both coreactant and buffer is also studied. The molecular structures of amine coreactants and coreactant buffers are shown in Figure 3.1 and Figure 3.2, respectively.

3.2 Experimental Section

Chemicals and Solutions. Tris(2,2′-bypyridyl)dichlororuthenium(II) hexahydrate, $Ru(bpy)_3Cl_2 \cdot 6H_2O$ (99.99 %), dibromomethane (99 %), 1,2-dibromoethane (99+ %), 1,3-dibromopropane (99 %), di-*n*-propylamine (99+ %), 1-bromopropane (99 %), piperidine (99.5+ %), bromoethane (99+ %), piperazine (99 %) were obtained from Aldrich (Milwaukee, WI) and used as received. Triethylamine (TEtA, 99.5 %), tri-*n*-propylamine (TPrA, 99+ %), *N,N,N′,N′*-tetraethylmethanediamine (TEDAM, 97 %), *N,N,N′,N′*-tetraethylethylenediamine

(a) Acyclic monoamine group

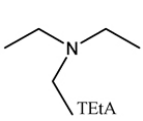

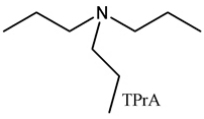

(b) Acyclic *N,N,N′,N′*-tetraethyldiamine group

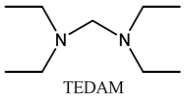

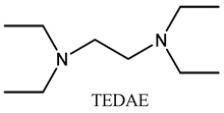

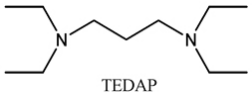

(c) Acyclic *N,N,N′,N′*-tetra-*n*-propyldiamine group

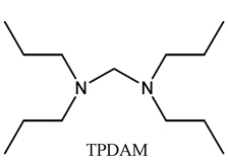

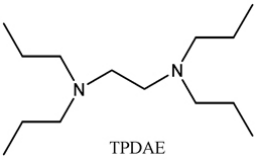

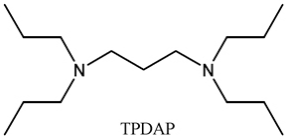

(d) Heteroalicyclic monoamine group

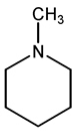

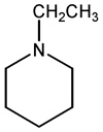

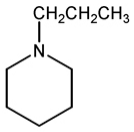

(e) Heteroalicyclic diamine group

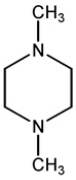

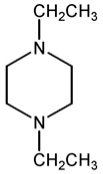

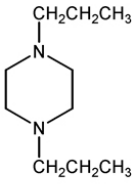

Figure 3.1. Molecular structures of amine coreactants. Acronyms are defined in the text.

(a) Morpholine group

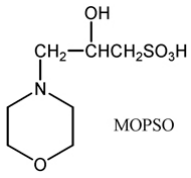

MOPSO

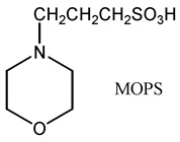

MOPS

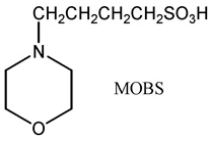

MOBS

(b) Piperazine group

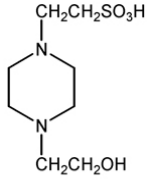

HEPES

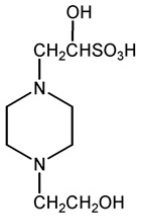

HEPPSO

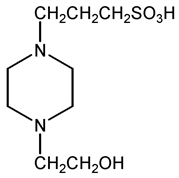

EPPS

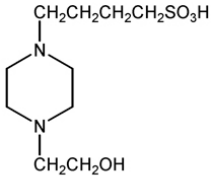

HEPBS

(c) Acyclic tertiary amine group

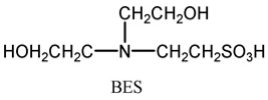

BES

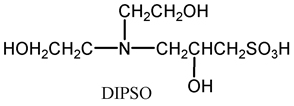

DIPSO

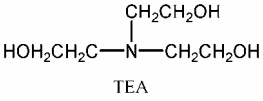

TEA

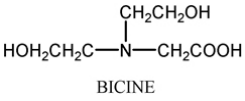

BICINE

Figure 3.2 *Continued on the next page.*

(d) Acyclic secondary amine group

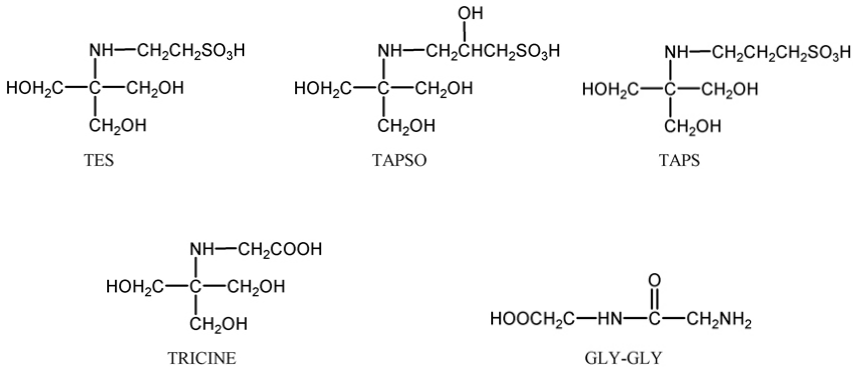

(e) Acyclic secondary diamine group

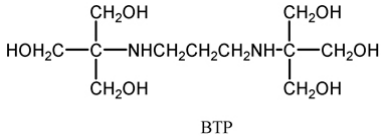

Figure 3.2. (*Cont.*) Molecular structures of coreactant buffers (CB). Acronyms are defined in the text.

(TEDAE, 98 %), *N,N,N′,N′*-tetraethyl-1,3-propanediamine (TEDAP, 97%), 1-methylpiperidine (MP, 98+ %), 1-ethylpiperidine (EP, 99 %), and 1,4-dimethylpiperazine (DMPz, 98 %) were purchased from Aldrich (Milwaukee, WI) and vacuum distilled before use. *N,N,N′,N′*-Tetra-*n*-propylmethanediamine (TPDAM), *N,N,N′,N′*-tetra-*n*-propylethylenediamine (TPDAE), *N,N,N′,N′*-tetra-*n*-propyl-1,3-propanediamine (TPDAP), 1-*n*-propylpiperidine (PP), 1,4-diethylpiperazine (DEPz), and 1,4-di-*n*-propylpiperazine (DPPz) were synthesized by direct alkylations from the appropriate starting materials (see Syntheses section). Molecular weights and structures of synthesized amines were confirmed by their mass spectra and nuclear magnetic resonance (NMR) spectra. Phosphoric acid (H_3PO_4, 85 %), monobasic- ($NaH_2PO_4 \cdot H_2O$), dibasic- ($Na_2HPO_4 \cdot 12H_2O$), and tribasic sodium phosphate ($Na_3PO_4 \cdot 7H_2O$) from Fisher Scientific Co. (Fair Lawn, NJ) were used without further purification. 3-[*N*-Morpholino]-2-hydroxypropanesulfonic acid (MOPSO), 1,3-bis[tris(hydroxymethyl)methylamino]propane (BTP), *N*,*N*-bis[2-hydroxyethyl]-2-aminoethanesulfonic acid (BES), 3-[*N*-morpholino]propanesulfonic acid (MOPS), *N*-tris[hydroxymethyl]methyl-2-aminoethanesulfonic acid (TES), *N*-[2-hydroxyethyl]piperazine-*N′*-[2-ethanesulfonic acid] (HEPES), 3-[*N*,*N*-bis(2-hydroxyethyl)amino]-2-hydroxypropanesulfonic acid (DIPSO), 4-[*N*-morpholino]butanesulfonic acid (MOBS), 3-[*N*-tris(hydroxymethyl)methylamino]-2-hydroxypropanesulfonic acid (TAPSO),

N–[2-hydroxyethyl]piperazine-*N*′-[2-hydroxypropanesulfonic acid] (HEPPSO), triethanolamine (TEA), *N*-[2-hydroxyethyl]piperazine-*N*′-[3-propanesulfonic acid] (EPPS), *N*-tris[hydroxymethyl]methylglycine (TRICINE), *N*-glycylglycine (GLY-GLY), *N*,*N*-bis[2-hydroxyethyl]glycine (BICINE), *N*-[2-hydroxyethyl]piperazine-*N*′-[4-butanesulfonic acid] (HEPBS), and *N*-tris[hydroxymethyl]methyl-3-aminopropanesulfonic acid (TAPS) were obtained from Sigma (St. Louis, MO) and used without further purification. 0.2 M phosphate buffer solutions with various pH values were prepared by a literature method.[13] 0.2 M coreactant buffer solutions were prepared by dissolving coreactant buffers in deionized water containing 0.1 M NaCl. The pH values of all buffer solutions were adjusted with either ~6 M sodium hydroxide (NaOH) or ~6 M hydrochloric acid (HCl) solution. Deionized water (Milli-Q, Millipore) was used to prepare all buffer solutions.

Syntheses of TPDAM, TPDAE, TPDAP, PP, DEPz, and DPPz. *N,N,N′,N′-Tetra-n-propylmethanediamine (TPDAM)*. TPDAM was synthesized by refluxing neat dibromomethane (10 ml) and excess di-*n*-propylamine (60 ml) at 120 °C without any solvent for 12 hrs. Once a reaction was done, white precipitates were formed. These precipitates were filtered and lightly washed with ether. Then they were dissolved in deionized water (50 ml) and this solution was saturated with sodium hydroxide (NaOH). Using ether, TPDAM was extracted from the NaOH saturated solution, and then vacuum distilled. [48 % of yield. ^{1}H

NMR ($CDCl_3$) δ 0.84 (*t*, 12H, *J* = 7.3 Hz, terminal CH_3–), 1.37 – 1.49 (*m*, at β-position of propyl branch), 3.14 (*s*, 2H, –CH_2– backbone). CI-MS (CH_4) *m*/*z* calculated for $C_{13}H_{30}N_2$ 214.37, found 215 $(M+1)^+$.]

N,N,N′,N′-Tetra-n-propylethylenediamine (TPDAE). TPDAE was synthesized by the same procedure as TPDAM synthesis. 12 ml of 1,2-dibromoethane and excess di-*n*-propylamine (60 ml) were used as starting materials. [64 % of yield. ^1H NMR ($CDCl_3$) δ 0.84 (*t*, 12H, *J* = 7.3 Hz, terminal CH_3–), 1.36 – 1.49 (*m*, 8H, –CH_2– at β-position of propyl branch), 2.33 – 2.38 (*m*, 8H, –CH_2– at α-position of propyl branch), 2.49 (*s*, 4H, –CH_2– in ethylene backbone). CI-MS (CH_4) *m*/*z* calculated for $C_{14}H_{32}N_2$ 228.39, found 229 $(M+1)^+$.]

N,N,N′,N′-Tetra-n-propylpropane-1,3-diamine (TPDAP). TPDAP was synthesized by the same procedure as TPDAM synthesis. 14 ml of 1,3-dibromopropane and excess di-*n*-propylamine (60 ml) were used as starting materials. [62 % of yield. ^1H NMR ($CDCl_3$) δ 0.84 (*t*, 12H, *J* = 7.3 Hz, terminal CH_3–), 1.36 – 1.48 (*m*, 8H, –CH_2– β-position in propyl branch), 1.50 – 1.60 (*m*, 2H, –CH_2– β-position in propylene backbone), 2.31 – 2.41 (*m*, 12H, –CH_2– at α-position). CI-MS (CH_4) *m*/*z* calculated for $C_{15}H_{34}N_2$ 242.41, found 243 $(M+1)^+$.]

1-Propylpiperidine (PP). PP was synthesized by the same procedure as TPDAM synthesis. 13 ml of 1-bromopropane and excess piperidine (45 ml) were used as starting materials. The temperature of reflux was 110 °C. [56 % of yield.

^{1}H NMR ($CDCl_3$) δ 0.86 (*t*, 3H, *J* = 7.4 Hz, terminal –CH_3), 1.10 – 1.80 (*m*, 8H, –CH_2– at β- and γ-position), 2.29 – 2.31 (*m*, 6H, –CH_2– at α-position). CI-MS (CH_4) *m*/*z* calculated for $C_8H_{17}N$ 127.21, found 128 $(M+1)^+$.]

1,4-Diethylpiperazine (DEPz). DEPz was synthesized with 12 g of piperazine and 35 ml of 1-bromoethane. Both of them were dissolved in 50 ml ethanol and then refluxed at 100 °C for 12 hrs. Once white precipitates were formed, they were filtered and gently washed with ethanol and then dried. These precipitates were dissolved in deionized water (50 ml) and then saturated with NaOH. After crude DEPz was extracted with ether, it was purified by vacuum distillation. [24 % of yield. ^{1}H NMR ($CDCl_3$) δ 0.99 (*t*, 6H, *J* =7.4 Hz, terminal –CH_3), 2.00 – 2.30 (*m*, 4H at α-position of ethyl group), 2.53 (*s*, 8H, –CH_2– at the ring). CI-MS (CH_4) *m*/*z* calculated for $C_8H_{18}N_2$ 142. 24, found 143 $(M+1)^+$.]

1,4-Dipropylpiperazine (DPPz). DPPz was synthesized by the same procedure as DEPz synthesis. Pure solid of piperazine and 1-bromopropane were used as starting materials. [22 % of yield. ^{1}H NMR ($CDCl_3$) δ 0.86 (*t*, 6H, *J* = 7.3 Hz, terminal –CH_3), 1.30 – 1.80 (*m*, 4H, –CH_2– at β-position of propyl group), 1.90 – 2.20 (*t*, 4H, at α-position of propyl group), 2.48 (*s*, 8H, –CH_2– at the ring). CI-MS (CH_4) *m*/*z* calculated for $C_{10}H_{22}N_2$ 170.30, found 171 $(M+1)^+$.]

Instrumentation and Procedures. A glassy carbon electrode (GCE, area = 0.07 cm^2) was polished prior to experiments, using 1 micron diamond

suspension on a nylon cloth and then 0.25 micron diamond suspension on a microcloth (Buehler, Lake Bluff, IL). In addition, the GCE was lightly polished with deionized water on a microcloth immediately before each measurement. For electrochemical and ECL measurements, a conventional three-electrode electrochemical cell was employed. A GCE (3 mm diameter) served as a working electrode, a Pt wire as a counter, and Ag/AgCl as a reference electrode. Cyclic voltammograms (CV) were measured with either the model 660 electrochemical workstation (CH Instruments, Austin, TX), or a home-built potentiostat. Simultaneous ECL signals with CV were recorded using a Hamamatsu R4220p photomultiplier tube (PMT) placed just beneath the electrochemical cell. A high-voltage power supply series 225 (Bertan High Voltage Co., Hicksville, NY) was used to provide – 750 V to a PMT for the appropriate sensitivity. All solutions were deaerated by bubbling N_2 gas before each measurement.

3.3 Results and Discussion

Electrochemistry of $Ru(bpy)_3^{2+}$ and 14 Different Amine Coreactants. In an organic solvent, such as acetonitrile (MeCN), $Ru(bpy)_3^{2+}$ usually displays a one-electron reversible oxidation and its oxidized form, $Ru(bpy)_3^{3+}$, can remain in contact with air for overnight.[14] On the other hand, the reversibility of electrochemical oxidation of $Ru(bpy)_3^{2+}$ in aqueous media depends on the pH of the solution. Figure 3.3 shows the cyclic voltammograms (CV) for

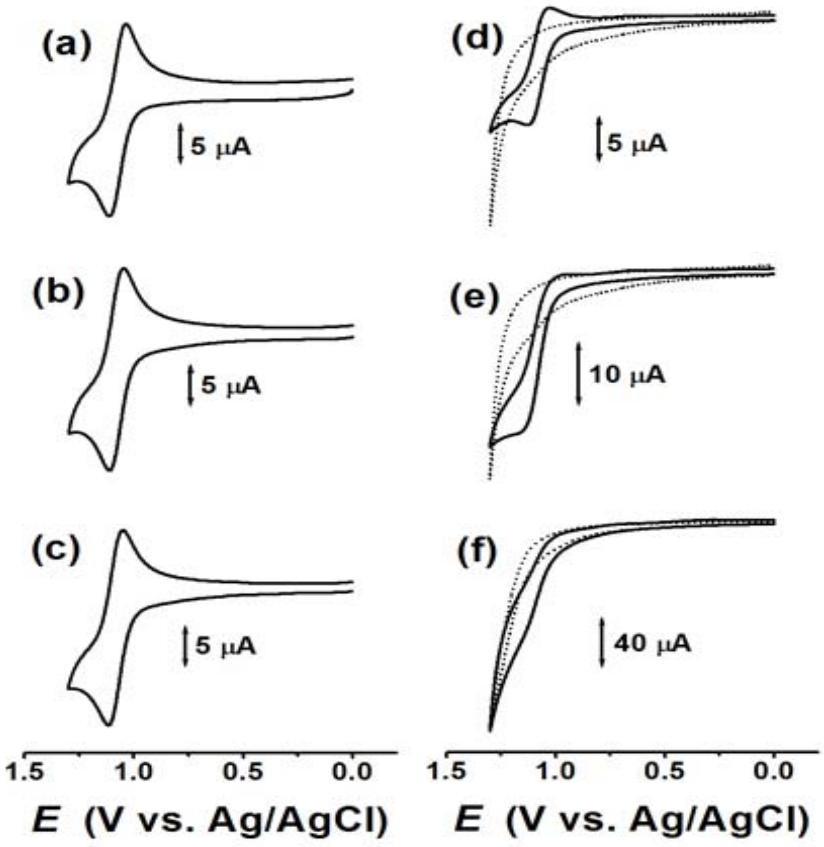

Figure 3.3. Cyclic voltammograms (CV) of 1 mM $Ru(bpy)_3^{2+}$ in (a) pH 2.5, (b) pH 6.5, (c) pH 9.5, (d) pH 10.5, (e) pH 11.5, and (f) pH 12.5 of 0.2 M PBS at 0.1 V/s using a glassy carbon electrode (area = 0.07 cm^2). The dotted lines are background CVs.

the electrochemical oxidation of $Ru(bpy)_3^{2+}$ in phosphate buffer solutions (PBS) of different pH values, measured at 0.1 V/s. In the range of pH 2.5 to pH 9.5, the peak potential separation (ΔE_p) of the $Ru(bpy)_3^{2+/3+}$ couple was ~ 63 mV, which was close to 59 mV for an one-electron reversible redox reaction, and the ratio of peak currents (i_c/i_a) for the $Ru(bpy)_3^{2+/3+}$ couple was ~ 1 (i_c/i_a = 0.91). The half-wave potential ($E_{1/2}$) was + 1.1 V vs. Ag/AgCl. Therefore, the electrochemical oxidation of $Ru(bpy)_3^{2+}$ was reversible in this pH range. However, the electrochemical oxidation of $Ru(bpy)_3^{2+}$ became more and more irreversible as the pH value of the solution increased. No reversible wave was shown even if the background current of the solvent was subtracted (pH 10.5 – pH 12.5). At pH 10.5, the electrochemical oxidation of $Ru(bpy)_3^{2+}$ was considered to be quasi-reversible, because its ΔE_p was 100 mV and i_c/i_a was ~ 0.6. At pHs 11.5 and 12.5, the electrochemical oxidation of $Ru(bpy)_3^{2+}$ might be irreversible probably due to oxidation of the solvent. Although there have been many arguments[15–21] on the stability and reactivity of both $Ru(bpy)_3^{2+}$ and $Ru(bpy)_3^{3+}$ with base, such as OH^-, its stability and reaction mechanism is still uncertain.

Electrochemical oxidations of most tertiary amines are well known[22–26] and follow the ECE process as shown in Scheme 3.4. Their CVs show one or two oxidation waves depending on the pH of the solution and the reactivity of free radicals of tertiary amines for hydrolysis. The second oxidation wave in the CV is

usually considered to be the oxidation of dialkylamine which is the hydrolysis product of an oxidized tertiary amine [the product (R_2NH) of eq. (3.13)].[24,25]

Scheme 3.4

$$R_2NCH_2R' - e \rightleftharpoons R_2N^{\bullet+}CH_2R' \quad (3.10)$$

$$R_2N^{\bullet+}CH_2R' \longrightarrow R_2NC^{\bullet}HR' + H^+ \quad (3.11)$$

$$R_2NC^{\bullet}HR' - e \rightleftharpoons R_2N^{+}=CHR' \quad (3.12)$$

$$R_2N^{+}=CHR' + H_2O \longrightarrow R_2NH + R'CHO + H^+ \quad (3.13)$$

With 10 mM concentrations of 14 different amines, cyclic voltammetry was carried out using a glassy carbon electrode (GCE) in the PBS of pH 12.5, where all amines existed as deprotonated forms. Each CV showed irreversible electrochemical oxidations. For a totally irreversible wave in CV where the first electron transfer is the rate determining step, the peak potential (E_p) is the function of scan rate as defined in eq. (3.14)[27]:

$$E_p = E^\circ + (RT/\alpha F)[0.780 + \ln(D^{1/2}/k^\circ) + \ln(\alpha F/RT)^{1/2}] + (2.303RT/2\alpha F)\log \nu \quad (3.14)$$

where E° is the standard potential, R is the gas constant, T is temperature, α is the

transfer coefficient, F is the faraday constant, D is the diffusion coefficient, $k°$ is the standard heterogeneous rate constant, and ν is the scan rate. In CV experiments, the anodic peak potentials ($E_{p,a}$) of amines used in this work were linearly shifted to more positive potentials as the scan rate logarithmically increased. For example, Figure 3.4 shows CVs of 10 mM TEtA in pH 12.5 PBS at various scan rates (10 mV/s – 200 mV/s) and dependence of $E_{p,a}$ on log ν. $E_{p,a}$ of the TEtA oxidation was linearly dependent on log ν. The transfer coefficients (α) of 14 amines could be calculated from the slope ($\partial E_{p,a}/\partial \log \nu$) of a plot of $E_{p,a}$ vs. log ν, and are summarized in Table 3.1. The α values of 14 amines were close to 0.5 (α = 0.42 ~ 0.56), indicating that a slow heterogeneous electron transfer reaction [eq. (3.10)] intervened in the overall chemical kinetic control [eq. (3.11)].[6]

Because of the compensation of the $TPrA^{\bullet}$ (free radical) oxidation current from the $TPrA^{\bullet+}$ (radical cation) reduction current, it is difficult to obtain a reversible oxidation wave of TPrA even from the fast scan CV to measure $E_{1/2}$ for eq. (3.2).[10] Analogously, the CVs of the other amines did not show reversible oxidation waves due to the same reason. From eq. (3.14), however, unknown $E°$ value for eq. (3.10) can be approximated from the y-intercept (C) of a plot of $E_{p,a}$ vs. log ν. Assuming that α is 0.5, D is 5×10^{-6} cm^2/s, and 0.001 cm/s $\leq k° \leq$ 1 cm/s, the y-intercept (C) term of eq. (3.14) can be shorten to eq. (3.15):

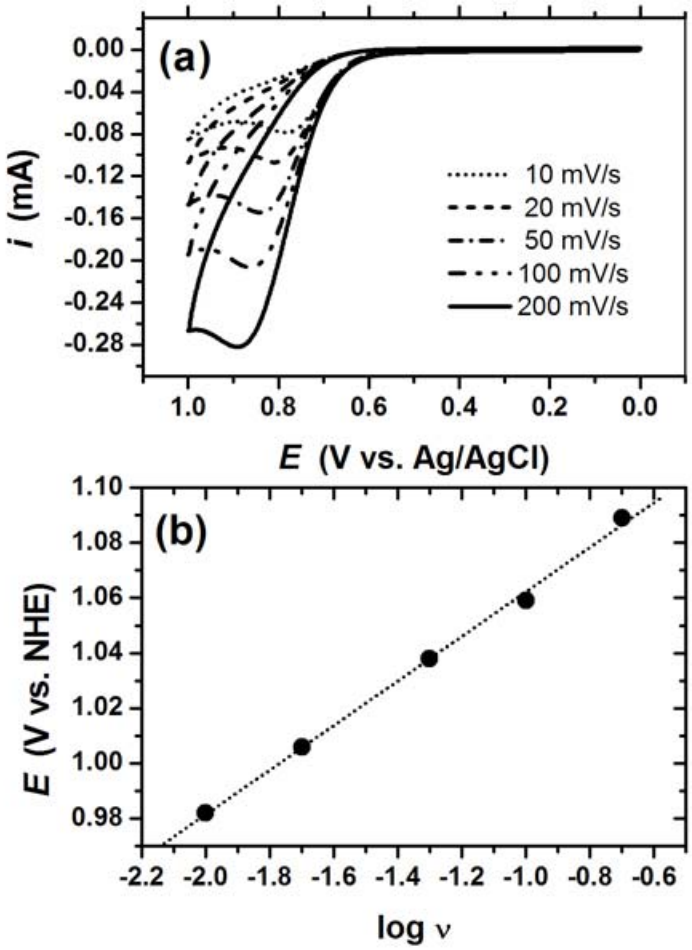

Figure 3.4. (a) Cyclic voltammograms of 10 mM TEtA in pH 12.5 PBS measured at various scan rates (ν). (b) Dependence of peak potentials for TEtA oxidation on log ν. A GCE (area = 0.07 cm^2) was used as a working electrode.

Table 3.1. Summary of Electrochemical Data for the Oxidation of Amines.

Amine	$\partial E_{p,a}/\partial \log \nu$ (mV/decade)	α	C (V)[a]	E_p (V)[b]
TEtA	69.8 ± 0.1	0.42	1.13	1.06
TPrA	52.8 ± 0.5	0.56	0.96	0.91
TEDAM	69.8 ± 0.1	0.42	1.50	1.43
TEDAE	69.8 ± 0.3	0.42	1.05	0.98
TEDAP	66.3 ± 0.5	0.45	1.18	1.11
TPDAM	54.9 ± 0.6	0.54	0.78	0.73
TPDAE	63.7 ± 0.4	0.46	0.79	0.75
TPDAP	69.6 ± 0.6	0.43	0.95	0.87
MP	69.4 ± 0.4	0.43	1.26	1.19
EP	69.4 ± 0.3	0.43	1.20	1.13
PP	69.8 ± 0.1	0.42	1.18	1.11
DMPz	54.4 ± 0.4	0.54	1.46	1.41
DEPz	69.8 ± 0.1	0.42	1.45	1.38
DPPz	60.4 ± 0.2	0.49	1.39	1.33

All Potentials were measured at a GCE (area = 0.07 cm^2) with an Ag/AgCl reference electrode and then converted to the potentials vs. NHE. Scan rate (ν) range : 10 mV/s – 200 mV/s.

a. The y-intercept of the plot of E_p *vs.* log υ.

b. Measured at the scan rate of 0.1 V/s.

$$E^\circ - 0.20 \leq C \leq E^\circ + 0.16 \quad (3.15)$$

$$C - 0.16 \leq E^\circ \leq C + 0.20 \quad (3.16)$$

Therefore, the *C* values summarized in Table 3.1 can be useful information to get a rough estimate of the E° values of radical cations of amines.

ECL of $Ru(bpy)_3^{2+}$ by amine coreactants. ECL of $Ru(bpy)_3^{2+}$ was observed when the electrode potential was anodically swept in a solution containing $Ru(bpy)_3^{2+}$ and an amine coreactant and followed the parallel process to Schemes 3.1, 3.2, and 3.3. Figure 3.5 shows simultaneous CV and ECL measured under the condition of 1 μM $Ru(bpy)_3^{2+}$ and 10 mM TEDAP in pH 7.5 PBS with the scan rate of 0.1 V/s. From the CV, TEDAP began to be oxidized at + 0.55 V vs. Ag/AgCl and it might generate both $TEDAP^{\bullet+}$ (radical cation) and $TEDAP^{\bullet}$ (free radical) that participated in the ECL reaction later. Similar to ECL by TPrA[10], TEDAP produced the first ECL wave before $Ru(bpy)_3^{2+}$ was oxidized ($E_{1/2}$ = + 1.1 V vs. Ag/AgCl). Then, the second ECL wave occurred at around + 1.1 V vs. Ag/AgCl, where $Ru(bpy)_3^{2+}$ was oxidized. The presence of the first ECL wave indicates that the radical cation of TEDAP is also produced and has a sufficient lifetime to reduce $Ru(bpy)_3^{+}$ to $Ru(bpy)_3^{2+}$* in the solution. On the other hand, Figure 3.6 is the simultaneous CV and ECL of 1 μM $Ru(bpy)_3^{2+}$ and 10 mM

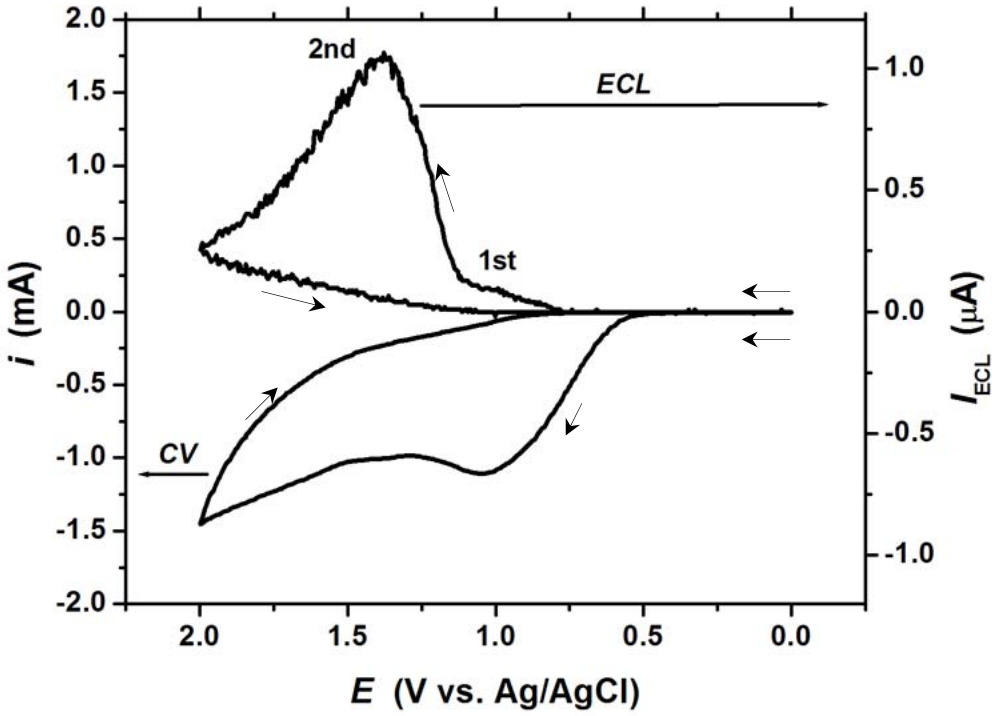

Figure 3.5. Simultaneous CV and ECL of 1 μM $Ru(bpy)_3^{2+}$ with 10 mM *N,N,N′,N′*-tetraethyl-1,3-propanediamine (TEDAP) in pH 7.5 PBS. Scan rate. = 0.1 V/s. A GCE (area = 0.07 cm^2) was used.

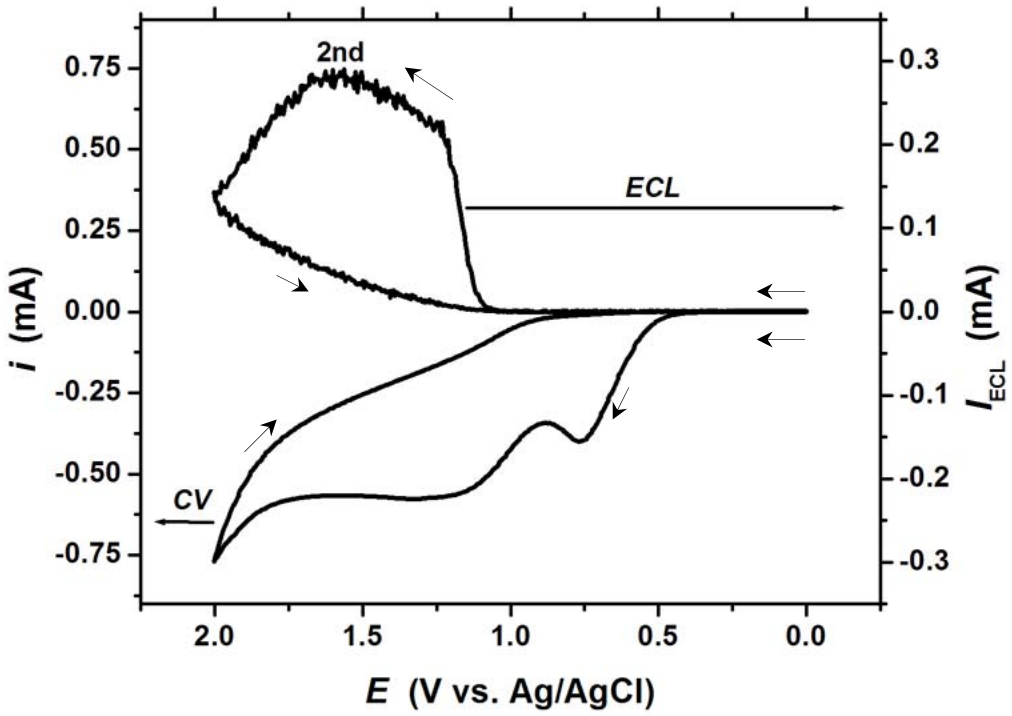

Figure 3.6. Simultaneous CV and ECL of 1 μM $Ru(bpy)_3^{2+}$ with 10 mM *N,N,N′,N′*-tetra-*n*-propylethylenediamine (TPDAE) in pH 7.5 PBS. Scan rate. = 0.1 V/s. A GCE (area = 0.07 cm^2) was used.

TPDAE in pH 7.5 PBS with the scan rate of 0.1 V/s. Although TPDAE also produced both $TPDAE^{\bullet+}$ (radical cation) and $TPDAE^{\bullet}$ (free radical) during its oxidation, TPDAE displayed only the second ECL wave.

The first ECL. The maximum intensities of the first ECL waves obtained with $Ru(bpy)_3^{2+}$ (1 μM) and each different amine coreactant (10 mM) in pH 7.5 PBS are shown in Figure 3.7. Like TPDAE shown in Figure 3.6, TPDAM also did not show the first ECL wave, because the radical cations of TPDAM and TPDAE, probably, were either extremely short-lived transients or not sufficiently energetic to produce $Ru(bpy)_3^{2+}$*. Based on the fact that TPDAP produced the first ECL, it could be speculated that the radical cations of TPDAM and TPDAE were not extremely short-lived. In general, the radical cation of an amine coreactant must have an $E°$ value that is more positive than at least + 0.94 V[28] vs. NHE in order to generate $Ru(bpy)_3^{2+}$* (2.12 eV)[29] from $Ru(bpy)_3^{+}$ ($E°$ of $Ru(bpy)_3^{2+/+}$ in water = – 1.28 V vs. NHE[29]). As shown in Table 3.1, the C values of TPDAM (+ 0.78 V) and TPDAE (+ 0.79 V), which are close to their real $E°$ values were much lower than the required value, + 0.94 V. As a result, radical cations of TPDAM and TPDAE were not strong enough to generate $Ru(bpy)_3^{2+}$*. In contrast, the C values of other amine coreactants were quite higher than + 0.94 V, so that the first ECL wave was observed.

In view of the first ECL wave, monoamine coreactant (TEtA, TPrA, MP, EP, and PP) gave much stronger emissions than did diamine coreactants

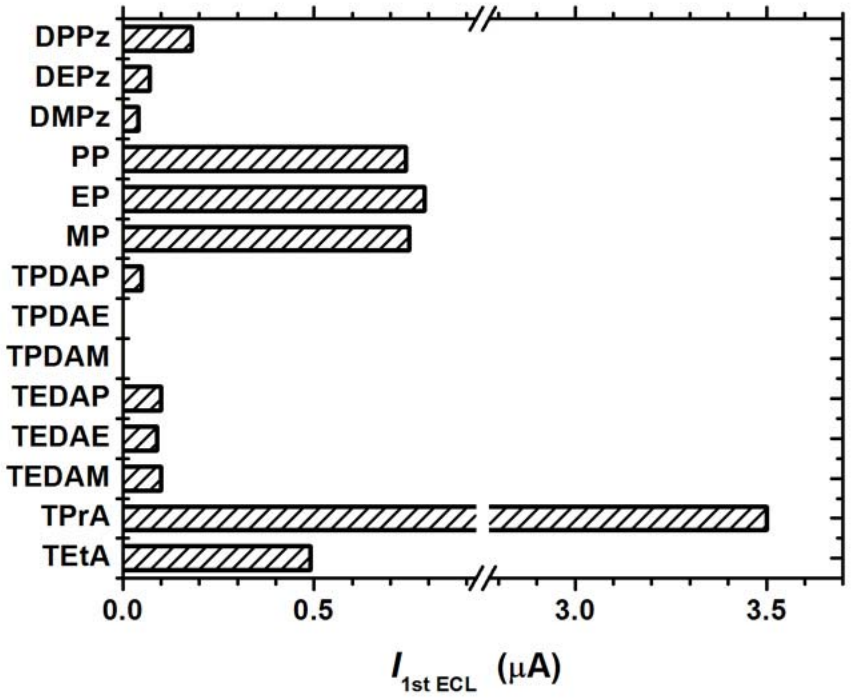

Figure 3.7. Comparison of the first ECL wave intensities of 1 μM $Ru(bpy)_3^{2+}$ generated with various amine coreactants (10 mM) in pH 7.5 PBS. Scan rate = 0.1 V/s. A GCE (area = 0.07 cm^2) was used.

(TEDAM, TEDAE, TEDAP, TPDAM, TPDAE, TPDAP, DMPz, DEPz, and DPPz). In order to produce a first ECL wave, the radical cations of amine coreactants must have the proper value of $E°$ for eq. (3.10) as well as a fairly long lifetime, which is closely related on the stability of radical cations. This stability strongly depends on the structure of a molecule. At pH 7.5, one nitrogen atom of a diamine had to be protonated[30] and the oxidation would occur on the other nitrogen atom. When the radical cations of diamines were formed, the positive charge on the protonated nitrogen could induce a faster deprotonation of the radical cations. Therefore, the relative amount of diamine radical cations would be much smaller than that of monoamine radical cations. Thus, the ECL intensity of diamines was much weaker than that of monoamines.

The second ECL. The pH dependence of the second ECL wave were investigated in the range of pH 2.5 to 9.5, because the oxidation of $Ru(bpy)_3^{2+}$ became irreversible (Figure 3.3) and the unknown background emission (probably by the reaction of $Ru(bpy)_3^{3+}$ with OH^-)[31] was significant above at pH 10.5. Figures 3.8 – 3.12 show the pH dependence of the second ECL wave of $Ru(bpy)_3^{2+}$ produced by 14 different amine coreactants. Below at pH 6, relatively low ECL intensities were observed for most amine coreactants except for TPDAP, which generated the highest ECL intensity at pH 5.5, because the protonated forms of amines became predominant over deprotonated forms and the deprotonation step, reaction (3.11), proceeded more slowly in the acidic pH

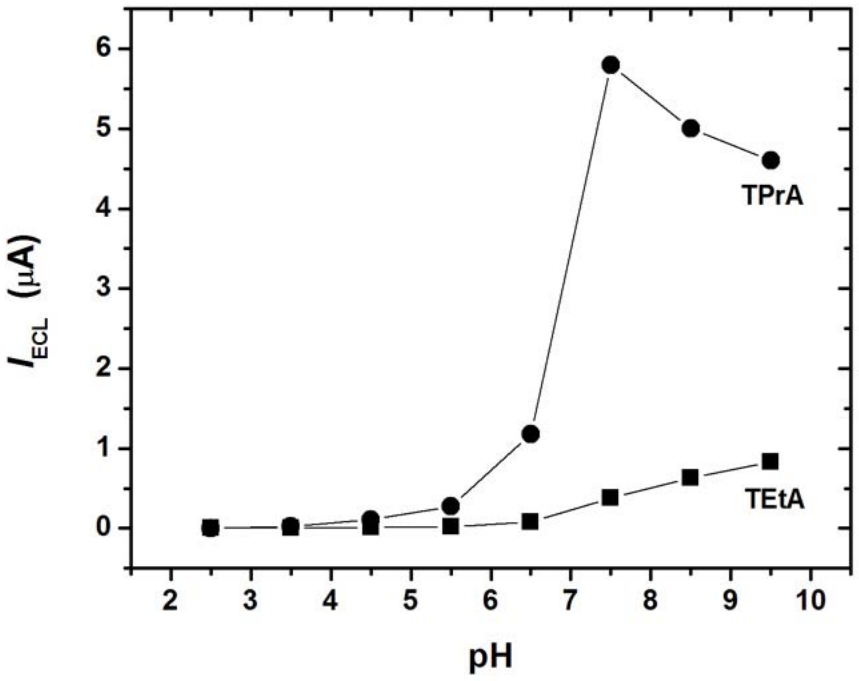

Figure 3.8. Dependence of the second ECL produced in a solution of 1 μM $Ru(bpy)_3^{2+}$ and 10 mM acyclic monoamine group coreactant (TEtA or TPrA) on the pH of PBS. Each data point is the average value of three measurements and contains less than 10 % deviation. A GCE (area = 0.07 cm^2) was used.

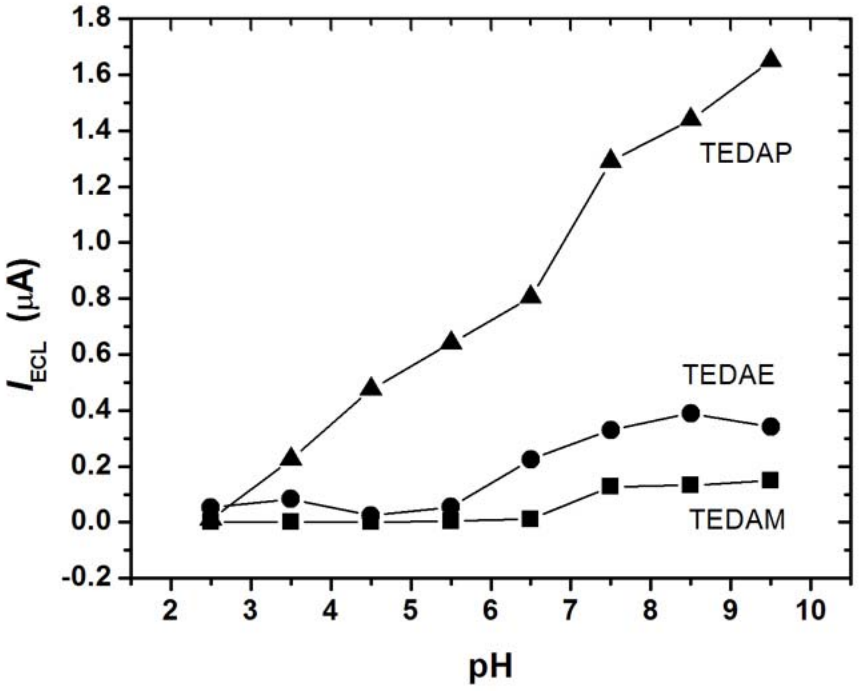

Figure 3.9. Dependence of the second ECL produced in a solution of 1 μM $Ru(bpy)_3^{2+}$ and 10 mM acyclic *N*,*N*,*N*′,*N*′-tetraethyldiamine group coreactant (TEDAM, TEDAE, or TEDAP) on the pH of PBS. Each data point is the average value of three measurements and contains less than 10 % deviation. A GCE (area = 0.07 cm^2) was used.

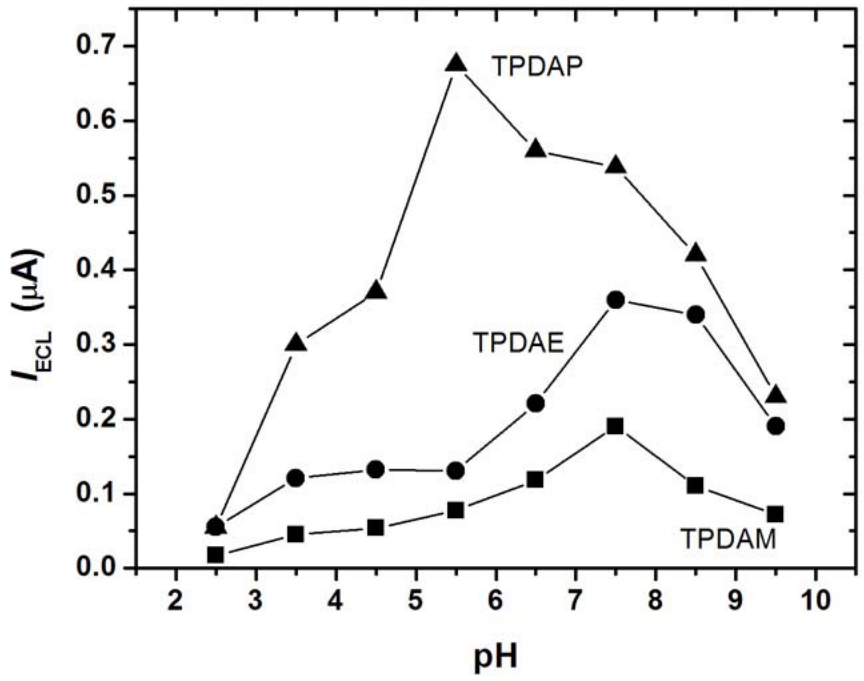

Figure 3.10. Dependence of the second ECL produced in a solution of 1 μM $Ru(bpy)_3^{2+}$ and 10 mM acyclic *N*,*N*,*N*′,*N*′-tetra-*n*-propyldiamine group coreactant (TPDAM, TPDAE, or TPDAP) on the pH of PBS. Each data point is the average value of three measurements and contains less than 10 % deviation. A GCE (area = 0.07 cm^2) was used.

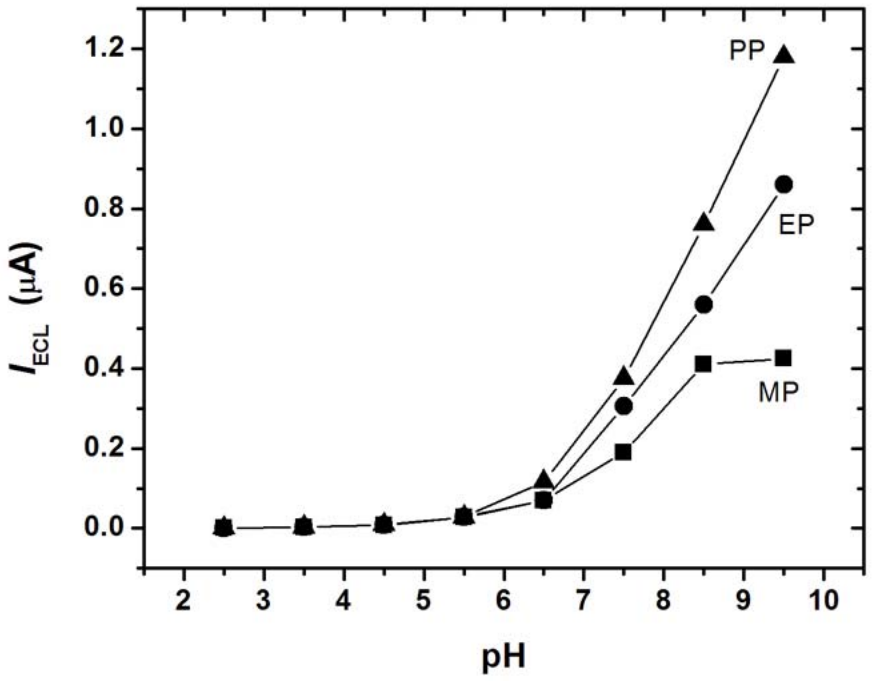

Figure 3.11. Dependence of the second ECL produced in a solution of 1 μM $Ru(bpy)_3^{2+}$ and 10 mM heteroalicyclic monoamine group coreactant (MP, EP, or PP) on the pH of PBS. Each data point is the average value of three measurements and contains less than 10 % deviation. A GCE (area = 0.07 cm^2) was used.

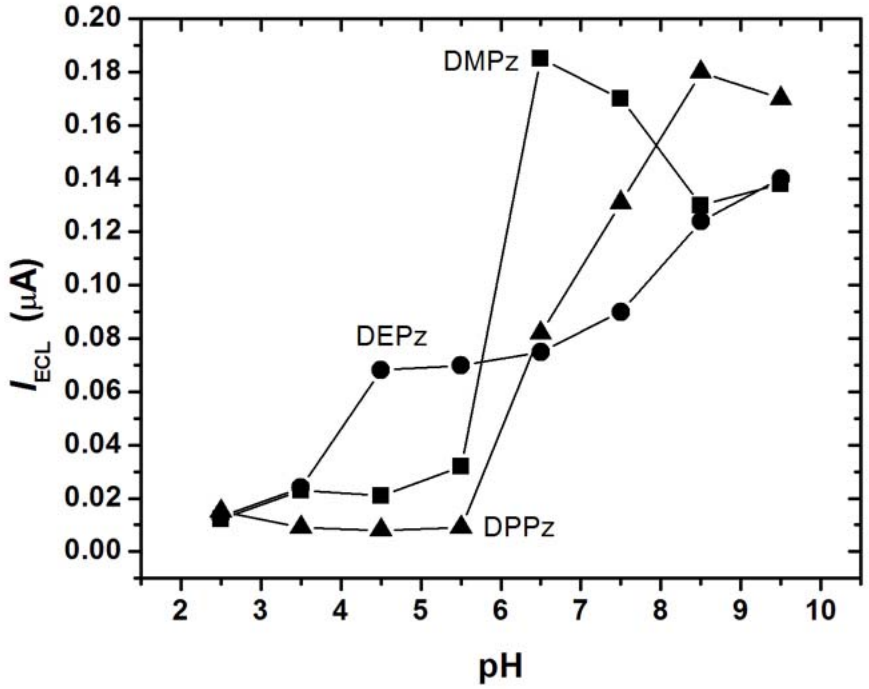

Figure 3.12. Dependence of the second ECL produced in a solution of 1 μM $Ru(bpy)_3^{2+}$ and 10 mM heteroalicyclic diamine group coreactant (DMPz, DEPz, or DPPz) on the pH of PBS. Each data point is the average value of three measurements and contains less than 10 % deviation. A GCE (area = 0.07 cm^2) was used.

region. In case of TPDAP, because of the hydrophobicity of TPDAP, the solubility of TPDAP in water decreased with the increasing pH of PBS. In fact, the oxidation peak current for TPDAP was highest at pH 5.5 (see Figure 3.13), so that its maximum ECL was shown at pH 5.5. On the other hand, the other amines generated their highest ECL intensities in a region of pH 7.5 – pH 9.5. Optimum pHs and the maximum ECL intensities of amine coreactants are summarized in Table 3.2.

Like the first ECL wave, monoamines gave a higher intensity of the second ECL wave than did diamines; the positive charge on the protonated nitrogen atom of a diamine molecule made the free radicals of diamines relatively less stable than those of monoamines. Except for DMPz, DEPz, and DPPz, the intensity of the second ECL wave tended to increase in order of methyl < ethyl < *n*-propyl substituent in the homolog of amines. Because of the electron-donating characteristics of alkyl group, amines having longer alkyl substituents produced more stable free radical and more intense ECL. However, the ECL tendency of DMPz, DEPz, and DPPz was totally unexpected.

The second ECL wave intensities of acyclic amines (e.g. TPrA and TEDAP) were higher than those of heteroalicyclic amines (PP and DPPz). The neutral molecule of an amine has the trigonal pyramid structure. When an amine molecule is oxidized, initially the loss of one electron occurs from the lone pair electrons on a nitrogen molecule and this causes the rearrangement of the amine

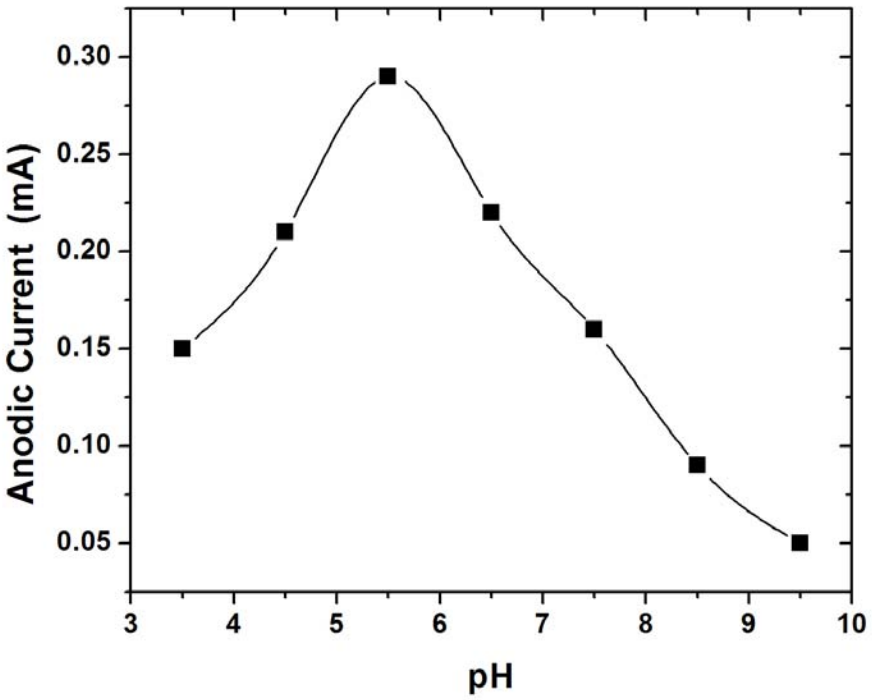

Figure 3.13. Dependence of the anodic current for the oxidation of 10 mM TPDAP on pH of PBS. Scan Rate = 0.1 V/s. A GCE (area = 0.07 cm^2) was used.

Table 3.2. List of pK_a Values of Coreactants, Optimum pH for the Second ECL and Its ECL intensities.

Coreactants	pK_a	Optimum pH	I_{ECL}[a] (μA)
TEtA	10.75[b]	9.5	0.83 ± 0.05
TPrA	10.66[c]	7.5	5.80 ± 0.07
TEDAM	< 1[d,f], 11.01[e,f]	9.5	0.15 ± 0.03
TEDAE	6.54[d,f], 9.84[e,f]	8.5	0.39 ± 0.05
TEDAP	8.20[d,g], 10.18[e,g]	9.5	1.65 ± 0.07
TPDAM	-[k]	7.5	0.19 ± 0.04
TPDAE	-[k]	7.5	0.36 ± 0.04
TPDAP	9.6[e,h]	5.5	0.68 ± 0.06
MP	10.38[b]	9.5	0.43 ± 0.08
EP	10.45[b]	9.5	0.86 ± 0.08
PP	10.41[i]	9.5	1.18 ± 0.03
DMPz	4.10[d,j], 8.40[e,j]	6.5	0.19 ± 0.07
DEPz	4.67[d,f], 8.83[e,f]	9.5	0.14 ± 0.04
DPPz	-[k]	8.5	0.18 ± 0.06

ECL was produced with 1 μM $Ru(bpy)_3^{2+}$ and 10 mM each coreactant in PBS.

a. Average values of 3 independent measurements for each coreactant. *b*. From ref. (32). *c*. From ref. (33). *d*. p$K_{a,1}$. *e*. p$K_{a,2}$. *f*. From ref. (34). *g*. From ref. (35). *h*. In this work. *i*. From ref. (36). *j*. From ref. (37). *k*. Not available.

molecule: the trigonal pyramid structure will be changed to the trigonal plane shape because the repulsion from the non-bonding orbital of nitrogen atom is diminished. Then, after deprotonation from the α-carbon, another rearrangement must occur because the orbital of unpaired non-bonding electron is filled again. Therefore, the rate of amine oxidation depends on how easy the rearrangement of a molecule occurs. Because acyclic amines (TPrA and TEDAP) have more flexible movement of substituents than do heteroalicyclic amines (PP and DPPz), acyclic amine coreactants generated the more intense second ECL wave than did heteroalicyclic amines.

ECL of $Ru(bpy)_3^{2+}$ in Coreactant Buffers. The new concept of buffer (coreactant buffer) solutions for ECL was developed using various biological buffers. The coreactant buffer (CB) can be defined as an agent used for a coreactant as well as the control of pH. Therefore, use of a CB may be useful especially when an added coreactant causes a side-reaction with an analyte. CBs used in this work have various amine structures (Figure 3.2), offer a useful pH of ~ 7.5 (pK_a 6.9 – 8.4), and are inert with most biological molecules. Figure 3.14 shows the simultaneous CV and ECL of 1 μM $Ru(bpy)_3^{2+}$ in the CB solution (0.2 M DIPSO, 0.1 M NaCl) at 0.1 V/s. Because DIPSO is a tertiary amine, it could be electrochemically oxidized (Figure 3.14, CV) via Scheme 3.4 and produce both a radical cation and a free radical. The other CBs were also oxidized by this scheme. Like amine coreactants discussed in the previous section, DIPSO

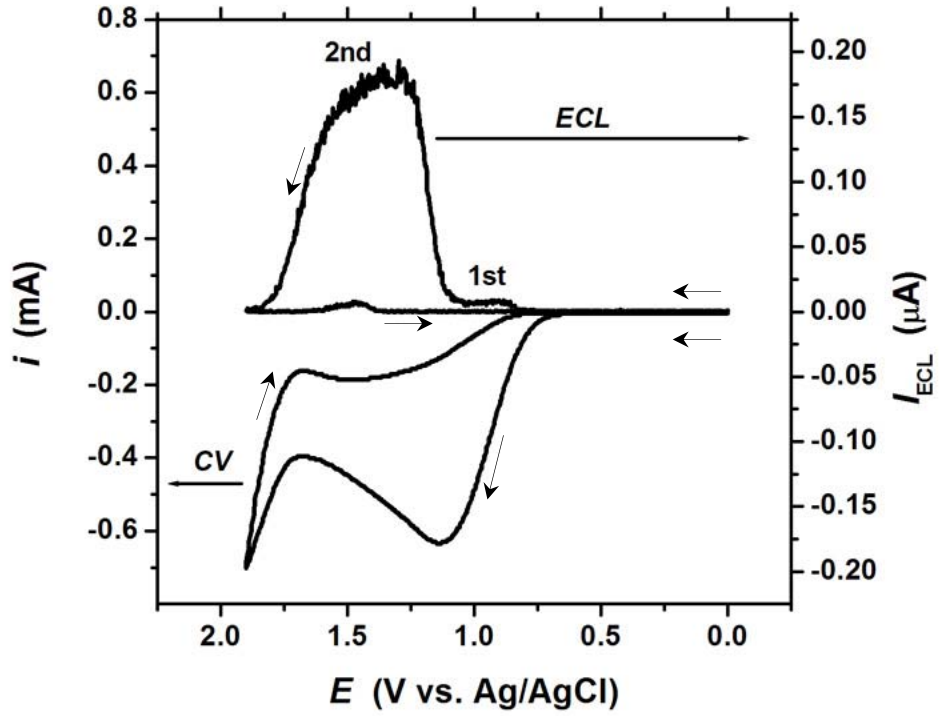

Figure 3.14. Simultaneous CV and ECL 1 μM $Ru(bpy)_3^{2+}$ in pH 7.5 of DIPSO buffer (0.2 M) solution containing 0.1 M NaCl as a supporting electrolyte. Scan rate = 0.1 V/s. A GCE (area = 0.07 cm^2) was used.

produced two ECL waves in a plot of the ECL intensity vs. potential (Figure 3.14, ECL) following the analogous mechanism to TPrA. Except for DIPSO, MOBS, and TEA, the other CBs did not show a first ECL wave because their oxidation occurred at more positive potentials (see Table 3.3) than $Ru(bpy)_3^{2+}$ oxidation ($E_{1/2}$ = + 1.1 V vs. Ag/AgCl). All electrochemical and ECL data are summarized in Table 3.3.

Like amine coreactants, the stability of the radical cation of a CB plays an important role to produce the first ECL wave. It was reported that the radical cation or free radical of amine having electron-withdrawing groups near a nitrogen atom or an α-carbon (within 2 carbon atoms) would be further destabilized.[5,38] As a result, MOBS produced the most intense first ECL among those that produced the first ECL waves because MOBS did not have any electron-withdrawing groups near a nitrogen atom in its molecular structure. In contrast, DIPSO and TEA have the $-CH_2CH_2OH$ and $-CH_2CH(OH)-$ groups, which function as electron-withdrawing groups by an inductive effect of an electronegative atom,[38,39] on their nitrogen atoms. Therefore, their first ECL wave intensities were much less than that of MOBS.

All CBs produced a second ECL wave of $Ru(bpy)_3^{2+}$ by the same way of Schemes 3.2 and 3.3. The second ECL wave intensities of $Ru(bpy)_3^{2+}$ (1 μM) generated with various CBs were compared with that generated with 10 mM TPrA in pH 7.5 PBS by calculating the ratio of the second ECL intensities,

Table 3.3. pK_a, Anodic Peak Potential (E_p), the First and Second ECL wave Intensities, and the Relative second ECL wave Intensity (I_{CB}/I_{TPrA}) of Coreactant Buffers.

Buffer	pK_a	E_p (V)[a]	1st ECL (nA)	2nd ECL (μA)	I_{CB}/I_{TPrA} (%)
MOPSO	6.9	1.30	-	0.82	14.1
MOPS	7.2	1.52	-	1.00	17.2
MOBS	7.6	1.20	50	1.40	24.1
HEPES	7.5	-[b]	-	0.17	2.9
HEPPSO	7.8	-[b]	-	0.03	0.5
EPPS	8.0	-[b]	-	0.09	1.6
HEPBS	8.3	1.55	-	0.09	1.6
BES	7.1	1.20	-	0.09	1.6
DIPSO	7.6	1.03	15	0.18	3.1
TEA	7.8	0.95	10	0.26	4.5
BICINE	8.3	0.99	-	0.03	0.5
TES	7.4	1.44	-	0.18	3.1
TAPSO	7.6	1.40	-	0.24	4.1
TAPS	8.4	1.23	-	0.63	10.9
TRICINE	8.1	1.29	-	0.01	0.2
GLY-GLY	8.2	-[b]	-	0.01	0.2
BTP	6.8	1.43	-	0.88	15.2

All buffer solutions contain 0.2 M buffering agents and 0.2 M NaCl.

a. Oxidation peak potential measured from CV on the GCE at 0.1 V/s

b. E_p was not measurable due to the broadness of wave.

I_{CB}/I_{TPrA}, (Table 3.3). Among them, MOPSO (14.1 %), BTP (15.2 %), MOPS (17.2 %), MOBS (24.1 %), and TAPS (10.9 %) generated more than 10 % of the second ECL produced with TPrA (10 mM) in PBS. Thus, these CBs could be candidates as substitutes of TPrA. In view of CB structures, a CB having an –OH group near at α-carbon definitely produced a lower intensity of the second ECL wave than did a CB not having this group. In addition, as the number of –OH groups increased in the same molecular structure of CBs, the ECL intensity decreased. Although MOPSO, MOPS, and MOBS have heteroalicyclic structures (their base structure is a morpholine), their ECL intensities were not lower than those of acyclic CBs because the electron-donating group (–O–) in a ring further stabilized free radical form of MOPSO, MOPS, and MOBS.

3.4 Conclusion

The structures of amine coreactants were correlated with their reactivity to produce the ECL of $Ru(bpy)_3^{2+}$. Of amine coreactants used in this work, TPrA generated the highest first and second ECL intensity of $Ru(bpy)_3^{2+}$, indicating that TPrA had the optimized structure to keep stabilizing both the radical cation and the free radical. Generally, diamines and heteroalicyclic amines do not give more intense first and second ECL than acyclic tertiary amines. In addition, electron-withdrawing groups in an amine molecule decreased the second ECL wave by destabilizing the free radical of an amine, while the electron-donating group in an

amine molecule enhanced the second ECL wave by stabilizing the free radical of an amine.

Based on the ECL results in CB solutions, MOPSO, BTP, MOPS, MOBS, and TAPS generated comparable ECL of $Ru(bpy)_3^{2+}$ to TPrA. Generally, morpholine group coreactants produced the most efficient ECL among CBs. Therefore, they can be used especially in the ECL analysis of immunoassays or DNA-probe assays without employing additional coreactants. Furthermore, since they are well-known biological buffers and there are no other components besides analytes and ECL labels, the biological reactivity of biomolecules, such as interaction between antibody and antigen, will not be interfered, and the decomposition or denaturalization of biomolecules is not expected.

References

(1) Faulkner, L. R.; Bard, A. J. In *Electroanalytical Chemistry*; Bard, A. J., Ed.; Marcel Dekker: New York, 1977; Vol. 10, p. 1.

(2) Knight, A. W.; Greenway, G. M. *Analyst* **1994**, *119*, 879.

(3) Bard, A. J.; Debad, J. D.; Leland, J. K.; Sigal, G. B.; Wilber, J. L.; Wohlstadter, J. N. In *Encyclopedia of Analytical Chemistry: Applications, Theory, and Instrumentation*; Meyers, R. A., Ed.; John Wiley & Sons: New York, 2000, Vol. 11, p. 9842.

(4) Leland, J. K.; Powell M. J. *J. Electrochem. Soc.* **1990**, *137*, 3127.

(5) Knight, A. W.; Greenway, G. M. *Analyst* **1996**, *121*, 101R.

(6) Kanoufi, F.; Zu, Y.; Bard, A. J. *J. Phys. Chem. B* **2001**, *105*, 210.

(7) Zu, Y.; Bard, A. J. *Anal. Chem.* **2001**, *73*, 3960.

(8) Gross, E. M.; Pastore, P.; Wightman, R. M. *J. Phys. Chem. B* **2001**, *105*, 8732.

(9) Zu, Y.; Bard, A. J. *Anal. Chem.* **2000**, *72*, 3223.

(10) Miao, W.; Choi, J. –P.; Bard, A. J. *J. Am. Chem. Soc.* **2002**, *124*, 14478.

(11) Noffsinger, J. B.; Danielson, N. D. *Anal. Chem*. **1987**, *59*, 865.

(12) Downey, T. M.; Nieman, T. A. *Anal. Chem.* **1992**, *64*, 261.

(13) Christian, G. D.; Purdy, W. C. *J. Electroanal. Chem.* **1962**, *3*, 363.

(14) Tokel-Takvoryan, N. E.; Hemingway, R. E.; Bard, A. J. *J. Am. Chem. Soc.* **1973**, *95*, 6582.

(15) Gillard, R. D.; Hughes, C. T.; Williams, P. A. *Transition Met. Chem.* **1976**, *1*, 51.

(16) Sagüés, J. A. A.; Gillard, R. D.; Lancashire, R. J.; Willaims, P. A. *J. Chem. Soc. Dalton Trans.* **1979**, 193.

(17) Constable, E. C.; Seddon, E. A. *J. Chem. Soc. Chem. Comm.* **1982**, 34.

(18) Constable, E. C. *Polyhedron* **1983**, *2*, 551.

(19) Creutz, C.; Sutin, N. *Proc. Nat. Acad. Sci.* **1975**, *72*, 2858.

(20) Serpon, N.; Bolletta, F. *Inorg. Chim. Acta.* **1983**, *75*, 189.

(21) Serpon, N.; Ponterini, G.; Jamieson, M. A.; Bolletta, F.; Maestri, M. *Coord. Chem. Rev.* **1983**, *50*, 209.

(22) For a general review on an nonaromatic amine oxidation, Chow, Y. L.; Danen, W. C.; Nelsen, S. F.; Rosenblatt, D. H. *Chem. Rev.* **1978**, *78*, 243.

(23) Mann, C. K. *Anal. Chem.* **1964**, *36*, 2424.

(24) Masui, M.; Sayo, H.; Tsuda, Y. *J. Chem. Soc. B* **1968**, 973.

(25) Portis, L. C.; Bhat, V. V.; Mann, C. K. *J. Org. Chem.* **1970**, *35*, 2175.

(26) Ross, S. D. *Tetrahedron Lett.* **1973**, *14*, 1237.

(27) Bard, A. J.; Faulkner, L. R. In *Electrochemical Method, 2nd Ed.* Wiley & Sons: New York, 2001, Chapter 6.

(28) Calculated from an equation: $E°\ [R_3N/R_3N^{\bullet+}] = E_s + E°\ [Ru(bpy)_3^{2+/+}] + 0.1$ eV where E_s is the excited singlet energy of $Ru(bpy)_3^{2+}$ and 0.1 eV is the entropy correction term.

(29) Kalyanasundaram, K. *Coord. Chem. Rev.* **1982**, *46*, 159.

(30) The first *pKa*'s of most diamines are below 5 and the second *pKa*'s are above 9.

(31) Hercules, D. M.; Lytle F. E. *J. Am. Chem. Soc.* **1966**, *88*, 4745.

(32) In *CRC Handbook of Chemistry and Physics, 83rd Ed.*, Lide, D. R. Ed., CRC Press:Boca Raton, FL, 2002/03, Section 8.

(33) Dean, J. A. In *Lange's Handbook of Chemistry, 15th Ed.*, McGraw-Hill, Inc.:New York, 1999, Section 8.

(34) Yu, Q.; Kandegedara, A.; Xu, Y.; Rorabacher, D. B. *Anal. Biochem.* **1997**, *253*, 50.

(35) Gero, A. *J. Am. Chem. Soc.* **1954**, *76*, 5158.

(36) Perrin, D. D. In *Dissociation Constants of Organic Bases in Aqueous Solution.* Butterworths:London, 1965.

(37) Dega-Szafran, Z.; Jaskólski, M.; Kurzyca, I.; Barczyński, P.; Szafran, M. *J. Mol. Struct.* **2002**, *614*, 23.

(38) Brune, S. N.; Bobbitt, D. R. *Anal. Chem.* **1992**, *64*, 166.

(39) March, J. In *Advanced Organic Chemistry: Reactions, Mechanisms, and Structure, 4th Ed.* Wiley & Sons: New York, 1992, Chapter 9.

Therefore, it is speculated that two successive one-electron reductions of NR can occur [paths (a) and (b) in Scheme 4.1]. Similarly, NRH^+ is supposed to be reduced as same manner. However, if the heterogeneous electron transfer rate of path (d) is very fast and path (d) occurs at same or more positive potential than the one for path (c), a two-electron reduction process of NRH^+ is expected. In our system, path (e) might be negligible because there was not a sufficient concentration of H^+. Similar phenomena were observed in electrochemical reductions of phenazine and protonated phenazine in DMF or DMSO.[28]

Scheme 4.1

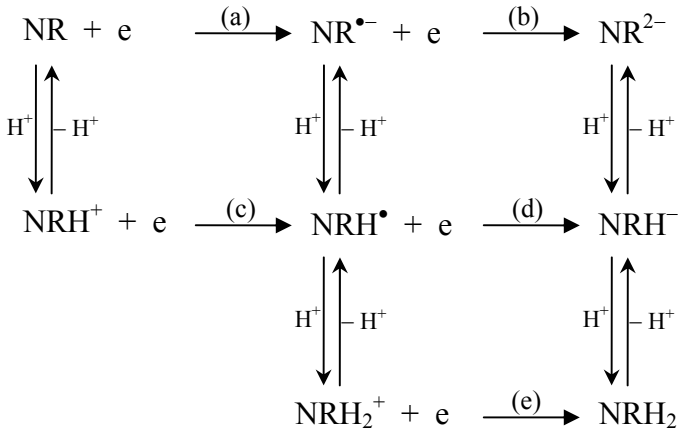

In summary, electrochemical reductions of NR and NRH^+ in MeCN are occurs as follows.

$$NR + e \longrightarrow NR^{\bullet -} \quad (4.8)$$

$$NRH^{+} + 2e \longrightarrow NRH^{-} \quad (4.9)$$

Electrogenerated Chemiluminescence (ECL) of NR. ECL by ion annihilation was not produced because neither NR nor NRH^{+} generated stable radical cations (no reversible oxidation shown in their CVs). Therefore, benzoyl peroxide (BPO) was used as a coreactant because it produced a sufficiently strong oxidizing agent, benzoate radical ($C_6H_5CO_2^{\bullet}$), via the ECE process.

$$BPO + e \longrightarrow BPO^{\bullet -} \quad (4.10)$$

$$BPO^{\bullet -} \longrightarrow C_6H_5CO_2^{\bullet} + C_6H_5CO_2^{-} \quad (4.11)$$

$$C_6H_5CO_2^{\bullet} + e \longrightarrow C_6H_5CO_2^{-} \quad (4.12)$$

Figure 4.8 shows the simultaneous CV and ECL response of the 1 mM NR/5 mM BPO system in MeCN containing 0.1 M TBAP at 0.1 V/s. From the CV, BPO was reduced at – 1.25 V vs. Ag QRE prior to the NR reduction and no ECL was found at this potential, indicating that no luminescence was generated by only BPO reduction. When the electrode potential approached to the reduction potential of NR, ECL emitted by NR was detected at the PMT.

The proposed ECL mechanism of NR generated with BPO is shown in Scheme 4.2. The electrochemical reduction of BPO displayed an irreversible

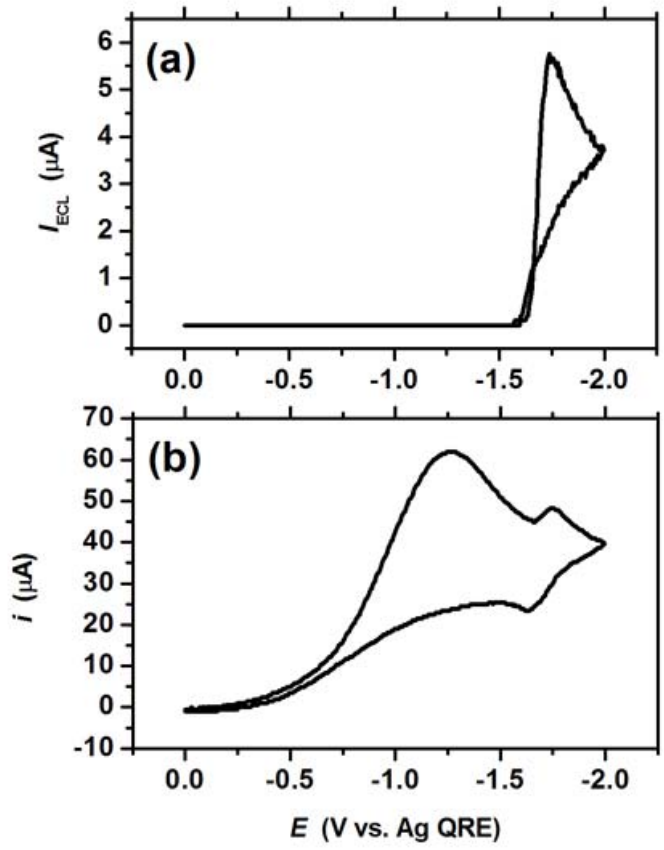

Figure 4.8. Simultaneous (a) ECL and (b) CV of 1 mM NR and 5 mM BPO in 0.1 M TBAP/MeCN at 0.1 V/s. A Pt electrode was used (area = 0.03 cm^2).

reduction wave in CV [Figure 4.8], and followed an ECE mechanism[29], [eq. (4.10) through eq. (4.12)] which was analogous to the one proposed by Chandross,[30] *et. al.*, where BPO is reduced by hydrocarbon radical anions. The generated $C_6H_5CO_2^{\bullet}$ was a sufficiently strong oxidizing agent, whose $E°$ ($C_6H_5CO_2^{\bullet}/C_6H_5CO_2^{-}$) values were reported as either + 0.8 V[31] or + 1.5 V[30] vs. SCE. Once NR was reduced, $C_6H_5CO_2^{\bullet}$ oxidized $NR^{\bullet-}$ to NR* [eq. (4.14)].

Scheme 4.2

$$BPO + e \longrightarrow BPO^{\bullet-} \qquad (4.10)$$

$$BPO^{\bullet-} \longrightarrow C_6H_5CO_2^{-} + C_6H_5CO_2^{\bullet} \qquad (4.11)$$

$$NR + e \longrightarrow NR^{\bullet-} \qquad (4.13)$$

$$NR^{\bullet-} + C_6H_5CO_2^{\bullet} \longrightarrow {}^1NR^* + C_6H_5CO_2^{-} \qquad (4.14)$$

$${}^1NR^* \longrightarrow NR + h\nu \qquad (4.15)$$

To check the energetic feasibility, the energy ($-\Delta H_{co}$)[32] available in the reaction between $C_6H_5CO_2^{\bullet}$ and $NR^{\bullet-}$ was calculated using $E_{1/2}$ ($NR/NR^{\bullet-}$) and $E°$ ($C_6H_5CO_2^{\bullet}/C_6H_5CO_2^{-}$), and compared with the lowest excited singlet state energy (E_s) of NR, which was ditermined from the fluorescence spectrum of NR.

From the equation (4.16),

$$-\Delta H_{co} = E^{\circ}(C_6H_5CO_2^{\bullet}/C_6H_5CO_2^{-}) - E_{1/2}(NR/NR^{\bullet-}) - 0.1\ eV \qquad (4.16)$$

where 0.1 eV is an estimate of the temperature-entropy approximation term ($T\Delta S$) at 25 °C, the calculated $-\Delta H_{co}$ is 2.34 eV if E° ($C_6H_5CO_2^{\bullet}/C_6H_5CO_2^{-}$) is + 0.8 V ($-\Delta H_{co}$ = 3.04 eV if E° of $C_6H_5CO_2^{\bullet}$ is + 1.5 V), which is larger than E_s (2.21 eV) of NR. Therefore, the lowest excited singlet state (^{1}NR*) of NR can be directly generated.

In contrast, no ECL signal was obtained with NRH^+ and BPO. Because the electrochemical reduction of NRH^+ is a two-electron transfer reaction and $-\Delta H_{co}$ (1.93 eV) estimated from the maximum value (+ 1.5 V) of E° ($C_6H_5CO_2^{\bullet}/C_6H_5CO_2^{-}$) is less than E_s (2.06 eV) of NRH^+, it is energetically unfavorable to directly generate $^1NRH^+$*.

To determine that the observed ECL was emitted from NR, ECL spectra were measured with a CCD camera and compared with its fluorescence. Figure 4.9 shows the ECL spectrum of 1 mM NR with 10 mM BPO produced by pulsing the electrode potential between 0 V and – 1.6 V vs. Ag QRE with the 0.1 sec pulse width and the fluorescence spectra of NR (5 μM) and NRH^+ (5 μM). The fluorescence maxima of NR and NRH^+ were found at 561 nm and 601 nm, respectively. Interestingly, the observed ECL spectrum of NR, which had a maximum intensity at 610 nm, corresponded to the fluorescence of NRH^+ rather

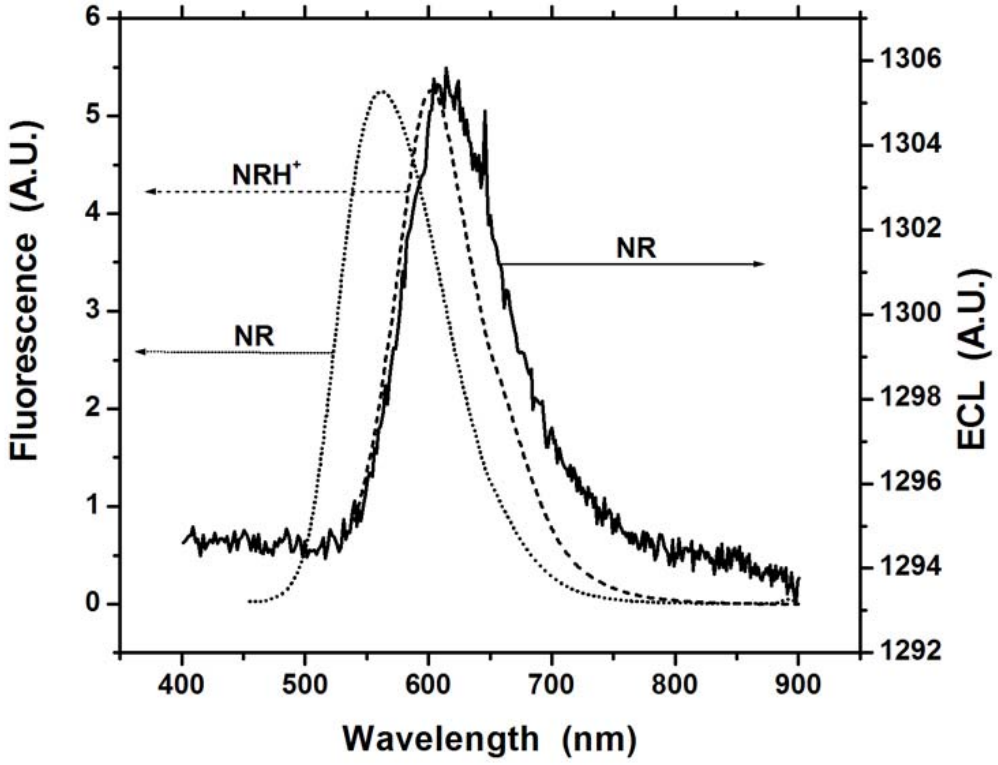

Figure 4.9. ECL (solid line) spectrum of 1 mM NR and fluorescence spectra of 5 μM NR (dotted line) and 5 μM NRH^+ (dashed line). ECL was generated with 10 mM BPO by pulsing the electrode potential between 0 V and – 1.6 V vs. Ag QRE (0.1 sec pulse-width and 5 min integration). λ_{ex} for NR and NRH^+ were 440 nm and 530 nm, respectively.

than NR. To check the presence of unknown fluorescing species produced during ECL, absorbance and fluorescence measurements were carried out again with the same NR/BPO solution as soon as the ECL experiment was finished. The resulting absorption and fluorescence spectra were identical with those measured before ECL experiments, suggesting that no emissive bulk by-product was formed during the ECL reaction. However, there may be still possibility that a small amount of by-products can be formed at (or near) the electrode during the ECL reaction.

Singh, *et. al.* reported the dual solvatochromism of NR in fluorescence.[33] They observed that the fluorescence maxima shifted to the longer wavelength region as the solvent polarity became higher, and suggested the existence of two closely spaced electronic excited states[33]. To check the solvatochromic effect on the NR ECL, several solvents having different polarities (dielectric constants) were used. Unlike in MeCN, the electrochemical reduction of NR was not reversible in tetrahydrofuran (THF) and benzonitrile (Bz) (See Supporting Information Figure4.2), indicating that the radical anions of NR were not stable in these solvents. As well, no ECL was observed in THF and Bz. However, NR was reversibly reduced in CH_2Cl_2 (See Supporting Information Figure 4.2) and its ECL was produced with BPO at 575 nm. Figure 4.10 shows the ECL spectra of 1 mM NR with 10 mM BPO in MeCN and CH_2Cl_2. Because MeCN usually provides better stability for radical anions than CH_2Cl_2,[32] the ECL produced in

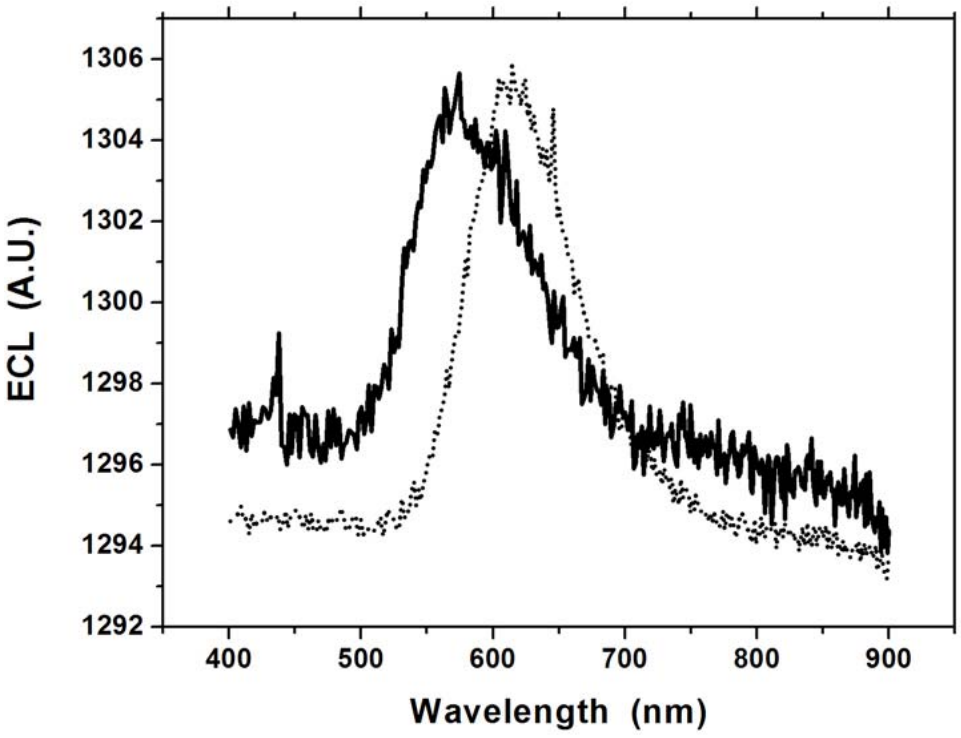

Figure 4.10. ECL spectra of 1 mM NR with 10 mM BPO in MeCN (dotted line) and CH_2Cl_2 (solid line). ECL was generated by pulsing the potential between 0 V and – 1.6 V vs. Ag QRE with 5 min integration time. The same Pt electrode was used for each measurement (area =0.03 cm^2).

MeCN is higher than that produced in CH_2Cl_2 with the same concentrations of NR and BPO. The ECL of NR in CH_2Cl_2 occurred at a ~ 30 nm shorter wavelength than in MeCN. This wavelength shift in the NR ECL is likely due to the difference in the dielectric constants (ε) of CH_2Cl_2 ($\varepsilon = 9.1$) and MeCN ($\varepsilon = 37.5$).

Concentration effects on the ECL of NR. The ECL of NR strongly depends on the concentrations of NR, H^+, and BPO. Figure 4.11 displays the concentration effect of NR on its ECL produced with 5 mM BPO. Each ECL was measured with a PMT by sweeping the electrode potential. The measured ECL intensities were linearly proportional to the concentrations of NR up to 0.25 mM. However, the ECL intensities gradually decreased from 0.5 mM to 2 mM of NR because of the inner filter effect (self-absorption) and self-quenching at such high concentrations. Generally, the inner filter effect occurs when the wavelength of emission overlaps an absorption band and becomes significant with an increasing concentration of emitter. The rate of self-quenching is expect to increase with increasing concentration of emitter because the average distance between emitting molecules is shorter so that probability of collisions between excited state molecules is greater at high concentration. Therefore, radiationless energy transfer becomes significant.

The ECL intensity of NR was strongly dependent on the concentration of H^+, because the protonated form of NR did not produce ECL. Figure 4.12 shows

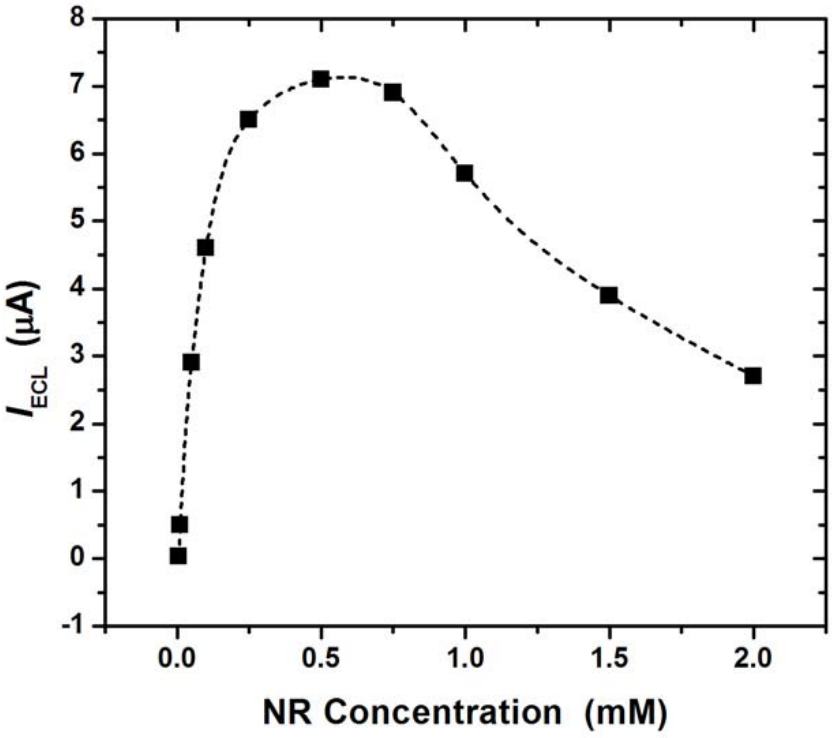

Figure 4.11. Effect of NR concentrations on its ECL produced with a fixed 5 mM BPO. ECL was measured with a PMT and by sweeping an electrode potential at 0.1 V/s. The same Pt electrode was used for each measurement (area =0.03 cm^2).

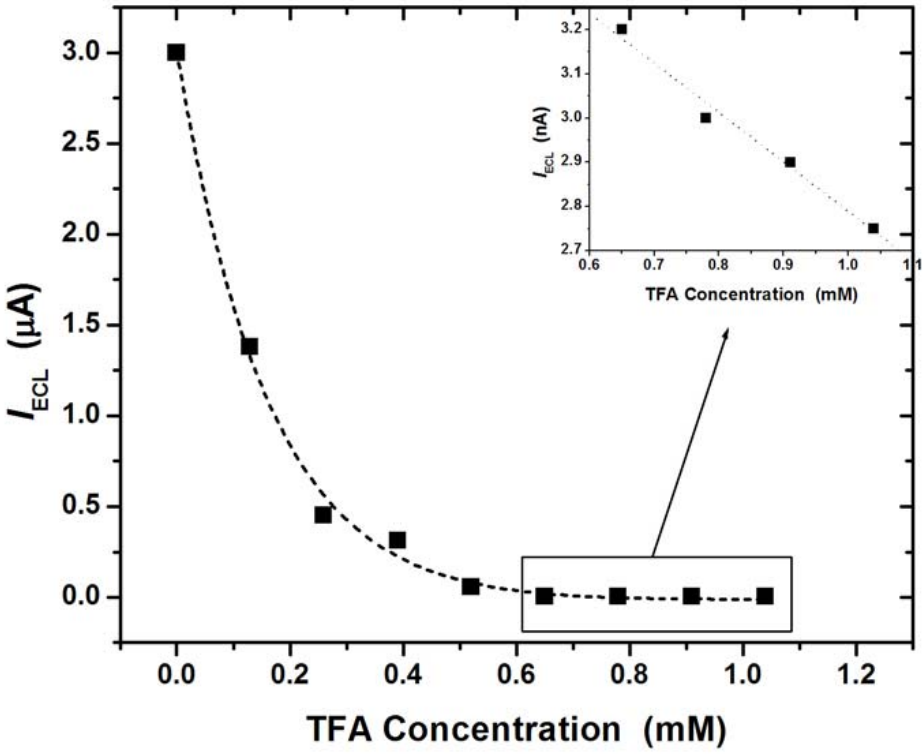

Figure 4.12. Effect of TFA concentrations on the ECL of 1 mM NR produced with 5 mM BPO. ECL was measured with a PMT and by sweeping an electrode potential at 0.1 V/s. The same Pt electrode was used for each measurement (area =0.03 cm^2).

the effect of H^+ concentrations on the ECL of 1 mM NR using TFA as a H^+ donor. As shown in Figure 4.12, the initial ECL intensities were dramatically affected by the small amount of acid and the total ECL intensity decayed exponentially although it decreased linearly in the relatively high concentration region [inset of Figure 4.12]. The decay of the ECL intensity by adding TFA is caused not only by the formation of NRH^+ but also by the inner filter effect of formed NRH^+. Because the absorption band (533 nm) of NRH^+ is located more closely to the ECL band (610 nm) of NR than that (441 nm) of NR, the inner filter effect by NRH^+ could occur more efficiently than by NR. In fact, larger portion of the absorption band of NRH^+ overlapped the ECL spectrum of NR than did the absorption band of NR: 15.8 % of NR ECL was overlapped to the NRH^+ absorption band, but 2.8 % to the NR absorption band (See Supporting Information Figure 4.3).

Figure 4.13 shows the ECL intensity of 0.5 mM NR as a function of the BPO concentration. The ECL intensity of 0.5 mM NR was linearly proportional to the concentration of BPO from 0 to 10 mM. Then the ECL intensities decreased as the concentration of BPO increased from 10 mM, implying that the ECL of NR was quenched by BPO in such high concentrations. It has already been reported that BPO was used as an effective quencher for the fluorescence of $Ru(bpy)_3^{2+}$ and aromatic hydrocarbons.[34,35] Similarly, ECL quenching might occur by electron transfer (ET) as follows;

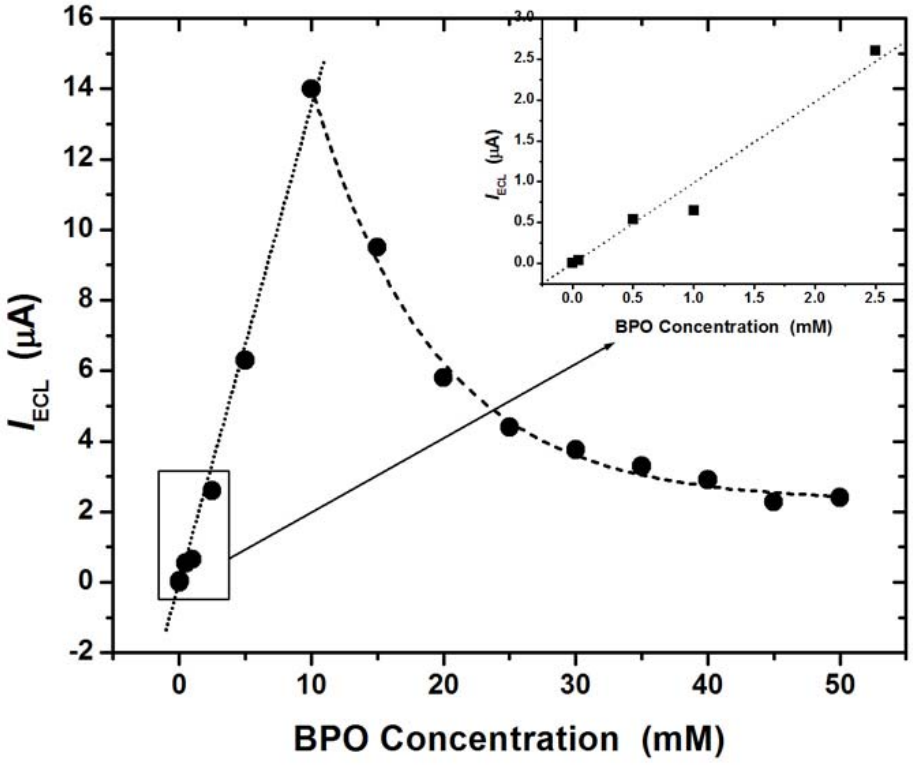

Figure 4.13. Effect of BPO concentrations on the ECL of 0.5 mM NR. ECL was measured with a PMT and by sweeping the electrode potential at 0.1 V/s. Inset represents the low concentration region (0 mM to 2.5 mM BPO). The same Pt electrode was used for each measurement (area =0.03 cm^2).

$$NR^* + BPO \xrightarrow{k_q} [NR^{\bullet+} \cdots BPO^-] \quad (4.15)$$

$$[NR^{\bullet+} \cdots BPO^-] \rightarrow NR^{\bullet+} + C_6H_5CO_2^{\bullet} + C_6H_5CO_2^- \quad (4.16)$$

$$[NR^{\bullet+} \cdots BPO^-] \rightarrow NR + BPO \quad (4.17)$$

Once the intermediate state, $[NR^{\bullet+} \cdots BPO^-]$, as shown in eq. (4.15) was formed, both the decomposition reaction [eq. (4.16)] and the back electron transfer reaction [eq. (4.17)] could occur. The quenching effect by BPO seemed not to be efficient below 10 mM BPO against the ECL of 0.5 mM NR.

The quenching experiments were performed with the fluorescence of NR to check whether NR was a quencher. The quenching effect of BPO was also observed in the fluorescence of NR. The fluorescence quenching rate constant (k_q) can be estimated from the Stern–Volmer relationship[36] in the absence of molecular oxygen as defined by

$$\frac{I_0}{I} = 1 + K_{SV}[BPO] = 1 + k_q \tau^s [BPO] \quad (4.18)$$

where I and I_0 denote the fluorescence intensity with BPO and the initial fluorescence intensity without BPO, respectively, K_{SV} is the Stern-Volmer quenching constant, k_q is the quenching rate constant, and τ^s is the lifetime of the

lowest excited singlet state. Figure 4.14 shows the Stern-Volmer plot of the NR fluorescence quenching. From the slope of this plot, K_{SV} and k_q were calculated as 68.95 M^{-1} and 1.64×10^{10} $M^{-1}s^{-1}$, respectively, by taking τ^s as 4.2 ns[33].

ECL of $Ru(bpy)_3^{2+}$ with BPO and ECL Efficiency. The new coreactant BPO was also applied to tris(2,2′-bipyridine)ruthenium(II), $Ru(bpy)_3^{2+}$ (bpy = 2,2′-bipyridine), which is a well-known ECL emitter. As shown in Figure 4.15, the $Ru(bpy)_3^{2+}$/BPO system produced ECL in 0.1 M TBAP/MeCN. When the electrode potential was swept in the cathodic direction, BPO was first reduced and followed by the production of $C_6H_5CO_2^{\bullet}$. No luminescence occurred until $Ru(bpy)_3^{2+}$ was reduced. Three reversible reductions for the $Ru(bpy)_3^{2+/+}$, $Ru(bpy)_3^{+/0}$, and $Ru(bpy)_3^{0/-}$ couples were observed in order [Figure 4.15 (a)] and $Ru(bpy)_3^{2+}$* (2.12 eV[37]) was produced by the energetic ET reaction ($-\Delta H_{co}$ = at least 2.2 eV[38]) with $C_6H_5CO_2^{\bullet}$ [Figure 4.15 (b)]. The produced ECL gave the orange emission having a maximum intensity at 623 nm [inset of Figure 4.15 (b)]. Although ECL was also produced at the potential where $Ru(bpy)_3^0$ and $Ru(bpy)_3^-$ were generated, only the first ECL produced by $Ru(bpy)_3^+$ would be considered here for the proposed ECL mechanism shown in Scheme 4.2. Besides the direct generation of $Ru(bpy)_3^{2+}$* [eq. (4.20)], $Ru(bpy)_3^{2+}$* can be produced by annihilation reaction. If the $E°$ value of $C_6H_5CO_2^{\bullet}$ is taken as + 1.5 V vs. SCE[30], it is energetically feasible for $C_6H_5CO_2^{\bullet}$ to oxidize $Ru(bpy)_3^{2+}$ to $Ru(bpy)_3^{3+}$ ($E°$ = +

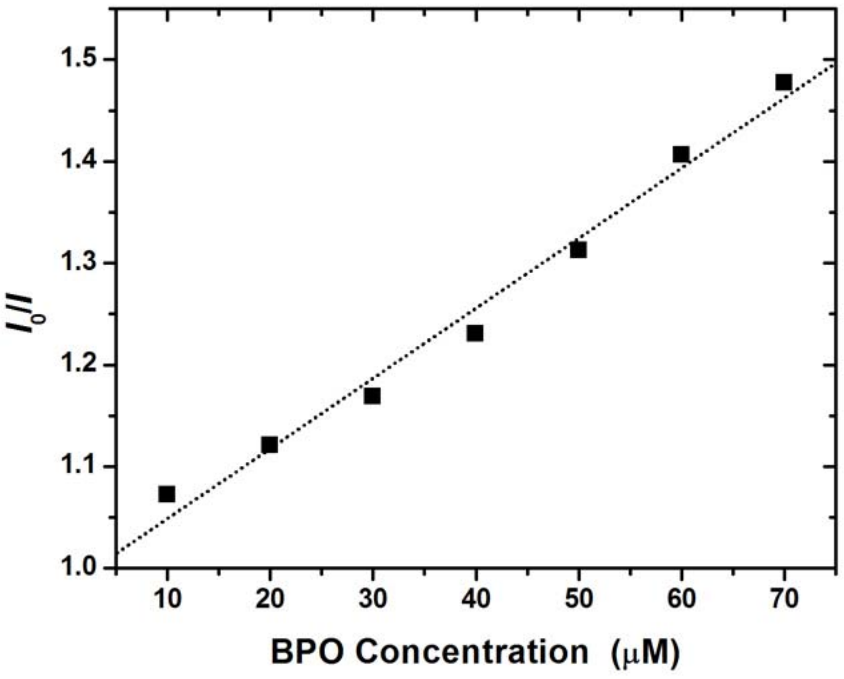

Figure 4.14. Stern-Volmer plot of the NR fluorescence quenching by BPO in the absence of molecular oxygen. C_{NR} = 1 μM. λ_{ex} = 440 nm.

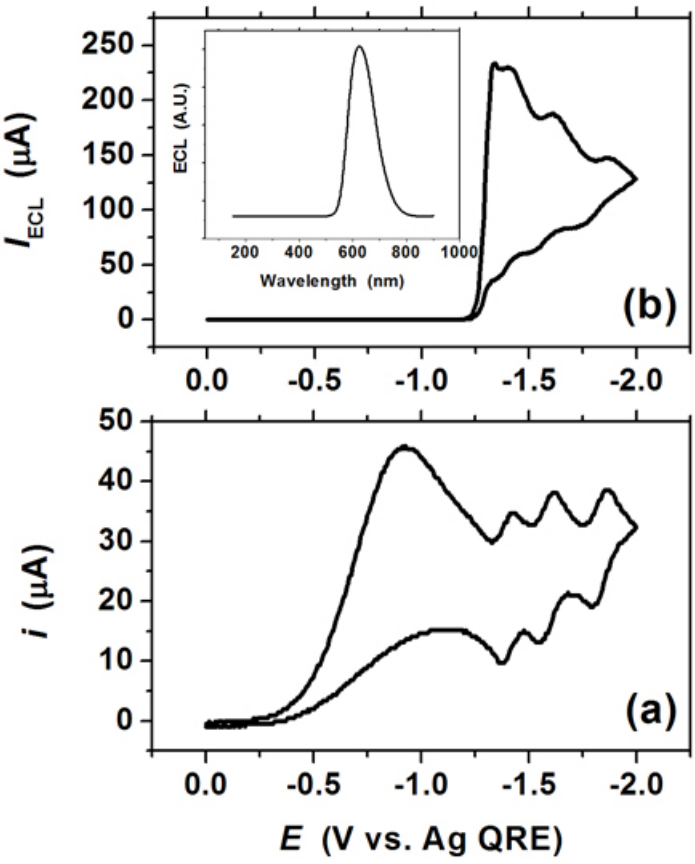

Figure 4.15. Simultaneous (a) cyclic voltammogram and (b) ECL wave of 1 mM $Ru(bpy)_3^{2+}$ and 5 mM BPO in 0.1 M TBAP/MeCN at 0.1 V/s. Inset of (b) represents the ECL spectra measured under the same condition.

1. 29 V vs. SCE) [eq. (4.21)]. Therefore, electrochemically generated $Ru(bpy)_3^{+}$ can be annihilated by $Ru(bpy)_3^{3+}$ to produce $Ru(bpy)_3^{2+}$* [eq. (4.22)].

Scheme 4.3

$$BPO + e \longrightarrow BPO^{-} \quad (4.8)$$

$$BPO^{-} \longrightarrow C_6H_5CO_2^{\bullet} + C_6H_5CO_2^{-} \quad (4.9)$$

$$Ru(bpy)_3^{2+} + e \longrightarrow Ru(bpy)_3^{+} \quad (4.19)$$

$$Ru(bpy)_3^{+} + C_6H_5CO_2^{\bullet} \longrightarrow Ru(bpy)_3^{2+}* + C_6H_5CO_2^{-} \quad (4.20)$$

or

$$Ru(bpy)_3^{2+} + C_6H_5CO_2^{\bullet} \longrightarrow Ru(bpy)_3^{3+} + C_6H_5CO_2^{-} \quad (4.21)$$

$$Ru(bpy)_3^{+} + Ru(bpy)_3^{3+} \longrightarrow Ru(bpy)_3^{2+}* + Ru(bpy)_3^{2+} \quad (4.22)$$

In general, the ECL efficiency (ϕ_{ECL}) is defined as photons emitted per redox event that is related to the total charge applied. In the NR/BPO ECL system, ϕ_{ECL} could not be estimated because the total charge did not represent the number of redox reactions between $NR^{\bullet-}$ and $C_6H_5CO_2^{\bullet}$. Therefore, the integrated ECL intensity of the NR/BPO system was compared with a refernence ECL emitter/BPO system. For this comparison, $Ru(bpy)_3^{2+}$ was employed as a reference because the ECL efficiency of the $Ru(bpy)_3^{2+}$ is well known (~ 5 %[39–42]).The integrated ECL intensity of NR was compared with that of $Ru(bpy)_3^{2+}$

obtained under the identical condition (0.5 mM NR/10 mM BPO and 0.5 mM $Ru(bpy)_3^{2+}$/10 mM BPO). The relative intensity ratio ($I_{NR}/I_{Ru(II)}$) was ~ 0.05.

4.4 Conclusion

NR can be used as an pH indicator (pK_a = 6.5) showing the yellow-to-red color change when a NR solution is titrated with acids. In addition, NR that generates the stable radical anion ($NR^{\bullet-}$) can also be used as a new ECL emitter (λ_{em} = 610 nm) in MeCN. Although NR produces the low ECL intensity ($I_{NR}/I_{Ru(II)}$ = ~ 5 %), it may be useful for an ECL label in immunoassay or DNA-probe assay analyses because of its non-toxic stain property for biological cells and pH indicator property in MeCN. The protonated form (NRH^+) of NR does not produce ECL because of its two-electron reduction and lack of sufficient energy for ECL generation.

BPO is introduced as a new coreactant. The chemical and electrochemical reduction of BPO generates a strong oxidizing agent, $C_6H_5CO_2^{\bullet}$, which oxidizes the radical anions of NR and $Ru(bpy)_3^{2+}$ to their excited states. The relatively high concentration of BPO (e.g. >10 mM compared to 5 mM NR) quenches both ECL and fluorescence. The optimum condition for NR to produce ECL is 0.5 mM NR/10 mM BPO in the absence of proton donors and molecular oxygens.

Supporting Information

The molecular structure of BPO, CVs of NR taken in various solvents, and the inner filter effect of NR and NRH^+ in ECL are available in this section.

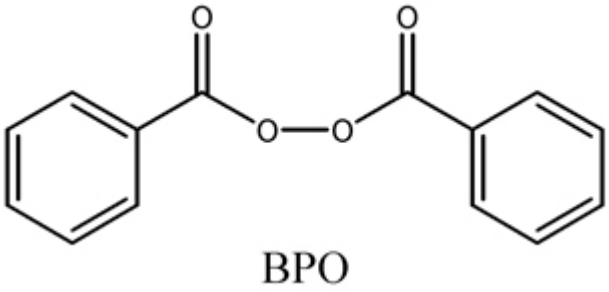

BPO

Supporting Information Figure 4.1. Molecular structure of benzoyl peroxide.

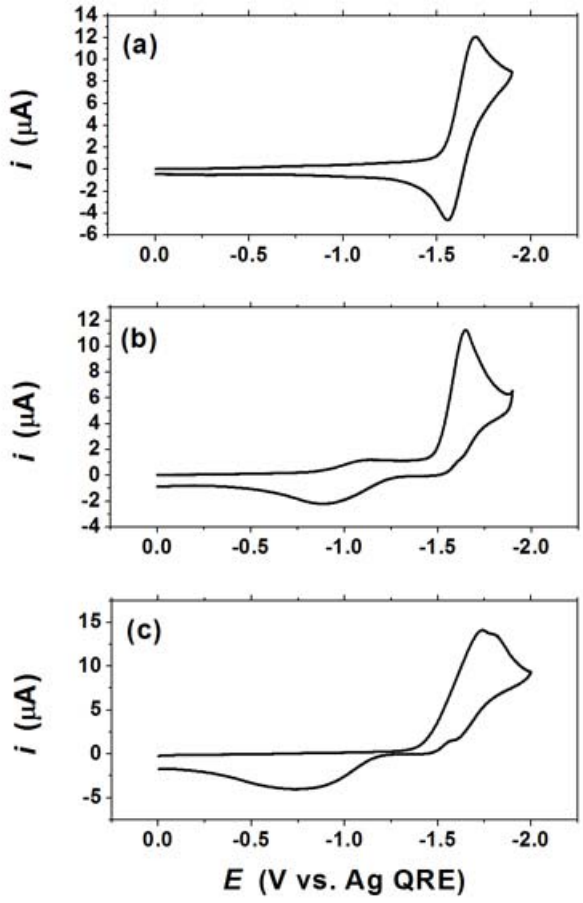

Supporting Information Figure 4.2. Cyclic voltammograms of 1 mM NR in (a) CH_2Cl_2, (b) benzonitrile, and (c) tetrahydrofuran (THF). Supporting electrolyte: 0.1 M TBAP. S.R. = 0.1 V/s

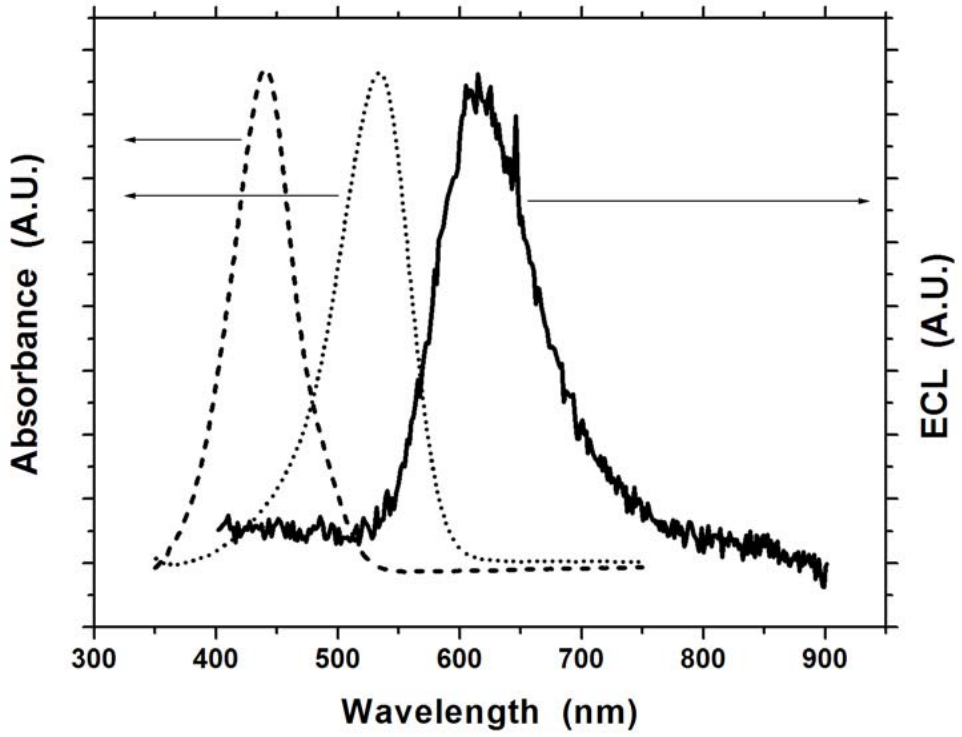

Supporting Information Figure 4.3. Electronic absorbance spectra of 10 μM NR (dashed line) and NRH^+ (dotted line) in MeCN and ECL spectrum of 1 mM NR (solid line) with 10 mM BPO in MeCN.

References

(1) Lamanna, J. C.; McCracken, K. A. *Anal. Biochem.* **1984**, *142*, 117.

(2) Haumann, M.; Junge, W. *Biochemistry*, **1994**, *33*, 864.

(3) Osborne, R.; Perkins, M. A. *Food Chem. Toxicol.* **1994**, *32*, 133.

(4) Gaullier, J. M., Geze, M.; Santus, R.; Sa e Melo, T.; Maziere, J. C.; Bazin, M.; Morliere, P.; Dubertret, L. *Photochem. Photobiol.* **1995**, *62*, 114.

(5) Woodburn, K. W.; Vardaxis, N. J.; Hill, J. S.; Kaye, A. H.; Phillips, D. R. *Photochem. Photobiol.* **1991**, *54*, 725.

(6) Chen, G.; Hanson, C. L.; Ebner, T. J. *J. Neurophysiol.* **1996**, *76*, 4169.

(7) Okada, D. *J. Neurosci. Methods* **2000**, *101*, 85.

(8) Walz Jr., F. G.; Terenna, B.; Rolince, D. *Biopolymers*, **1975**, *14*, 825.

(9) For general reviews, (a) Faulkner, L. R.; Glass, R. S. In *Chemical and Biological Generation of Excited States*, Adam, W.; Cilento, G., Eds.; Academic Press: New York, Chapter 6, 1982, p. 191. (b) Knight, A. W.; Greenway, G. M. *Analyst* **1994**, *119*, 879. (c) Bard, A. J.; Debad, J. D.; Leland, J. K.; Sigal, G. B.; Wilbur, J. L.; Wohlstadter, J. N. In *Encyclopedia of Analytical Chemistry: Applications, Theory, and Instrumentation*, Meyer, R. A. Ed.; John Wiley & Sons: New York, 2000, p. 9842.

(10) White, H. S.; Bard, A. J. *J. Am. Chem. Soc.* **1982**, *104*, 6891.

(11) Bolleta, F.; Ciano, M.; Balzani, V.; Serpone, N. *Inorg. Chim. Acta.* **1982**, *62*, 207.

(12) Becker, W. G.; Seung, H. S.; Bard, A. J. *J. Electroanal. Chem.* **1984**, *167*, 127.

(13) Bard, A. J.; Whitesides, G. M. *U.S. Patents* 5 221 605, 1993; 5 238 808, 1993; and 5 310 687, 1994.

(14) Blackburn, G. F.; Shah, H. P.; Kenien, J. H.; Leland, J.; Kamin, R. A.; Link, J.; Peterman, J.; Powell, M. J.; Shah, A.; Talley, D. B.; Tyagi, S. K.; Wilkins, E.; Wu, T. –G.; Massey, R. J. *J. Clin. Chem.* **1991**, *37*, 1534.

(15) Coetzee, J. F.; Kolthoff, I. M. *J. Am. Chem. Soc.* **1957**, *79*, 6110.

(16) Debad, J. D.; Morris, J. S.; Magnus, P.; Bard, A. J. *J. Org. Chem.* **1997**, *62*, 530.

(17) McCord, P.; Bard, A. J. *J. Electroanal. Chem.* **1991**, *318*, 91.

(18) Kolthoff, I. M.; Bruckenstein, S.; Chantooni, M. K. *J. Am. Chem. Soc.* **1961**, *83*, 3927.

(19) Halliday, C. S.; Matthews, D. B. *Aust. J. Chem.* **1983**, *36*, 507.

(20) Bauldreay, J. M.; Archer, M. D. *Electrochim. Acta* **1983**, *28*, 1515.

(21) Creager, S. E.; Marks, G. T.; Aikens, D. A.; Richtol, H. H. *J. Electroanal. Chem.* **1983**, *152*, 197.

(22) Witt, E. *Ber. Dtsch. Chem. Ges.* **1878**, *12*, 931.

(23) Denuault, G.; Mirkin, M. V.; Bard, A. J. *J. Electroanal. Chem.* **1991**, *308*, 27.

(24) Wightman, R. M.; Wipf, D. O. In *Electroanalytical Chemistry*; Bard, A. J., Ed.; Marcel Dekker: New York, 1988, Vol. 15. p. 267.

(25) Bard, A. J.; Fan, F. –R.; Kwak, J.; Lev, O. *Anal. Chem.* **1989**, *61*, 132.

(26) Oldham, K. B. *J. Electroanal. Chem.* **1981**, *122*, 1.

(27) Oldham, K. B.; Zoski, C. G. *J. Electroanal. Chem.* **1988**, *256*, 11.

(28) Sawyer, D. T.; Komai, R. Y. *Anal. Chem.* **1972**, *44*, 715.

(29) Bard, A. J.; Faulkner, L. R. In *Electrochemical Methods*, 2nd Ed., John Wiley & Sons: New York, 2001, Chapter 12, p 476.

(30) Chandross, E. A.; Sonntag, F. I. *J. Am. Chem. Soc.* **1966**, *88*, 1089.

(31) Akins, D. L.; Birke, R. L. *Chem. Phys. Lett.* **1974**, *29*, 428.

(32) Faulkner, L. R.; Bard, A. J. In *Electroanalytical Chemistry*; Bard, A. J., Ed; Marcel Dekker: New York, 1977; Vol. 10, p 1.

(33) Singh, M. K.; Pal, H.; Bhasikuttan, A. C.; Sapre, A. V. *Photochem. Photobiol.* **1998**, *68*, 32.

(34) Oishi, S.; Tajime, K.; Shiojima, I. *J. Mol. Catal.* **1982**, *14*, 383.

(35) Urano, T.; Kitamura, A.; Sakuragi, H.; Tokumaru, K. *J. Photochem.* **1984**, *26*, 69.

(36) Wilkinson, F. In *Fluorescence: Theory, Instrumentation, and Practice*; Guilbault, G. G., Ed; Marcel Dekker: New York, 1967; Chapter 1.

(37) Kalyanasundaram, K. *Coor. Chem. Rev.* **1982**, *46*, 159.

(38) Calculated by eq. (4.14) with $E°$ ($C_6H_5CO_2^{\bullet}/C_6H_5CO_2^{-}$) = + 0.8 V from ref. (30) and $E°$ ($Ru(bpy)_3^{2+/+}$) = – 1.5 V from ref. (10)

(39) Tokel-Takvoryan, N. E.; Hemingway, R. E.; Bard, A. J. *J. Am. Chem. Soc.* **1973**, *95*, 6582.

(40) Wallace, W. L.; Bard, A. J. *J. Phys. Chem.* **1979**, *83*, 1350.

(41) Itoh, K.; Honda, K. *Chem. Lett.* **1979**, 99.

(42) Luttmer, J. D.; Bard, A. J. *J. Phys. Chem.* **1981**, *85*, 1155.